國立臺灣海洋大學

河海工程學系

碩士學位論文

指導教授：陳正宗 終身特聘教授

加法定理及疊加技巧在含圓形邊界承受集中力與螺旋差排之反平面問題的應用

Applications of addition theorem and superposition technique to anti-plane problems with circular boundaries subject to concentrated force and screw dislocation

研究生：周克勳 撰

中華民國 97 年 7 月

加法定理及疊加技巧在含圓形邊界承受集中力與螺旋差排之反平面問題的應用

Applications of addition theorem and superposition technique to anti-plane problems with circular boundaries subject to concentrated force and screw dislocation

研 究 生：周克勳　　Student：Ke-Hsun Chou

指導教授：陳正宗　　Advisor：Jeng-Tzong Chen

國 立 臺 灣 海 洋 大 學
河 海 工 程 學 系
碩 士 論 文

A Thesis
Submitted to Department of Harbor and River Engineering
College of Engineering
National Taiwan Ocean University
In Partial Fulfillment of the Requirements
for the Degree of
Master of Science
in
Harbor and River Engineering
July 2008
Keelung, Taiwan, Republic of China

中華民國 97 年 7 月

誌 謝

兩年的碩士生涯隨著論文的完成而進入的結束的階段，學生的生涯也暫時告一段落，想當初進入海大之時，在還不知研究室的情況下，毅然決然地進入了 陳正宗 終身特聘教授的力學聲響振動實驗室中。在這兩年的學習及成長的過程中，讓我深刻的體驗到什麼是嚴謹的求學態度、實事求是的精神，老師對於做研究的認真程度更是我難以望其項背的。在研究所這兩年的求學體驗，正如實驗室門聯上所寫的一樣『教學良心事，研究天酬勤』，在這兩年中有相當深刻的體驗。由衷的感謝教授在研究期間所投入的時間與心力，並在撰寫論文期間，教授不厭其煩地審閱修正，得以完成論文的定稿。

論文口試期間，承蒙台灣科技大學機械工程系 趙振綱 教授、中華技術學院機械工程系 李為民 副教授、國立高雄海洋科技大學造船工程系 陳義麟 副教授、宜蘭大學土木工程學系 陳桂鴻 助理教授、中華技術學院航空機械系 呂學育 助理教授與台灣大學 徐文信 博士，不吝指教並提供寶貴的意見使文章更為完備，深表謝意。

在求學期間除了憑藉著自已的毅力與努力之外，還要感謝研究室諸位學長：應德、奐禎、佳男等學長的細心教導，無論是課業上或是程式撰寫上的建議與修正。以及研究室學弟：聖凱、羿州、祥志、家瑋，感謝他們願意分擔研究室細微的工作。同時也要感謝相處多年的好友：文謙、育加、璟照、奕銓、哲瑋、明修、哲平、思佑於求學路程上的陪伴與鼓勵。更要感謝國科會計畫 NSC 96-2221-E-019-041 提供之碩士生研究助學金，以及中華顧問工程司(台灣世曦工程顧問公司)所頒發之工程科技獎學金，讓我於做研究時無經濟壓力，更能專心致力於學業及研究上。最後並感謝國科會及 NTOU/MSV 經費補助之下，得以在京都發表論文，實屬難得。

研究生的生活即將告一段落了，雖然這段旅程即將結束，但是這又意味著另一段的旅程的啟程，期許自已能夠順利地渡過一個個即將到來的歷練。

周克勳 Ke-Hsun Chou

2008/07/28 於力學聲響振動實驗室

中文摘要

本論文利用加法定理及疊加技巧來求解集中力與螺旋差排問題的格林函數。此兩類問題均可利用疊加技巧分為兩部份。一部分為基本解的問題;另一部份為典型的邊界值問題。於基本解的部份，我們利用加法定理展開成退化核的型式。而在求解螺旋差排問題時，將角度型的基本解展成退化核的型式，這在作者的認知中文獻並未發現。我們引入疊加技巧及加法定理來決定典型邊界值問題之邊界條件。再利用NTOU/MSV在零場積分方程結合傅立葉級數求解典型邊界值問題之成功經驗，第二部份的解將能迎刃而解。將兩部分的場解做疊加即可得到完整的格林函數。另外，選取不同項數的傅立葉級數進行收斂性分析來測試本方法的收斂速率。最後，我們將利用含圓形邊界(洞及夾雜)之集中力與螺旋差排問題，來驗證此方法的準確性。本法最大特色可免除傳統邊界元素法中的五項缺點:(1)奇異積分的主值計算、(2)病態矩陣、(3)邊界層效應、(4)線性收斂及(5)網格切割。

關鍵字：加法定理、疊加技巧、螺旋差排、格林函數

Abstract

In this thesis, we employ the addition theorem and superposition technique to derive the Green function of the concentrated forces and screw dislocation problems. By using the superposition technique, the problems can be decomposed into two parts. One is the problem of the fundamental solution and the other is a typical boundary value problem (BVP). The fundamental solution is expanded into the degenerate kernel by using the addition theorem. The angle-type fundamental solution of the screw dislocation problem has not been expanded into the degenerate form before to our best knowledge. Following the success of null-filed integral formulation for solving the typical BVP with Fourier boundary densities in the NTOU/MSV group, the second part boundary condition can be easily obtained by introducing the superposition technique and addition theorem. After superposing the two solutions, the Green function can be obtained. Convergence rate using various numbers of terms for Fourier series is also examined. Finally, some concentrated force and screw dislocation problems with circular boundaries, including holes and inclusions, were demonstrated to see the validity of present method. Five disadvantages, (1) calculation of principal value, (2) ill-posed model, (3) boundary-layer effect, (4) linear convergence and (5) mesh generation, can be avoided by using the present approach in comparison with the conventional BEM.

Keyword: addition theorem, superposition technique, screw dislocation, Green function

Applications of addition theorem and superposition technique to problems with circular boundaries subject to concentrated force and screw dislocation

Contents

Table captions

Figure captions

Notations

μ	Shear modulus
φ	Fundamental solution of the screw dislocation
∇^2	Laplacian operator
$\delta(\mathrm{x}-\mathrm{s})$	Dirac-delta function
ξ	Location of the source point
ρ_i	Radius of the ith circle
a_i	radius of the ith circle
a_n , b_n	Fourier coefficients of boundary density $u(s)$
B	Boundary
b	Burger's vector
$C.P.V.$	Cauchy principal value
D	Domain of interest
D^c	Complementary domain
$F(z)$	Complex function
$G(x,\xi)$	Green's function
$H.P.V.$	Hadamard principle value
N	Number of the circles
n	Normal vector
n_s	Normal vector at the source point s
n_x	Normal vector at the field point x
$L(\mathrm{s},\mathrm{x})$	Kernel function in the hypersingular formulation
$L^I(\mathrm{s},\mathrm{x})$	Degenerate kernel function of $L(\mathrm{s},\mathrm{x})$ for $R>\rho$
$L^E(\mathrm{s},\mathrm{x})$	Degenerate kernel function of $L(\mathrm{s},\mathrm{x})$ for $\rho>R$
M	Number of the terms of the Fourier series
$M(\mathrm{s},\mathrm{x})$	Kernel function in the hypersingular formulation
$M^I(\mathrm{s},\mathrm{x})$	Degenerate kernel function of $M(\mathrm{s},\mathrm{x})$ for $R\geq\rho$
$M^E(\mathrm{s},\mathrm{x})$	Degenerate kernel function of $M(\mathrm{s},\mathrm{x})$ for $\rho>R$
R_i	Distance between the source point and ith center of the circle
$R.P.V.$	Riemann principal value
r	distance between the source point s and the field point x , $r\equiv\lvert x-s\rvert$
$T(\mathrm{s},\mathrm{x})$	Kernel function in the singular formulation
$T^I(\mathrm{s},\mathrm{x})$	Degenerate kernel function of $T(\mathrm{s},\mathrm{x})$ for $R>\rho$

$T^E(\mathrm{s},\mathrm{x})$	Degenerate kernel function of $T(\mathrm{s},\mathrm{x})$ for $\rho > R$
$t(s)$	Normal derivative of $u(s)$ at s, $\dfrac{\partial u(s)}{\partial n_s}$
$t(x)$	Normal derivative of $u(x)$ at x, $\dfrac{\partial u(x)}{\partial n_x}$
t^I	normal derivative of u^I
t^M	normal derivative of u^M
p_n, q_n	Fourier coefficients for the boundary density of $\partial u(s)/\partial n_s$
$U(\mathrm{s},\mathrm{x})$	Kernel function in the singular formulation
$U^I(\mathrm{s},\mathrm{x})$	Degenerate kernel function of $U(\mathrm{s},\mathrm{x})$ for $R \geq \rho$
$U^E(\mathrm{s},\mathrm{x})$	Degenerate kernel function of $U(\mathrm{s},\mathrm{x})$ for $\rho > R$
$u(s)$	Potential function at the source point s
$u(x)$	Potential function at the field point x
u^I	Fourier coefficients of boundary densities for the inclusion
u^M	Fourier coefficients of boundary densities for the matrix
s	Source point
w	Anti-plane displacement
x	Field point
z_x	Position vector for the field point (complex variable)
z_s	Position vector for the source point (complex variable)
$[\mathbf{U}]$	Influence matrix of the kernel function $U(\mathrm{s},\mathrm{x})$
$\{\mathbf{u}\}$	Column vector of Fourier coefficients $\{a_0 \quad a_1 \quad b_1 \quad \cdots \quad a_M \quad b_M\}^T$
$[\mathbf{T}]$	Influence matrix of the kernel function $T(\mathrm{s},\mathrm{x})$
$\{\mathbf{t}\}$	Column vector of Fourier coefficients $\{p_0 \quad p_1 \quad q_1 \quad \cdots \quad p_M \quad q_M\}^T$
$[\boldsymbol{\mu}]$	Diagonal matrix of shear modulus
(R,θ)	Polar coordinate of s
(ρ,ϕ)	Polar coordinate of x
θ	Polar angle measured with respect to the x direction
"I"	Index of inclusion
"M"	Index of matrix

Chapter 1 Introduction

1.1 Motivation of the research and literature review

Many engineering problems can be formulated as mathematical models of the boundary value problems. In order to solve such problems, researchers proposed several numerical methods as shown in the Table 1-1, e.g., boundary element method (BEM), finite element method (FEM), finite difference method (FDM). Figure 1-1 shows growth of number of papers for FEM and BEM. FDM is the simplest way of approximating a differential operator and is extensively used in solving a differential equation. FDM has some difficulties in modeling the boundary condition of complicated curved geometries. In such problems, FDM can't exactly capture the geometry of the problem. In the recent years, FEM has been widely applied to solve many engineering problems. The development of the FEM is often based on the energy principle, e.g., the virtual work principle or the minimum potential. FEM has some disadvantages when modeling infinite regions, moving boundary problems and dealing with domain discretization. Among various numerical methods, BEM is one of the most popular numerical approaches for solving boundary value problems. The method requires only discretization of the boundary thus reducing one-dimension discretization in numerical implementation. BEM is convenient for the general boundaries, no matter what the dimension of the problem is. The most important advantage to FEM is that BEM can deal with the problem with the infinite domain without artificially truncating the domain. Although BEM has been involved as an alternative numerical method for solving engineering problems, five critical issues are of concern.

(1) Treatment of weak, strong and hypersingular singularity

BEM is based on the fundamental solution to solve the partial differential equation. The fundamental solution is a two-point function which is singular as the source and field points coincide. Most researchers have focused on the singular boundary integral equation for problems with ordinary boundaries. When a problem contains the degenerate boundary, fictitious frequency and spurious eigenvalue, the singular boundary integral equation is not sufficient. Thus, the hypersingular boundary integral equation has been proposed. A review article of Chen and Hong [Chen and Hong, 1999] can be consulted for readers. In order to directly face the Cauchy, Riemann and Hadamard principal values, researchers have published a large amount of papers by using the bump contour approach. Guiggiani [Guiggiani, 1995] has derived the free terms for the Laplace and Navier equations by using the differential geometry and bump contour approach in Figure 1-2 (a). Gray and Manne [Gray and Manne, 1993] have employed a limiting process to ensure a finite value from an interior point to boundary by using a symbolic software in Figure 1-2 (b). Waterman [Waterman, 1965] introduced the null-field approach (so-called extended boundary condition method (ECBM) or T-matrix method) to deal with the singularity problem. Achenbach *et al*. [Achenbach, Kechter and Xu, 1988] proposed the off-boundary approach in order to overcome the fictitious frequencies free of singularity. Although the fictitious BEM and the null-field approach can avoid directly calculating the singular and hypersingular integrals, they may result in an ill-posed model which will be elaborated on later.

(2) Ill-posed model

When the null-field approach or fictitious BEM are used to avoid directly calculating the singular and hypersingular integrals, it result in an ill-posed model. The influence matrix is not diagonally dominated and needs preconditioning. A well-posed model can be reconstructed, when the fictitious boundary locates on the real boundary or the null-field point is pushed on the real boundary. However, the singularity appears as the first issue mentioned.

(3) Boundary-layer effect

It is well known that boundary-layer effect appears in the conventional BEM. Kisu and Kawahara [Kisu and Kawahara, 1988] proposed a concept of relative quantity to eliminate the boundary-layer effect. Chen and Hong in Taiwan [Chen and Hong, 1994] as well as Chen et al. in China [Chen, Lu and Schnack, 2001] independently extended the idea of relative quantity to two regularization techniques which the boundary densities are subtracted by constant and linear terms. Sladek et al. [Sladek and Sladek, 1991] used a regularized version of the stress boundary integral equation (σ BEM) to compute the correct values of stresses close to the boundary. Others proposed a regularization of the integrand by using variable transformations. For example, Telles [Telles, 1987] used a cubic transformation such that its Jacobian is a minimum at the point on the boundary close to the collocation point and can smooth the integrand. Similarly, Huang and Cruse [Huang and Cruse, 1993] proposed rational transformations which can regularize the nearly singular integrals. To eliminate the boundary-layer effect, correct calculation for the nearly singular integral is the main concern.

(4) Convergence rate

In the recent years, BEM is very popular for boundary value problems with general geometries since it requires discretiztion on the boundary only. Regarding to constant, linear and quadratic elements, the discretization scheme does not take the special geometry into consideration. It leads to the slow convergence rate. Different boundary shapes have different interpolation functions to approximate the boundary density on the specific geometry. Fourier series for circular boundary, spherical harmonic function for surface of sphere, Legendre and Chebyshev polynomials for the boundary densities on the regular and degenerate straight boundaries and Methieu function for the boundary densities of elliptic boundaries were incorporated into BEM, respectively. Figure 1-3 shows randomly distributed apertures and/or inclusions with square, elliptic and circular shapes, etc. Bird and Steele [Bird, 1992; Bird and Steele, 1991; Bird and Steele, 1992] presented a Fourier series procedure to solve Laplace and biharmonic problems with circular holes by using the similar concept of Trefftz bases of the interior and exterior problems. T-complete functions can be extracted out in the degenerate kernel of fundamental solution [Chen, Wu, Lee and Chen, 2007]. The boundary potential and normal derivative of Laplace problem have been solved in the Caulk and Barone work [Barone and Caulk, 1981, 1982, 1985, 2000; Caulk, 1983, 1983, 1983, 1984] by using the special boundary integral equations in conjunction with the Fourier series. Crouch and Mogilevskaya [Crouch and Mogilevskaya, 2003] solved the elasticity problems with circular boundaries by using the Somigliana's formula and Fourier series. Although the boundary integral equations in conjunction with the Fourier series expansion were used in the previous researchers' work, but no one introduced the degenerate kernel in boundary integral equations. The exponential convergence instead of the algebraic convergence by using the degenerate kernel and Fourier expansion in the BEM has been proved in the Kress book [Kress, 1989]. Also, the collocation approach in the RBF meshless method also results in the exponential convergence and this finding receives attention. This thesis will take the advantage of the higher-order convergence rate to solve the problems with circular boundaries by using the Fourier series and degenerate kernels in the boundary integral equations.

(5) Mesh generation

In Figure 1-4, the numeral methods can be decomposed into two parts. One is the domain type methods, FEM and FDM, which have been widely used to solve the engineering problems. The other is the boundary type methods, BEM, MFS and Trefftz method, which are popular in the recent years. Although BEM is free of the domain disscretization, the boundary mesh is also required since the collocation point is on the real boundary. Thus, we introduced the Fourier series for problems with circular boundaries. By using the generalized coordinate, only collocation is required and mesh is free.

You may wonder is it possible to have an approach free of the five disadvantages of conventional BEM. The answer is yes. In this thesis, we propose a BIE approach to have five gains, singularity free, boundary-layer effect free, exponential convergence, well-posed model, mesh-free generation.

In mathematics, Green's function is an important tool to solve the ordinary and partial differential equations [Kellogg, 1953; Bergman and Schiffer, 1953; Morse and Fechbach, 1953; Courant and Hilbert, 1962; Melnikov, 1977; Roach, 1982]. Analytical Green's function for the concentrated forces have been presented for only a few simple configurations, Boley [Boley, 1956] analytically constructed the Green's function by using the successive approximation. Adewale [Adewale, 2006] proposed an analytical solution for an annular plate subjected to a concentrated load. Later, it was corrected by Chen et al.. Numerical Green's function has received attention by many researchers [Telles, Castor and Guimaraes, 1995; Guimaraes and Telles, 2000;

Ang and Telles, 2004]. Melnikov [Melnikov, 1982, 1995; Melnikov and Melnikov, 2001] utilized the method of modified potentials (MMP) to solve boundary value problems from various areas of computational mechanics. Later, Melnikov [Melnikov and Melnikov, 2006] studied in computing Green's functions and matrices of Green's type for mixed boundary value problems stated on 2-D regions of irregular configuration. For different field problems, dynamic Green's functions for time-harmonic problems [Kitahara, 1985; Denda, Wang and Yong, 2003; Denda, Araki and Yong, 2004], piezoelectricity problems [Wang and Zhong, 2003; Chen and Wu, 2006], and scattering problems in elastodynamics [Willis, 1980a, b; Talbot and Willis, 1983] have been solved by using BEM. In the recent years, the null-field BIEs were employed to solve Laplace, Helmholtz, Biharmonic, BiHelmholtz and Navier problems. In 2008, Chen and Ke [Chen and Ke, 2008] successfully used the null-field integral equation in conjunction with the Fourier series and degenerate kernels to construct the Green's function for the concentrated force by way of Green's third identiry.

Analytical Green's functions for the screw dislocation were derived by using the complex-variable function. Smith [Smith, 1968] solved the screw dislocation problems with circular or elliptic inclusion contained within an infinite body. Also, a uniform applied shear stress at infinity was considered. Dundurs [Dundurs, 1969] also solved such problems with circular hole or inclusion by using the image technique. Sendeckyj [Sendecky, 1970] extended a single inclusion to an arbitrary number of circular inclusions by employing the complex-varialbe function in conjunction with the inverse point method. Honein et al. [Honein et al., 1992] solved the problem of an elastic body containing circular inclusions subject to arbitrary loading by using the Möbius transformation. Sudak [Sudak, 2002] and Jin and Fang [Jin and Fang. 2008] solved the screw dislocation problem interacting with an imperfect interface by using the complex-variable technique. In 2006, Fang and Liu [Fang and Liu, 2006] extended the complex-variable function and Riemann-Schwarz's symmetry principle to solve the problem of the interaction of a screw dislocation with a circular nano-inhomogeneity incorporating interface stress. All the above papers utilized the complex-variable approach. We may propose an alternative formulation by using real-variable function.

For the inclusion problem, subdomain approach in a similar way of taking free body was used by Chen and Wu [Chen and Wu, 2006]. To derive the Green's function for a source singularity, Chen and Ke [Chen and Ke, 2008] directly solved the problems by using the Green's third identity. In stead of using the above approach, this thesis derives the Green function by using the superposition technique and addition theorem. The mathematical equivalence between Ke's and the present approaches is addressed in this thesis. Many addition theorems can be found in the mathematical handbook. Two-point function of fundamental solution is the main ingredient in BIEM. Difference-type $|\underset{\sim}{x}-\underset{\sim}{s}|$ kernel can be expanded in a separable form. The addition theorem and degenerate kernel are very similar if the position vector of $\underset{\sim}{s}$ changes sign. Therefore, degenerate kernel belongs to one kind of addition theorem.

In the Fredholm integral equations, the degenerate kernel (or so-called separate kernel) plays an important role. However, its applications in practical problems seem to have taken a back seat to other methods as mentioned by Golberg [Golberg, 1978]. This method can be seen as one kind of approximation methods, and the kernel function is expressed as finite sums of products by two functions of source and field point, respectively. The concept of generating "optimal" degenerate kernels has been proposed by Sloan et al. [Sloan, Burn and Datyner, 1975]. They also proved it to be equivalent to the iterated Petrov-Galerkin approximation. Later, Kress [Kress, 1989] proved that the integral equations of the second kind in conjunction with degenerate kernels have the convergence rate of exponential order instead of the linear algebraic order. The convergence rate is better than that of conventional BEM. Recently, Chen et al. applied the degenerate kernels in conjunction with null-field integral equations to solve many engineering problems including the Laplace [Chen et al. 2005, 2006, 2006, 2007], Helmholtz [Chen, 2005; Chen, Chen and Chen, 2005; Chen, Chen and Chen, 2005], biharmonic [Chen, Hsiao and Leu, 2006] and biHelmholtz [Lee, Chen and Lee, 2007] problems with holes and/or inclusions. The degenerate kernels are summarized in Table 1-2. Following the success of null-field integral formulation for a typical BVP as shown in Figure 1-5, the second part of the Green's function in the superposition approach can be easily solved. Main gains of their approach have five folds: avoid the improper integrals, well-posed model, boundary-layer effect free, exponential convergence and mesh-free generation. Based on the degenerate kernel, Chen and Wu had a new point of view for finding the image location [Chen and Wu, 2006]. Also, NTOU/MSV group linked the two numerical methods, Trefftz method and method of fundamental solutions for both Laplace and biharmonic problems, by using degenerate kernels [Chen, Wu, Lee and Chen, 2007] not only for the circular domain but also annular case. They found that the bases of T-complete sets are embedded in the degenerate kernel when the fundamental solution is expanded into degenerate form. Therefore, these two methods, Trefftz method and method of fundamental solutions, can be seen as mathematically equivalent. The similar viewpoint was also found by Schaback. However, Schaback claimed that MFS is closely connected to the Trefftz method but they are not mathematically equivalent as the number of d.o.f. becomes infinity. For the finite number of d.o.f.s, they are not equivalent in error analysis. He found that the MFS for the source points on the far-away filed yield a trial space that is a space of harmonic polynomials [Schaback, 2007]. In a word, the degenerate kernel can transform the integral equation to a linear algebraic system, once the closed-form kernel functions is replaced by the degenerate kernels.

In this thesis, we focus on the application of the addition theorem and superposition technique to problems with circular boundaries subject to concentrated forces or screw dislocations. The fundamental solution for the concentrated force has been already expanded into separable form in the polar coordinate by using the addition theorem. But, no one expanded the angle-type fundamental solution of the screw dislocation into the degenerate form to our best knowledge both in mathematics or engineering literature. Thus, we will separate the angle-type fundamental solution into the degenerate form by using the addition theorem. After introducing the superposition technique, the original problem can be decomposed into two parts. One is the fundamental solution and the other is the typical BVP with circular boundaries. The typical BVP of the second part is solved by using the null-field integral equation in conjunction with degenerate kernels and Fourier series following the successes of NTOU/MSV group. When the degenerate kernels and Fourier series are introduced, five advantages can be expected, (1) singularity free, (2) boundary-layer effect free, (3) exponential convergence, (4) well-posed model, (5) mesh-free generation. Regarding to the typical BVP using the null-field integral formulation, the adaptive observer system is proposed to fully employ the property of degenerate kernel. All the boundary integrals are easily obtained through the orthogonal property between the degenerate kernel and Fourier series. The Fourier coefficients can be obtained by using the linear algebraic equation after collocating the null-field point exactly on the real boundary and matching the boundary condition. In addition, the convergence test with various number of terms for Fourier series is studied. Problems of the concentrated force and screw dislocation are both demonstrated to see the validity of present method.

1.2 Organization of the thesis

The frame of the thesis is shown in Figure 1-6. In this thesis, the addition theorem and the superposition technique are the two key tools to derive the Green's function for the concentrated force and screw dislocation problems with circular holes and/or inclusions. The organization of this thesis is summarized below:

In chapter 2, we employ the present method to construct the Green's function of source singularity for the Laplace problem. After using the superposition technique, the Green's function can be decomposed into two parts. One is the fundamental solution and the other is a typical BVP with circular boundaries. In order to fully employ the geometry of circular boundary, the Fourier series for boundary densities, degenerate kernels for fundamental solutions and the adaptive observer system are all used in the null-field integral formulation. After collocating points on each circular boundary and satisfying the boundary conditions, the linear algebraic equation is obtained. Thus, the unknown boundary densities can be obtained easily. It is straightforward to obtain the field solution by substituting the unknown coefficients to the integral equation for the domain point. After superimposing the fundamental solution and the typical problem, the Green's function is obtained. Green's functions for eccentric or half-plane problems with a circular hole as well as an aperture and a semi-circular inclusion are found. The results of eccentric case and half-plane problems with a circular aperture or an aperture and a semi-circular inclusion are compared with those by Melnikov and Melnikov [Melnikov and Melnikov, 2001, 2006]. The comparison of the present thesis and Ke's is also made.

In chapter 3, we focus on the applications in deriving the solution of the screw dislocation for the Laplace equation with circular holes and/or inclusions. In this chapter, the angle-type fundamental solution is first expanded into the separable form. To our best knowledge, the degenerate kernel for the angle-type fundamental solution was not found in the literature before. Finally, some illustrative examples, infinite plane with a circular hole subjected to the Dirichlet or Neumann boundary condition and infinite plane with one and two circular inclusions were demonstrated to see the validity of the present method.

In chapter 4, we draw out some conclusions item by item and indicate some topics deserved for further study.

Table 1-1 Bibliographic database search based on the Web of Science [Cheng A. H. D. and Cheng D. T. (2005)]

Number of papers of FEM, FDM, FVM, CM and BEM		
Numerical method	Search phrase in topic field	No. of entries
FEM	‘Finite element’ or ‘finite element’	66,237
FDM	‘Finite difference’ or ‘finite difference’	19,531
BEM	‘Boundary element’ or ‘boundary element’ or ‘boundary integral’	10,126
FVM	‘Finite volume method’ or ‘finite volume method’	1695
CM	‘Collocation method’ or ‘collocation method’	1615

Table 1-2 Degenerate kernels and addition theorems

1-D	
$e^{x-s}=\dfrac{e^{x}}{e^{s}}$	
$\sin(x-s)=\sin x\cos s-\cos x\sin s$	
$\cos(x-s)=\cos x\cos s+\sin x\sin s$	
$U(s,x)=\dfrac{1}{2}\lvert x-s\rvert=\begin{cases}\dfrac{1}{2}x-\dfrac{1}{2}s, & x\ge s\\ \dfrac{1}{2}s-\dfrac{1}{2}x, & s>x\end{cases}$	(source singularity for a rod problem)
2-D	
$U(s,x)=\ln r=\begin{cases}\ln R-\sum_{m=1}^{\infty}\dfrac{1}{m}\left(\dfrac{\rho}{R}\right)^{m}\cos m(\theta-\phi), & R\ge\rho\\ \ln\rho-\sum_{m=1}^{\infty}\dfrac{1}{m}\left(\dfrac{R}{\rho}\right)^{m}\cos m(\theta-\phi), & \rho>R\end{cases}$	(source singularity for the Laplace problem)
$U(s,x)=\varphi=\begin{cases}\theta+\sum_{m=1}^{\infty}\dfrac{1}{m}\left(\dfrac{\rho}{R}\right)^{m}\sin m(\theta-\phi), & R\ge\rho\\ \phi-\pi-\sum_{m=1}^{\infty}\dfrac{1}{m}\left(\dfrac{R}{\rho}\right)^{m}\sin m(\theta-\phi), & \rho>R\end{cases}$	(screw dislocation for the Laplace problem)

$H_0^{(1)}(kr) = J_0(kr) + iY_0(kr)$ $H_0^{(2)}(kr) = J_0(kr) - iY_0(kr)$ $\rightarrow$ $J_0(kr) = \begin{cases} \sum_{m=-\infty}^{\infty} J_m(kR) J_m(k\rho)\cos(m(\theta-\phi)), & R \ge \rho \\ \sum_{m=-\infty}^{\infty} J_m(k\rho) J_m(kR)\cos(m(\theta-\phi)), & \rho > R \end{cases}$ $Y_0(kr) = \begin{cases} \sum_{m=-\infty}^{\infty} Y_m(kR) J_m(k\rho)\cos(m(\theta-\phi)), & R \ge \rho \\ \sum_{m=-\infty}^{\infty} Y_m(k\rho) J_m(kR)\cos(m(\theta-\phi)), & \rho > R \end{cases}$	(source singularity for the Helmholtz problem)
$I_0(kr) = \begin{cases} \sum_{m=-\infty}^{\infty} (-1)^m I_m(kR) I_m(k\rho)\cos(m(\theta-\phi)), & R \ge \rho \\ \sum_{m=-\infty}^{\infty} (-1)^m I_m(k\rho) I_m(kR)\cos(m(\theta-\phi)), & \rho > R \end{cases}$	(source singularity for the modified Helmholtz problem)
$K_0(kr) = \begin{cases} \sum_{m=-\infty}^{\infty} K_m(kR) I_m(k\rho)\cos(m(\theta-\phi)), & R \ge \rho \\ \sum_{m=-\infty}^{\infty} K_m(k\rho) I_m(kR)\cos(m(\theta-\phi)), & \rho > R \end{cases}$	(source singularity for the modified Helmholtz problem)

$$U(s,x)=r^2\ln r=\begin{cases}U^I(s,x)=\rho^2(1+\ln R)+R^2\ln R-[R\rho(1+2\ln R)+\frac{1}{2}\frac{\rho^3}{R}]\cos(\theta-\phi)-\sum_{m=2}^{\infty}[\frac{1}{m(m+1)}\frac{\rho^{m+2}}{R^m}-\frac{1}{m(m-1)}\frac{\rho^m}{R^{m-2}}]\cos[m(\theta-\phi)], & R\geq\rho\\ U^E(s,x)=R^2(1+\ln\rho)+\rho^2\ln\rho-[\rho R(1+2\ln\rho)+\frac{1}{2}\frac{R^3}{\rho}]\cos(\theta-\phi)-\sum_{m=2}^{\infty}[\frac{1}{m(m+1)}\frac{R^{m+2}}{\rho^m}-\frac{1}{m(m-1)}\frac{R^m}{\rho^{m-2}}]\cos[m(\theta-\phi)], & \rho>R\end{cases}$$ (source singularity for the biHarmonic problem)
$$U(s,x)=\frac{1}{8k^2D}\left[Y_0(kr)-iJ_0(kr)+\frac{2}{\pi}K_0(kr)\right]=\begin{cases}\frac{1}{8k^2D}\sum_{m=0}^{\infty}\varepsilon_m\{J_m(k\rho)[Y_m(kR)-iJ_m(kR)]+\frac{2}{\pi}I_m(k\rho)K_m(kR)\}cos\left[m\left(\theta\text{-}\varphi\right)\right], & R\geq\rho\\ \frac{1}{8k^2D}\sum_{m=0}^{\infty}\varepsilon_m\{J_m(kR)[Y_m(k\rho)-iJ_m(k\rho)]+\frac{2}{\pi}I_m(kR)K_m(k\rho)\}cos\left[m\left(\theta\text{-}\varphi\right)\right], & R<\rho\end{cases}$$ (source singularity for the biHelmholtz problem)
3-D
$$U(s,x)=\frac{1}{r}=\begin{cases}k\sum_{n=0}^{\infty}(2n+1)\sum_{m=0}^{n}\varepsilon_m\frac{(n-m)!}{(n+m)!}\cos\left[m\left(\phi-\bar{\phi}\right)\right]P_n^m(\cos\theta)P_n^m(\cos\bar{\theta})j_n(k\bar{\rho})j_n(k\rho), & \bar{\rho}\geq\rho\\ k\sum_{n=0}^{\infty}(2n+1)\sum_{m=0}^{n}\varepsilon_m\frac{(n-m)!}{(n+m)!}\cos\left[m\left(\phi-\bar{\phi}\right)\right]P_n^m(\cos\theta)P_n^m(\cos\bar{\theta})j_n(k\rho)j_n(k\bar{\rho}), & \rho>\bar{\rho}\end{cases}$$ (source singularity for the Lapalce problem)
$$U(s,x)=-\frac{e^{-ikr}}{r}=\begin{cases}ik\sum_{n=0}^{\infty}(2n+1)\sum_{m=0}^{n}\varepsilon_m\frac{(n-m)!}{(n+m)!}\cos\left[m\left(\phi-\bar{\phi}\right)\right]P_n^m(\cos\theta)P_n^m(\cos\bar{\theta})j_n(k\rho)h_n^{(2)}(k\bar{\rho}), & \bar{\rho}\geq\rho\\ ik\sum_{n=0}^{\infty}(2n+1)\sum_{m=0}^{n}\varepsilon_m\frac{(n-m)!}{(n+m)!}\cos\left[m\left(\phi-\bar{\phi}\right)\right]P_n^m(\cos\theta)P_n^m(\cos\bar{\theta})j_n(k\bar{\rho})h_n^{(2)}(k\rho), & \rho>\bar{\rho}\end{cases}$$ (source singularity for the Helmholtz problem)

Fig. 1-1 The growth of number of papers for FEM and BEM

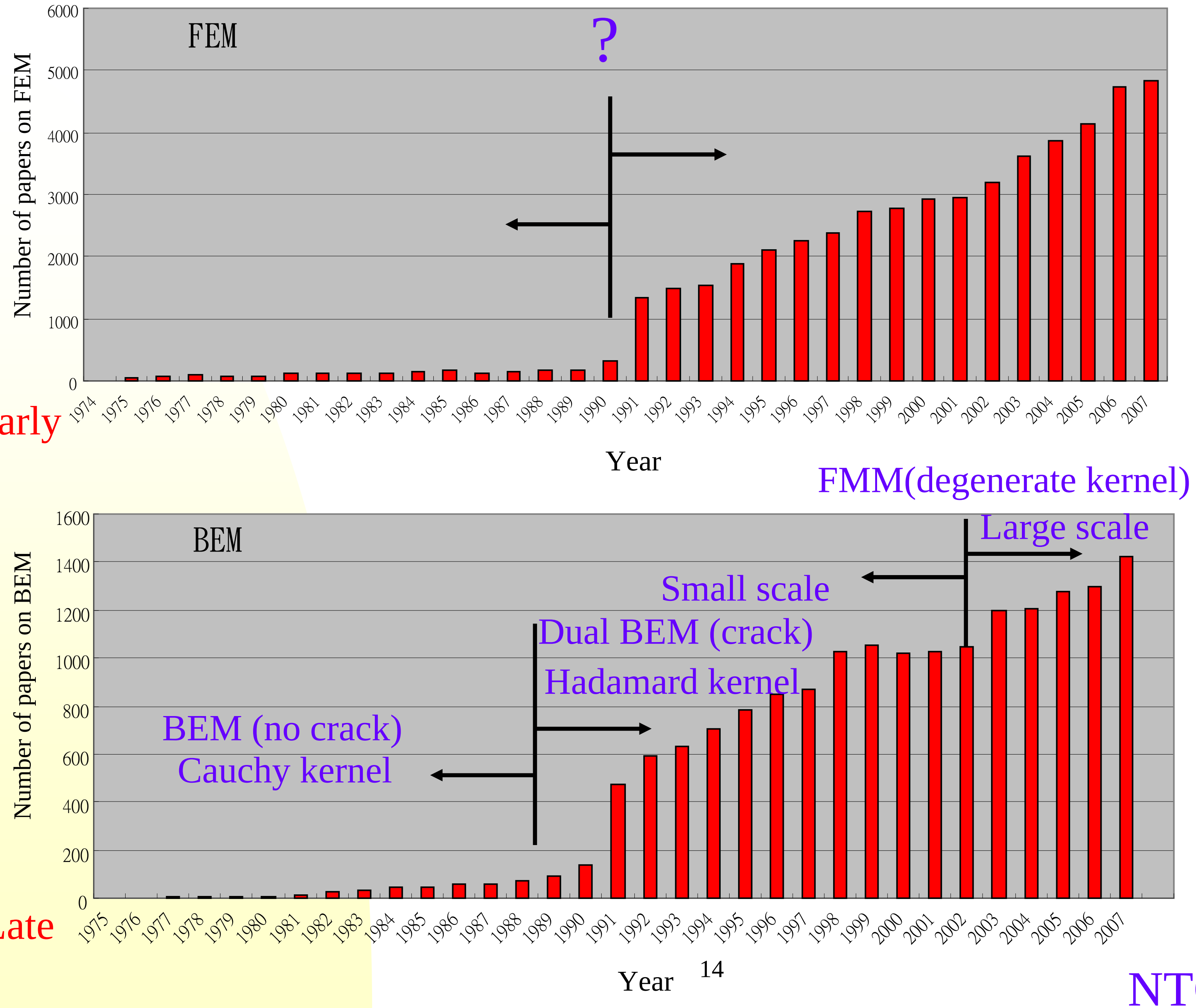

Early

Late

3.5

:

1

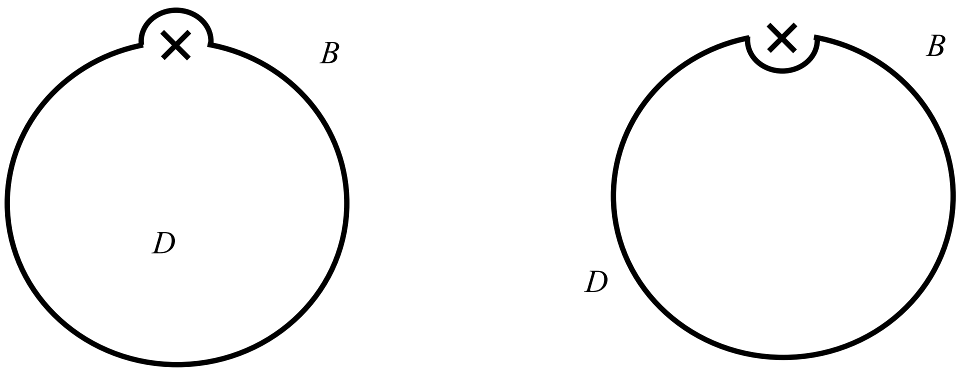

Figure 1-2 (a) Bump contour

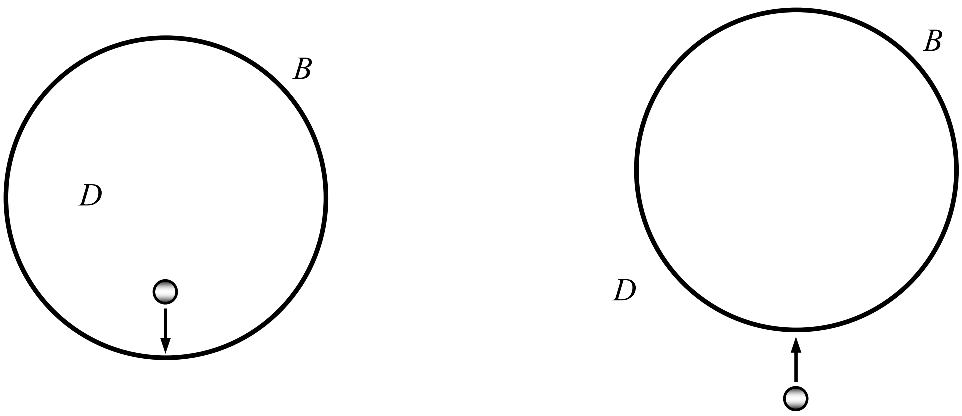

Figure 1-2 (b) Limiting process

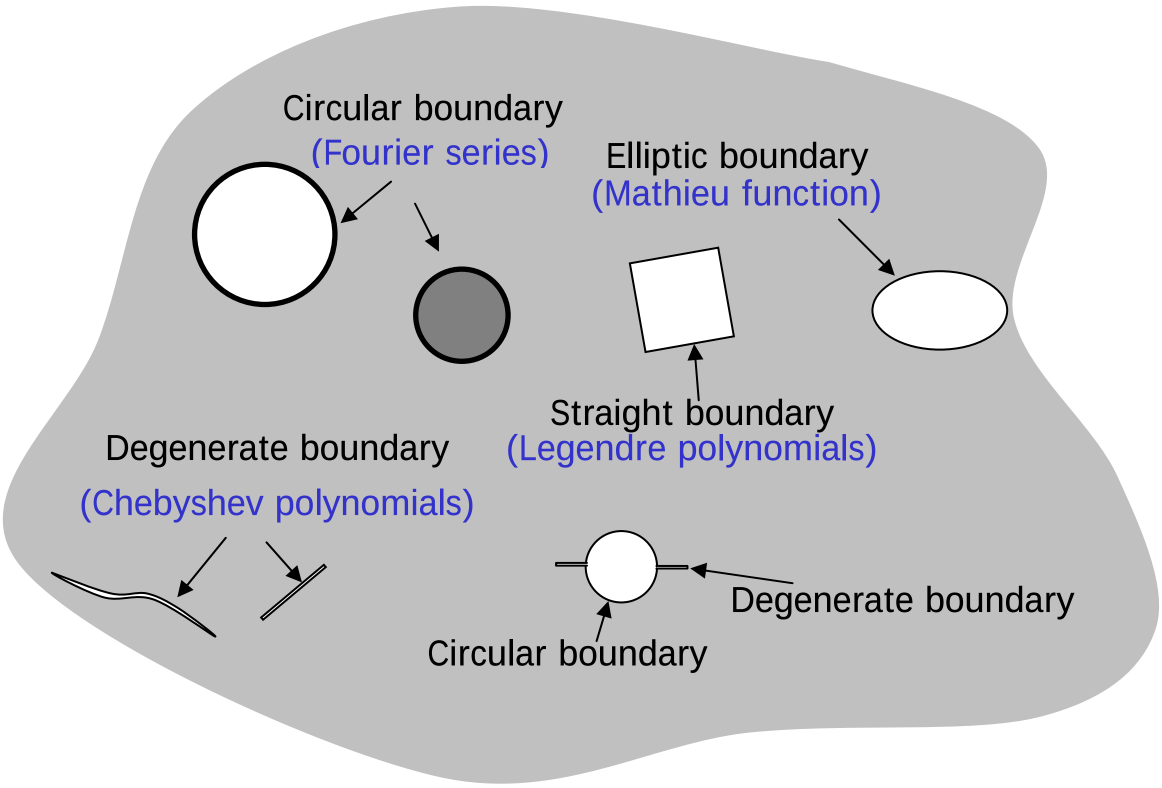

Fig. 1-3 A typical BVP with arbitrary boundaries

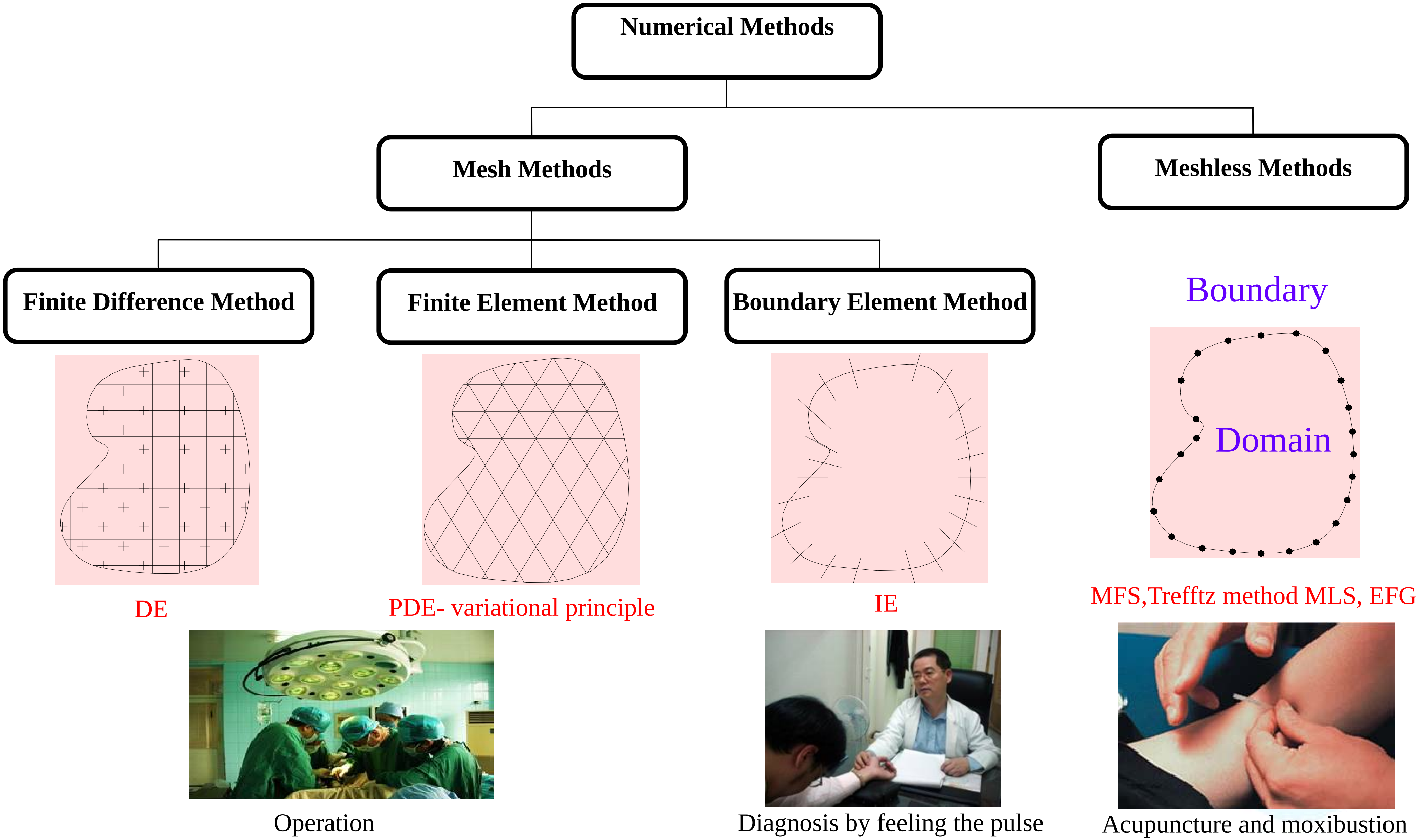

Fig. 1-4 Mesh generation for various methods

Fig. 1-5 Research topics of NTOU / MSV LAB on null-field BIEs (2003-2008)

Research topics of NTOU / MSV LAB on null-field BIEs (2003-2008)

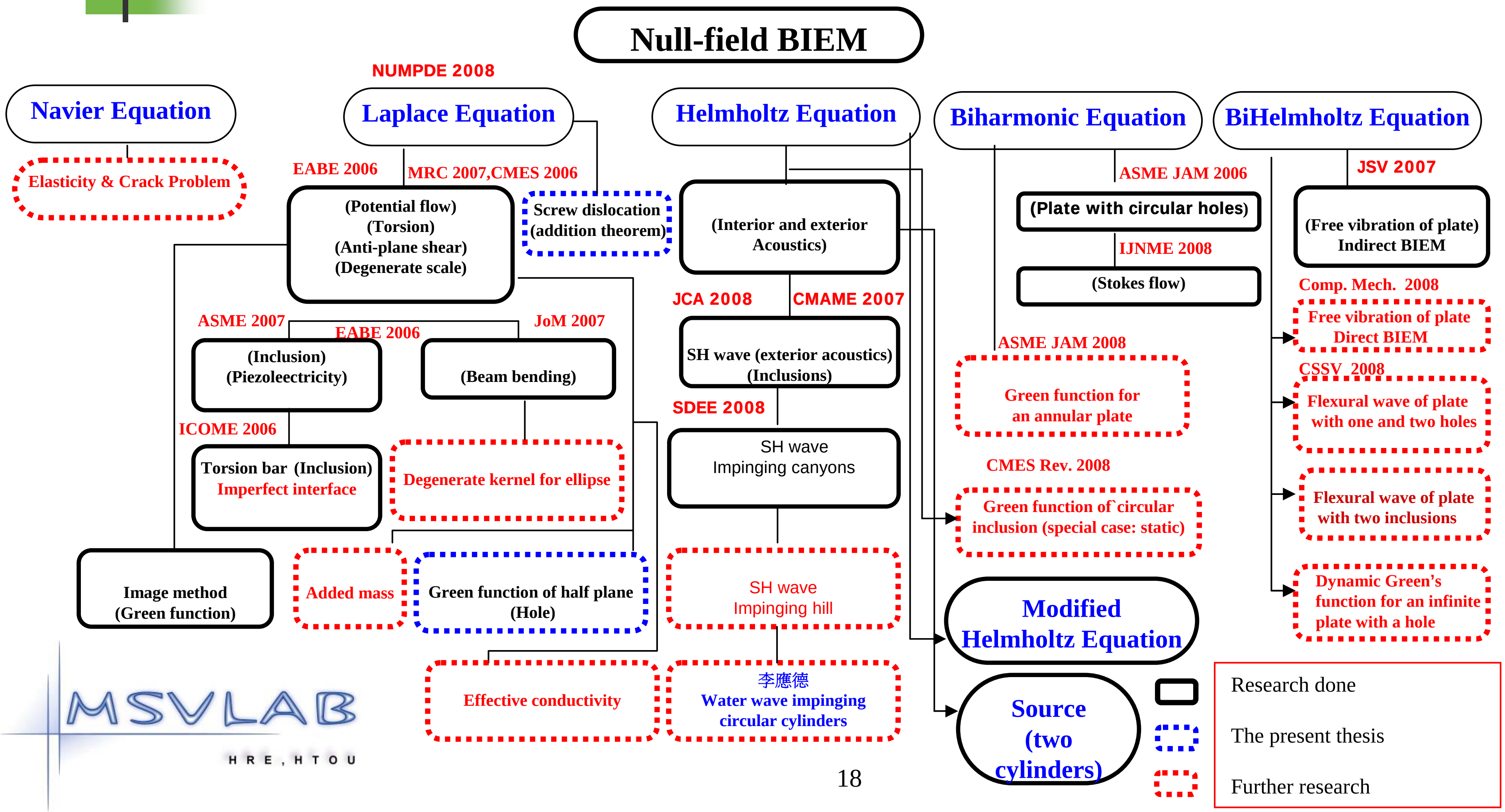

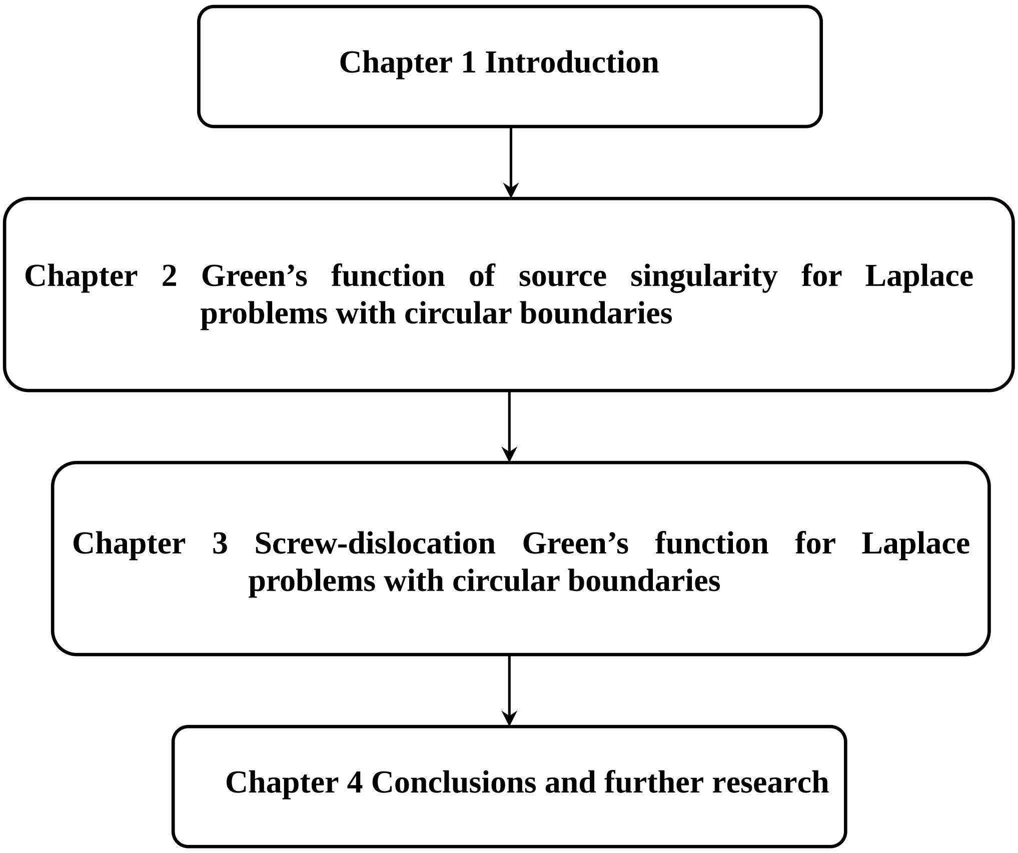

Fig. 1-6 The frame of this thesis

Chapter 2 Derivation of Green's function for Laplace problems with circular boundaries using addition theorem and superposition technique

Summary

Following the success of null-field integral equation to solve BVP of the Laplace equation, we employ the addition theorem and superposition technique to revisit the Green's function of the Laplace problem with circular boundaries. The Green's function is decomposed into two parts. One is the fundamental solution and the other is an infinite plane of circular boundary subject to the specified boundary conditions derived from the addition theorem. After superimposing the two solutions, the governing equation and boundary condition are both satisfied automatically. Several examples are demonstrated to see the validity of the present method.

Keyword: null-field integral equation, addition theorem, superposition, Laplace problem, Green's function.

2.1 Introduction

Mathematicians as well as engineers have studied Green's function in many fields [Jaswon and Symm, 1977; Melnikov, 1977]. Green's functions are useful building blocks for attacking more realistic problems. But only a few of simple regions allow a closed-form Green's function for the Laplace equation. For example, one aperture or circular sector in half-plane, infinite strip, semi-strip or infinite wedge are mapped by elementary analytic functions, making their Green's function expressed in a closed form. A closed-form Green's function for the Laplace equation by using the mapping function becomes impossible for the complicated domain except for very simple cases. Numerical Green's function has received attention from BEM researchers by Telles et al. [Telles et al., 1995; Guimaraes and Telles, 2000; Ang and Telles , 2004]. Melnikov [Melnikov, 1982, 1995; Melnikov and Melnikov, 2001] utilized the method of modified potentials (MMP) to solve boundary value problems from various areas of computational mechanics. Later, Melnikov and Melnikov [Melnikov and Melnikov, 2006] studied in computing Green's functions and matrices of Green's type for mixed boundary value problems (BVP) stated on 2-D regions of irregular configuration. For the image method, Thompson [Thomson, 1848] proposed the concept of reciprocal radii to find the image source to satisfy the homogeneous Dirichlet boundary condition. Chen and Wu [Chen and Wu, 2006] proposed an alternative way to find the location of image through the degenerate kernel. Chen and Ke [Chen and Ke, 2008] have constructed the Green's function of multiply-connected domain problems by using the null-field integral equation derived from the Green's third identity.

In this paper, the Green's function is decomposed into two parts. One is the fundamental solution and the other is an infinite plane of circular boundary subject to the specified boundary conditions, derived from the addition theorem. After superimposing the two solutions, the governing equation and boundary conditions are both satisfied. The main difference between the present paper and Chen and Ke [Chen and Ke, 2008] is that we do not directly employ the Green's third identity to derive the Green's function. Following the success of null-filed integral equation approach [Chen and Shen, 2007] for a typical boundary value problem with Fourier boundary densities, it can be easily extended to derive the Green's function by introducing the superposition technique and addition theorem in the present thesis. The null-field equation approach offers a few attractive features. First, the integrals involved are made simple by avoiding the senses of Cauchy and Hadamard principal values. Secondly, boundary-layer effect is eliminated since we introduce the addition theorem for the interior and exterior regions, respectively. Finally, this method can be seen as one kind of meshless method since no boundary element discretization is required. Finally, several illustrative examples, annular, eccentric and half-plane cases are demonstrated to see the validity of the present method.

2.2 Review of the null-field integral formulation for a typical boundary value problem with Fourier boundary densities

Considering the problem with N randomly distributed circular cavities and/or inclusions bounded in the domain D and enclosed with the boundaries, B_i ($i = 0, 1, 2, \cdots, N$) as shown in Figure 2-1. We define

$$B = \bigcup_{i=0}^{N} B_i \qquad (2\text{-}1)$$

In mathematical physics, many engineering problems can be described by the Laplace equation as shown below:

$$\nabla^2 u(x) = 0, \quad x \in D \tag{2-2}$$

where ∇^2 is the Laplacian operator, $u(x)$ is the potential function and D is the domain of the interest. The integral equation for the domain point can be derived from the third Green's third identity, we have

$$2\pi u(x) = \int_B T^E(\mathrm{s},\mathrm{x}) u(s) dB(\mathrm{s}) - \int_B U^E(\mathrm{s},\mathrm{x}) t(s) dB(\mathrm{s}), \quad \mathrm{x} \in D \cup B \tag{2-3}$$

$$2\pi \frac{\partial u(x)}{\partial n_x} = \int_B M^E(\mathrm{s},\mathrm{x}) u(s) dB(\mathrm{s}) - \int_B L^E(\mathrm{s},\mathrm{x}) t(s) dB(\mathrm{s}), \quad \mathrm{x} \in D \cup B \tag{2-4}$$

where the kernel functions (U^E, T^E, L^E, M^E) should be represented by using the exterior form of degenerate forms (see the next section), s and x are the source and field points, respectively, B is the boundary, n_x denotes the outward normal vector at the field point x and the kernel function $U(\mathrm{s},\mathrm{x}) = \ln r$, ($r \equiv |\mathrm{x}-\mathrm{s}|$), is the fundamental solution which satisfies

$$\nabla^2 U(\mathrm{s},\mathrm{x}) = 2\pi \delta(\mathrm{x}-\mathrm{s}), \tag{2-5}$$

in which $\delta(\mathrm{x}-\mathrm{s})$ denotes the Dirac-delta function. The other kernel functions, $T(\mathrm{s},\mathrm{x})$, $L(\mathrm{s},\mathrm{x})$ and $M(\mathrm{s},\mathrm{x})$, are defined by

$$T(\mathrm{s},\mathrm{x}) \equiv \frac{\partial U(\mathrm{s},\mathrm{x})}{\partial n_{\mathrm{s}}}, \quad L(\mathrm{s},\mathrm{x}) \equiv \frac{\partial U(\mathrm{s},\mathrm{x})}{\partial n_{\mathrm{x}}}, \quad M(\mathrm{s},\mathrm{x}) \equiv \frac{\partial^2 U(\mathrm{s},\mathrm{x})}{\partial n_{\mathrm{s}} \partial n_{\mathrm{x}}}, \tag{2-6}$$

where n_s denotes the outward normal vector at the source point s. By collocating the field point x locates outside the domain, the null-field integral equations of the direct method in Eqs. (2-3) and (2-4) yield

$$0 = \int_B T^I(\mathrm{s},\mathrm{x}) u(\mathrm{s}) dB(\mathrm{s}) - \int_B U^I(\mathrm{s},\mathrm{x}) t(\mathrm{s}) dB(\mathrm{s}), \quad \mathrm{x} \in D^c \cup B, \tag{2-7}$$

$$0 = \int_B M^I(\mathrm{s},\mathrm{x}) u(\mathrm{s}) dB(\mathrm{s}) - \int_B L^I(\mathrm{s},\mathrm{x}) t(\mathrm{s}) dB(\mathrm{s}), \quad \mathrm{x} \in D^c \cup B, \tag{2-8}$$

where the kernels should be represented by using the interior form of degenerate forms (see the next section), D^c is the complementary domain. It is worth noting that the null-field integral equations are not singular since s and x never coincide.

2.2.1 Expansion of kernel function and boundary density

Based on the separable property, the kernel function $U(\mathrm{s},\mathrm{x})$ can be expanded into series form by separating the field point $x(\rho,\phi)$ and source point $s(R,\theta)$ in the polar coordinate:

$$U(s,x)=\begin{cases} U^{I}(R,\theta;\rho,\phi)=\ln R-\sum_{m=1}^{\infty}\frac{1}{m}\left(\frac{\rho}{R}\right)^{m}\cos m(\theta-\phi), & R\geq\rho \\ U^{E}(R,\theta;\rho,\phi)=\ln\rho-\sum_{m=1}^{\infty}\frac{1}{m}\left(\frac{R}{\rho}\right)^{m}\cos m(\theta-\phi), & \rho>R \end{cases} \tag{2-9}$$

where the superscripts I and E denote the interior and exterior cases, respectively. It is noted that the leading term and the numerator in Eq. (2-9) involve the larger argument to ensure the log singularity and the series convergence, respectively. The other kernel functions, $T(\mathrm{s},\mathrm{x})$, $L(\mathrm{s},\mathrm{x})$ and $M(\mathrm{s},\mathrm{x})$ are obtained by their definition. The unknown boundary densities are represented by using the Fourier series as shown below:

$$u(\mathrm{s}_k)=a_0^k+\sum_{n=1}^{\infty}(a_n^k\cos n\theta_k+b_n^k\sin n\theta_k),\quad \mathrm{s}_k\in B_k,\quad k=1,2,\cdots,N, \tag{2-10}$$

$$t(\mathrm{s}_k)=p_0^k+\sum_{n=1}^{\infty}(p_n^k\cos n\theta_k+q_n^k\sin n\theta_k),\quad \mathrm{s}_k\in B_k,\quad k=1,2,\cdots,N, \tag{2-11}$$

where a_n^k, b_n^k, p_n^k and q_n^k $(n=0,1,2,\cdots)$ are the Fourier coefficients, θ_k is the polar angle measured related to the x-direction and N is the number of circular boundaries. In the real computation, the finite number of terms (M) for expansion of kernel and boundary density are adopted.

2.2.2 Adaptive observer system

In order to fully employ the property of degenerate kernels for circular boundaries, an adaptive observer system is addressed. For the integration, the origin of the observer system can be adaptively located on the center of the corresponding boundary contour. The dummy variable in the circular boundary integration is the angle θ instead of radial coordinate R. By using the adaptive system, all the integrations can be easily calculated for multiply-connected problems.

2.2.3 Linear algebraic equation

By moving the null-field point x_i to the ith circular boundary in the limit sense for Eq. (2-7), we have the linear algebraic equation

$$[\mathbf{U}]\{\mathbf{t}\}=[\mathbf{T}]\{\mathbf{u}\} \tag{2-12}$$

where $[\mathbf{U}]$ and $[\mathbf{T}]$ are the influence matrices with a dimension of $(N+1)(2M+1)$ by $(N+1)(2M+1)$, $\{\mathbf{u}\}$ and $\{\mathbf{t}\}$ denote the column vectors of Fourier coefficients with a dimension of $(N+1)(2M+1)$ by 1 in which $[\mathbf{U}]$, $[\mathbf{T}]$, $\{\mathbf{u}\}$ and $\{\mathbf{t}\}$ are defined as shown below:

$$[\mathbf{U}]=\begin{bmatrix} \mathbf{U}_{00} & \mathbf{U}_{01} & \cdots & \mathbf{U}_{0N} \\ \mathbf{U}_{10} & \mathbf{U}_{11} & \cdots & \mathbf{U}_{1N} \\ \vdots & \vdots & \ddots & \vdots \\ \mathbf{U}_{N0} & \mathbf{U}_{N1} & \cdots & \mathbf{U}_{NN} \end{bmatrix},\quad [\mathbf{T}]=\begin{bmatrix} \mathbf{T}_{00} & \mathbf{T}_{01} & \cdots & \mathbf{T}_{0N} \\ \mathbf{T}_{10} & \mathbf{T}_{11} & \cdots & \mathbf{T}_{1N} \\ \vdots & \vdots & \ddots & \vdots \\ \mathbf{T}_{N0} & \mathbf{T}_{N1} & \cdots & \mathbf{T}_{NN} \end{bmatrix}, \tag{2-13}$$

$$\{\mathbf{u}\}=\begin{Bmatrix} \mathbf{u}_0 \\ \mathbf{u}_1 \\ \mathbf{u}_2 \\ \vdots \\ \mathbf{u}_N \end{Bmatrix},\quad \{\mathbf{t}\}=\begin{Bmatrix} \mathbf{t}_0 \\ \mathbf{t}_1 \\ \mathbf{t}_2 \\ \vdots \\ \mathbf{t}_N \end{Bmatrix}, \tag{2-14}$$

where the vectors $\{\mathbf{u}_j\}$ and $\{\mathbf{t}_j\}$ are in the forms of $\{a_0^j \quad a_1^j \quad b_1^j \quad \cdots \quad a_M^j \quad b_M^j\}^T$ and $\{p_0^j \quad p_1^j \quad q_1^j \quad \cdots \quad p_M^j \quad q_M^j\}^T$, respectively; the first subscript “ i ” ($i=0,1,2,\cdots,N$) in $[\mathbf{U}_{ij}]$ and $[\mathbf{T}_{ij}]$ denotes the index of the ith circle where the collocation point is located and the second subscript “ j ” ($j=0,1,2,\cdots,N$) denotes the index of the jth circle where boundary data $\{\mathbf{u}_j\}$ or $\{\mathbf{t}_j\}$ are specified, N is the number of circular apertures in the domain and M indicates the truncated number of terms in Fourier series. The coefficient matrix of the linear algebraic system is partitioned into blocks, and each off-diagonal block corresponds to the influence matrices between two different circular cavities. The diagonal blocks are the influence matrices due to itself in each individual hole. After uniformly collocating the point along the jth circular boundary, the submatrix can be written as

$$[\mathbf{U}_{ij}]=\begin{bmatrix} U_{ij}^{0c}(\phi_1) & U_{ij}^{1c}(\phi_1) & U_{ij}^{1s}(\phi_1) & \cdots & U_{ij}^{Mc}(\phi_1) & U_{ij}^{Ms}(\phi_1) \\ U_{ij}^{0c}(\phi_2) & U_{ij}^{1c}(\phi_2) & U_{ij}^{1s}(\phi_2) & \cdots & U_{ij}^{Mc}(\phi_2) & U_{ij}^{Ms}(\phi_2) \\ U_{ij}^{0c}(\phi_3) & U_{ij}^{1c}(\phi_3) & U_{ij}^{1s}(\phi_3) & \cdots & U_{ij}^{Mc}(\phi_3) & U_{ij}^{Ms}(\phi_3) \\ \vdots & \vdots & \vdots & \ddots & \vdots & \vdots \\ U_{ij}^{0c}(\phi_{2M}) & U_{ij}^{1c}(\phi_{2M}) & U_{ij}^{1s}(\phi_{2M}) & \cdots & U_{ij}^{Mc}(\phi_{2M}) & U_{ij}^{Ms}(\phi_{2M}) \\ U_{ij}^{0c}(\phi_{2M+1}) & U_{ij}^{1c}(\phi_{2M+1}) & U_{ij}^{1s}(\phi_{2M+1}) & \cdots & U_{ij}^{Mc}(\phi_{2M+1}) & U_{ij}^{Ms}(\phi_{2M+1}) \end{bmatrix} \tag{2-15}$$

$$
[\mathbf{T}_{ij}] = \begin{bmatrix}
T_{ij}^{0c}(\phi_1) & T_{ij}^{1c}(\phi_1) & T_{ij}^{1s}(\phi_1) & \cdots & T_{ij}^{Mc}(\phi_1) & T_{ij}^{Ms}(\phi_1) \\
T_{ij}^{0c}(\phi_2) & T_{ij}^{1c}(\phi_2) & T_{ij}^{1s}(\phi_2) & \cdots & T_{ij}^{Mc}(\phi_2) & T_{ij}^{Ms}(\phi_2) \\
T_{ij}^{0c}(\phi_3) & T_{ij}^{1c}(\phi_3) & T_{ij}^{1s}(\phi_3) & \cdots & T_{ij}^{Mc}(\phi_3) & T_{ij}^{Ms}(\phi_3) \\
\vdots & \vdots & \vdots & \ddots & \vdots & \vdots \\
T_{ij}^{0c}(\phi_{2M}) & T_{ij}^{1c}(\phi_{2M}) & T_{ij}^{1s}(\phi_{2M}) & \cdots & T_{ij}^{Mc}(\phi_{2M}) & T_{ij}^{Ms}(\phi_{2M}) \\
T_{ij}^{0c}(\phi_{2M+1}) & T_{ij}^{1c}(\phi_{2M+1}) & T_{ij}^{1s}(\phi_{2M+1}) & \cdots & T_{ij}^{Mc}(\phi_{2M+1}) & T_{ij}^{Ms}(\phi_{2M+1})
\end{bmatrix} \quad (2\text{-}16)
$$

where ϕ_i, $i = 1, 2, \cdots, 2M+1$, are the angles of collocation along the circular boundary. Although both the matrices in Eqs. (2-15) and (2-16) are not sparse, it is found that the higher order harmonic is considered, the lower influence coefficient in numerical experiments is obtained. It is noted that the superscript "$0c$" in Eqs. (2-15) and (2-16) indicates the first term of Fourier series. The elements of $[\mathbf{U}_{ij}]$ and $[\mathbf{T}_{ij}]$ are defined respectively as

$$
U_{ij}^{nc}(\phi_m) = \int_{B_j} U(\mathrm{s}_j, \mathrm{x}_m) \cos(n\theta_j)\, R_j d\theta_j, \quad n = 0, 1, 2, \cdots, M, \quad m = 1, 2, \cdots, 2M+1 \quad (2\text{-}17)
$$

$$
U_{ij}^{ns}(\phi_m) = \int_{B_j} U(\mathrm{s}_j, \mathrm{x}_m) \sin(n\theta_j)\, R_j d\theta_j, \quad n = 1, 2, \cdots, M, \quad m = 1, 2, \cdots, 2M+1 \quad (2\text{-}18)
$$

$$
T_{ij}^{nc}(\phi_m) = \int_{B_j} T(\mathrm{s}_j, \mathrm{x}_m) \cos(n\theta_j)\, R_j d\theta_j, \quad n = 0, 1, 2, \cdots, M, \quad m = 1, 2, \cdots, 2M+1 \quad (2\text{-}19)
$$

$$
T_{ij}^{ns}(\phi_m) = \int_{B_j} T(\mathrm{s}_j, \mathrm{x}_m) \sin(n\theta_j)\, R_j d\theta_j, \quad n = 1, 2, \cdots, M, \quad m = 1, 2, \cdots, 2M+1 \quad (2\text{-}20)
$$

where $\mathrm{s}_j = (R_j, \theta_j)$, and ϕ_m is the polar angle of the collocation point x_m. The influence coefficient of $U_{ij}^{nc}(\phi_m)$ in Eq. (2-17) denotes the response at x_m due to $\cos n\theta$ distribution. The direction of contour integration should be taken care, *i.e.*, counterclockwise and clockwise directions are for the interior and exterior problems, respectively. By rearranging the known and unknown sets, the Fourier coefficients can be obtained easily. After obtaining unknown boundary densities, the field solution can be obtained by using Eq. (2-3).

2.3. Present approach for constructing the Green's function

Considering the problem with N randomly distributed circular cavities and/or inclusions bounded in the domain D and enclosed with the boundaries, B_i ($i = 0, 1, 2, \cdots, N$) as shown in Figure 2-2 (a), we define

$$B = \bigcup_{i=0}^{N} B_i \tag{2-21}$$

In mathematical physics, Green's function problems subjected to the boundary conditions and concentrated source satisfies

$$\nabla^2 G(x, \xi) = \delta(x - \xi), \quad x \in D \tag{2-22}$$

where $G(x, \xi)$ is the Green's function and can be seen as the potential, ξ denotes the location of the concentrated force and ∇^2 indicates the Laplacian operator. The boundary conditions of the problem are shown in the Figure 2-2 (a). Instead of using the Green's third identity in [Chen and Ke, 2008], the problem is decomposed into two parts. One is the fundamental solution and the other is an infinite plane of circular boundary subject to the specified boundary conditions, which are shown in Figures 2-2 (b) and (c), respectively. For boundary value problems with circular holes, it is usually convenient to take the origin of coordinate on the center of hole. This implies that it is likely to be convient to shift the origin during the solution procedure. Such shifts can be accomplished with the aid of addition theorems or so-called degenerate kernels which exist for the Laplace equation in the polar coordinate system. For simplicity, we use the Dirichlet boundary condition ($G(\theta) = 0$) to demonstrate our formulation. The fundamental solution is governed by:

$$\nabla^2 G^1(s, x) = \delta(x - s), \tag{2-23}$$

where $G^1(s, x)$ is the fundamental solution for the Laplace problem and the superscript 1 denotes the first-part solution. Based on the addition theorem, the fundamental solution can be separated into the series form in Eq. (2-9). To fully use the objectivity of the frame indifference, the origin of the observer system can be adaptively located on each center of the corresponding cycle. The boundary condition along the ith circular boundary is expressed as

$$G_i^1(\theta)=\begin{cases}\dfrac{\ln R_i}{2\pi}-\displaystyle\sum_{m=1}^{\infty}\frac{1}{2\pi m}\left(\frac{a_i}{R_i}\right)^m\cos m(\theta_i-\theta), & R_i\geq a_i\\[2ex]\dfrac{\ln a_i}{2\pi}-\displaystyle\sum_{m=1}^{\infty}\frac{1}{2\pi m}\left(\frac{R_i}{a_i}\right)^m\cos m(\theta_i-\theta), & a_i>R_i\end{cases},\quad x\in B_i \tag{2-24}$$

where the superscript 1 of $G(\theta)$ denotes the first-part B.C. on B_i boundary due to the fundamental solution, R_i and θ_i are the distance and the angle between the source point and the ith center of the corresponding circle, respectively, a_i denotes the radius of the ith circle and B_i is the ith circular boundary. In order to satisfy the boundary condition, the second part is a typical problem subject to the specified boundary condition ($G_i^2(x)=-G_i^1(x)$) which can be expressed in terms of Fourier series after using the addition theorem. The governing equation is shown below:

$$\nabla^2 G^2(s,x)=0,\ \ x\in D \tag{2-25}$$

where the superscript 2 of $G(s,x)$ denotes the second-part solution. This part can be seen as a typical BVP with circular boundaries and can be easily solved by using the null-field formulation as shown in Figure 2-2 (c). After superimposing the two solutions, the boundary condition automatically satisfies the Dirichlet boundary condition. Thus, the boundary condition in the second part is shown below:

$$G_i^2(\theta)=-G_i^1(\theta)=\begin{cases}-\dfrac{\ln R_i}{2\pi}+\displaystyle\sum_{m=1}^{\infty}\frac{1}{2\pi m}\left(\frac{a_i}{R_i}\right)^m\cos m(\theta_i-\theta), & R_i\geq a_i\\[2ex]-\dfrac{\ln a_i}{2\pi}+\displaystyle\sum_{m=1}^{\infty}\frac{1}{2\pi m}\left(\frac{R_i}{a_i}\right)^m\cos m(\theta_i-\theta), & a_i>R_i\end{cases},x\in B_i \tag{2-26}$$

where the superscript 2 of $G(\theta)$ denotes the second-part B.C.. By using the present approach, the problem can be solved in two stages. One is fundamental solution (Figure 2-2 (b)) and the other is a typical problem (Figure 2-2 (c)). After superimposing the two solutions, the Green's function can be obtained easily. The equivalence between the Green's third identity used in Ke's thesis and the superposition technique for the Green's function in the present chapter are shown in the Appendix 1.

2.4. Numerical examples

Case 1: An annular case (analytical solution)

Figure 2-3(a) depicts the Green's function of the annular ring. The boundary conditions along the inner and outer circles are the Dirichlet types. The source point is located at $\xi = (7.5, 0)$. The two radii of inner and outer circles are $a = 4.0$ and $b = 10.0$. The center of the inner and outer circles is $(0, 0)$. The analytical solution is obtained as

$$G(x)=\begin{cases} G^I(x)=\frac{1}{2\pi}\ln R-\frac{1}{2\pi}\sum_{m=1}^{\infty}\frac{1}{m}(\frac{\rho}{R})^m\cos m(\theta_\xi-\phi)+ \\ \quad \frac{1}{4\pi}\sum_{m=1}^{\infty}\frac{1}{m}(\frac{a^2}{\rho R})^m\cos m(\theta-\phi)-a\ln\rho a_0+ \\ \quad \frac{1}{2}\sum_{m=1}^{\infty}\frac{1}{m}\frac{a^{m+1}}{\rho^m}(a_m\cos m\phi+b_m\sin m\phi)-\frac{1}{2\pi}\ln b+ & , \quad R\ge\rho\ge a \\ \quad \frac{1}{4\pi}\sum_{m=1}^{\infty}\frac{1}{m}(\frac{\rho R}{b^2})^m\cos m(\theta-\phi)-b\ln bp_0+ \\ \quad \frac{1}{2}\sum_{m=1}^{\infty}\frac{1}{m}\frac{\rho^m}{b^{m-1}}(p_m\cos m\theta+q_m\sin m\theta) \\ G^E(x)=\frac{1}{2\pi}\ln\rho-\frac{1}{2\pi}\sum_{m=1}^{\infty}\frac{1}{m}(\frac{R}{\rho})^m\cos m(\theta_\xi-\phi)+ \\ \quad \frac{1}{4\pi}\sum_{m=1}^{\infty}\frac{1}{m}(\frac{a^2}{\rho R})^m\cos m(\theta_\xi-\phi)-a\ln\rho a_0+ \\ \quad \frac{1}{2}\sum_{m=1}^{\infty}\frac{1}{m}\frac{a^{m+1}}{\rho^m}(a_m\cos m\phi+b_m\sin m\phi)-\frac{1}{2\pi}\ln b+ & , \quad R<\rho<b \\ \quad \frac{1}{4\pi}\sum_{m=1}^{\infty}\frac{1}{m}(\frac{\rho R}{b^2})^m\cos m(\theta-\phi)-b\ln bp_0+ \\ \quad \frac{1}{2}\sum_{m=1}^{\infty}\frac{1}{m}\frac{\rho^m}{b^{m-1}}(p_m\cos m\theta+q_m\sin m\theta) \end{cases} \tag{2-27}$$

where the R denotes the distance between the source point and the origin, θ is the polar angle and the Fourier coefficients are shown below:

$$\begin{Bmatrix} a_0 \\ a_m \\ b_m \end{Bmatrix} = \begin{Bmatrix} \dfrac{\ln R - \ln b}{2\pi a(\ln a - \ln b)} \\ -\dfrac{a^{m-1}R^{-m}(a^{2m}+b^{2m}-2R^{2m})}{2\pi(a^{2m}-b^{2m})}\cos m\theta \\ -\dfrac{a^{m-1}R^{-m}(a^{2m}+b^{2m}-2R^{2m})}{2\pi(a^{2m}-b^{2m})}\sin m\theta \end{Bmatrix}, \qquad m=1,2,3\ldots$$

$$\begin{Bmatrix} p_0 \\ p_m \\ q_m \end{Bmatrix} = \begin{Bmatrix} \dfrac{\ln b - \ln R}{2\pi b(\ln a - \ln b)} \\ \dfrac{b^{-m-1}R^{-m}(-2a^{2m}b^{2m}+(a^{2m}+b^{2m})R^{2m})}{2\pi(-a^{2m}+b^{2m})}\cos m\theta \\ \dfrac{b^{-m-1}R^{-m}(-2a^{2m}b^{2m}+(a^{2m}+b^{2m})R^{2m})}{2\pi(-a^{2m}+b^{2m})}\sin m\theta \end{Bmatrix}, \qquad m=1,2,3\ldots \tag{2-28}$$

Figures 2-3(b) and 2-3(c) show the potential distribution by using the BIE approach and the present method, respectively. Good agreement is made.

Case 2: An infinite plane with an aperture (analytical solution)

Figure 2-4(a) depicts the Green's function for an infinite plane with an aperture with the Neumann boundary condition. The source point is located at $\xi = (1.25, 0)$. The center and radius of the aperture are $(0,0)$ and $a = 1.0$, respectively. By using the present formulation, the analytical solution is shown below:

$$G(x) = \begin{cases} G^I(x) = \dfrac{1}{2\pi}\ln R - \dfrac{1}{2\pi}\sum_{m=1}^{\infty}\dfrac{1}{m}(\dfrac{\rho}{R})^m \cos m(\theta-\phi) - \\ \qquad \dfrac{1}{2\pi}\sum_{m=1}^{\infty}\dfrac{1}{m}(\dfrac{a^2}{\rho R})^m \cos m(\theta-\phi), & R \ge \rho \ge a \\ G^E(x) = \dfrac{1}{2\pi}\ln \rho - \dfrac{1}{2\pi}\sum_{m=1}^{\infty}\dfrac{1}{m}(\dfrac{R}{\rho})^m \cos m(\theta-\phi) - \\ \qquad \dfrac{1}{2\pi}\sum_{m=1}^{\infty}\dfrac{1}{m}(\dfrac{a^2}{\rho R})^m \cos m(\theta-\phi), & R < \rho < \infty \end{cases} . \tag{2-29}$$

Figures 2-4(b) and 2-4(c) show the potential distribution by using the image method and the present method, respectively. Good agreement is made. The stress distribution is shown in Figures 2-4(d) and 2-4(e). After comparing with the two figures, we obtain the stress concentration factor of 2. When the location of the source point moving to far away, the problem can be seen as a remote shear problem with a circular hole where concentration factor is also 2 [Wu, 2006]. The local maximums occur at the angles of $\dfrac{\pi}{2}$ and $\dfrac{3\pi}{2}$.

Case 3: An eccentric ring (semi-analytical solution)

Figure 2-5(a) depicts the Green's function of the eccentric ring with the Dirichlet boundary condition. The source point is located at $\xi = (0, 0.75)$. The two radii of inner and outer circles are $a = 0.4$ and $b = 1.0$. The two centers of the inner and outer circles are (-0.4, 0) and (0,0), respectively. Figures 2-5(b) and 2-5(c) show the potential distribution by using Melnikov's approach [Melnikov and Melnikov, 2001] and the present method, respectively. We can also obtain consistent data by using our method as well as the Green's function $G(x,\xi)$ by MMP method.

Case 4: A half plane with an aperture (semi-analytical solution)

Figure 2-6(a) depicts the Green's function for the half plane with a hole with the Dirichlet boundary condition. The source point is located at $\xi = (2,1)$. The center and radius of the aperture are $(0,3)$ and $a = 1.0$. Figures 2-6(b) and 2-6(c) show the potential distribution by using the Melnikov's approach and the present method, respectively. Good agreement is made.

Case 5: A half-plane problem with a circular boundary subject to the Robin boundary condition (semi-analytical solution)

A half-plane problem with an aperture is considered. The governing equation and boundary condition are shown in Figure 2-7(a). The center and radius of the aperture are $(2,2)$ and $a = 1.0,$ respectively. The concentrated source is located at $(0,3.5)$. The Robin boundary condition $\frac{\partial G(x,\xi)}{\partial n_x} = -2G(x,\xi)$ is imposed on the aperture. Figures 2-7(b) and 2-7(c) show the potential distribution by using the Melnikov's approach and the present method, respectively. Good agreement is obtained.

Case 6: An infinite-plane problem with a circular inclusion (analytical solution)

An infinite-plane problem with an circular inclusion is considered. The governing equation and boundary condition are shown in Figure 2-8(a). The center and radius of the inclusion are $(0,0)$ and $a = 1.0,$ respectively. The concentrated source is located at $(1.1,0)$. Figure 2-8(b) shows the stress distribution along the interface. After comparing the present approach with the Wang and Sudak [Wang and Sudak, 2007], good agreement is obtained. After using the Parseval's theorem to test the convergence rate, Figures 2-8(c) and 2-8(d) are obtained.

2.5. Conclusions

For the Green's function with circular boundaries, we have proposed an indirect approach to construct the Green's function by using the addition theorem and superposition technique. Several examples, including two analytical solutions (*an annular case and an infinite plane with an aperture)* and three semi-analytical solutions (*an eccentric ring, a half plane with an aperture and a half-plane problem with a circular boundary subject to the Robin boundary condition*) were demonstrated to check the validity of the present formulation. The present method has more physical sense (taking free body) to solve the Green's function for the Laplace problems with circular boundaries. Our advantages are five folds: (1) mesh-free generation (2) well-posed model (3) principal-value free (4) elimination of boundary-layer effect (5) exponential convergence.

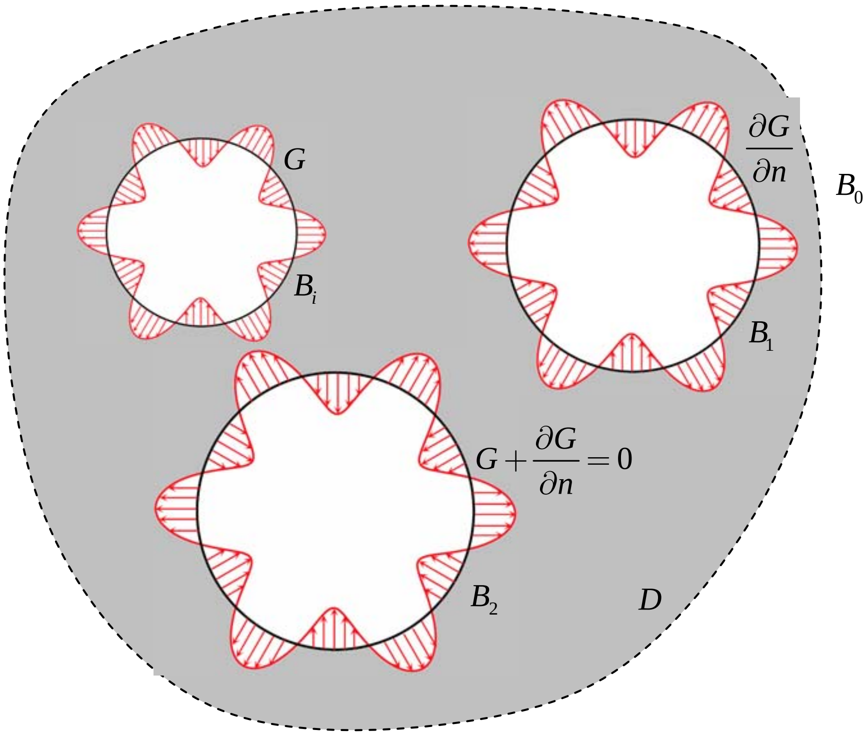

Figure 2-1 A typical boundary value problem with Fourier boundary densities of Dirichlet, Neumann and Robin boundary conditions

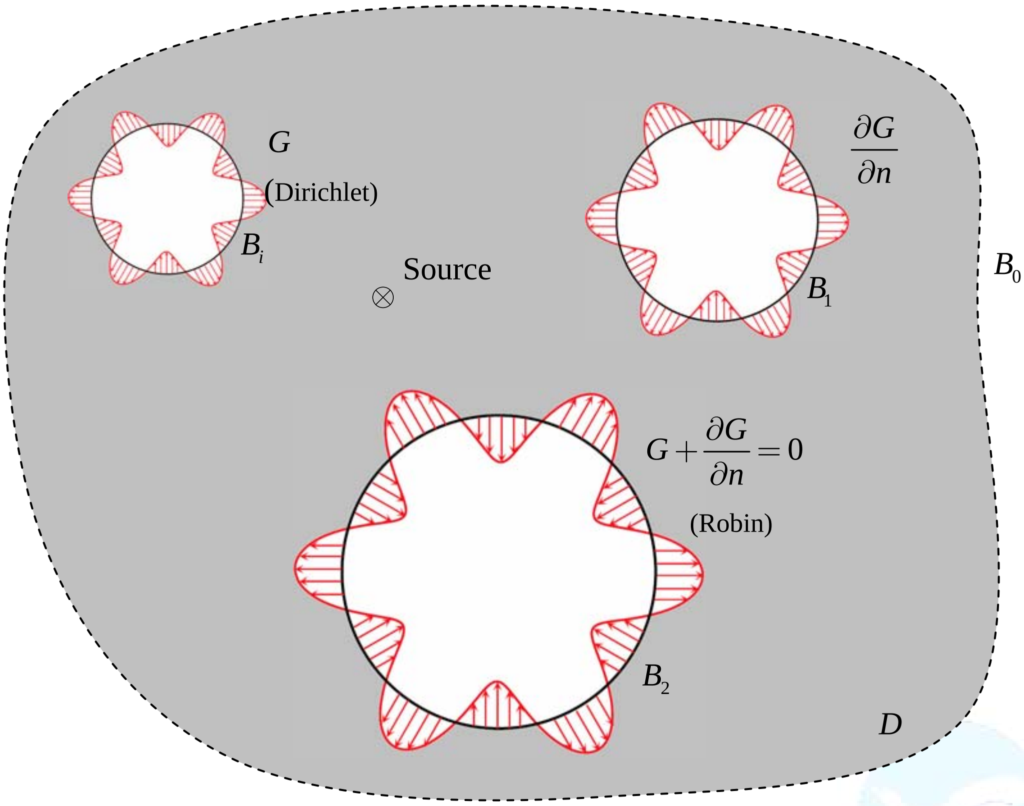

Figure 2-2 (a) Green's function for the Laplace problem with Fourier boundary densities of the Dirichlet, Neumann and Robin types

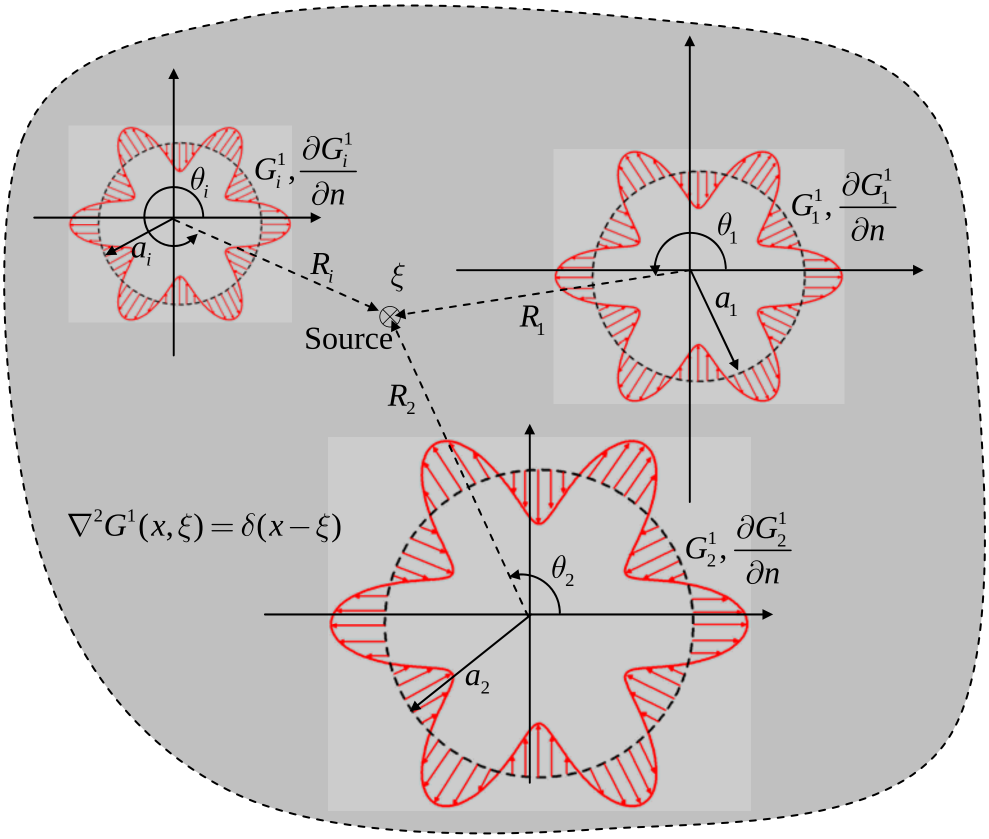

Figure 2-2 (b) The first part of the Green's function-fundamental solution

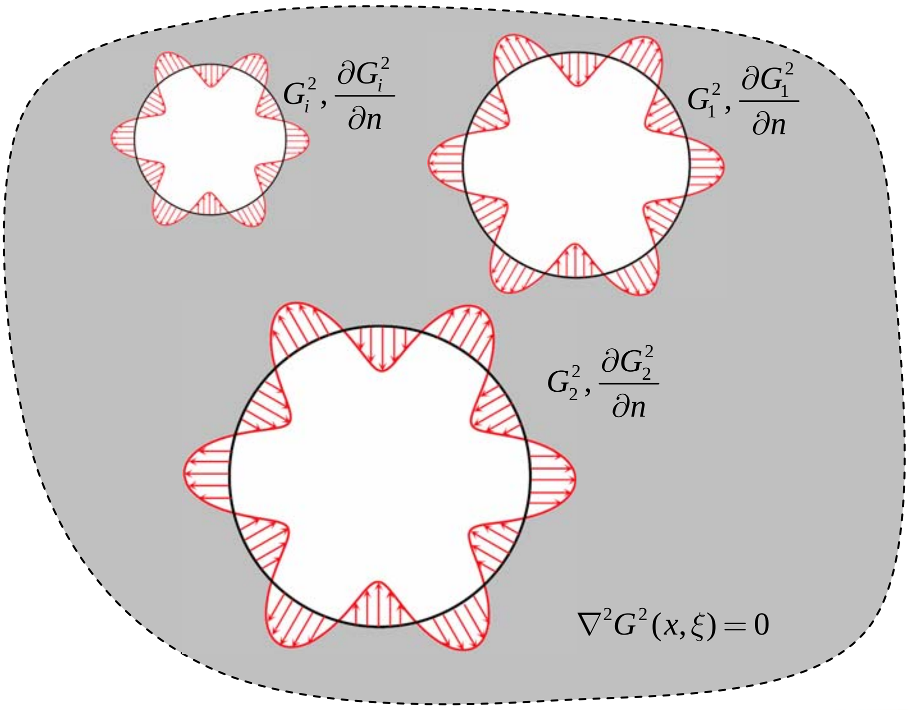

Figure 2-2 (c) The second part of the Green's function-fundamental solution-an infinite plane with circular boundary subject to the specified boundary conditions

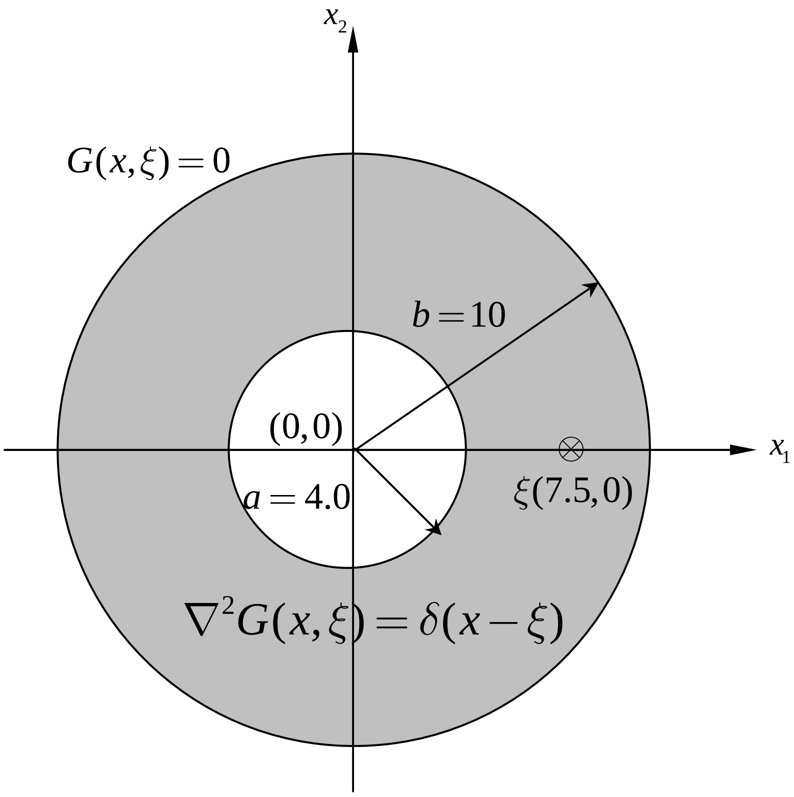

Figure 2-3 (a) Green's function for the annular ring

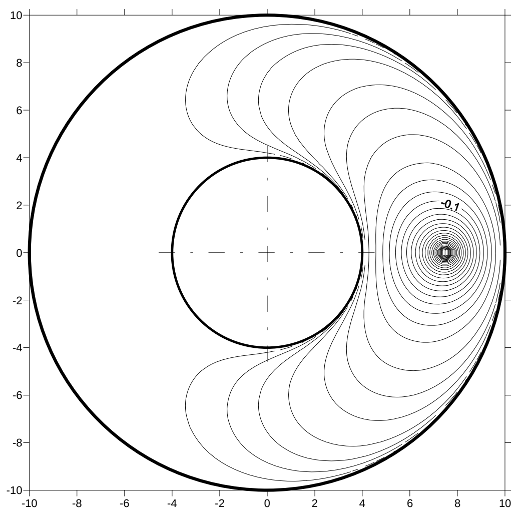

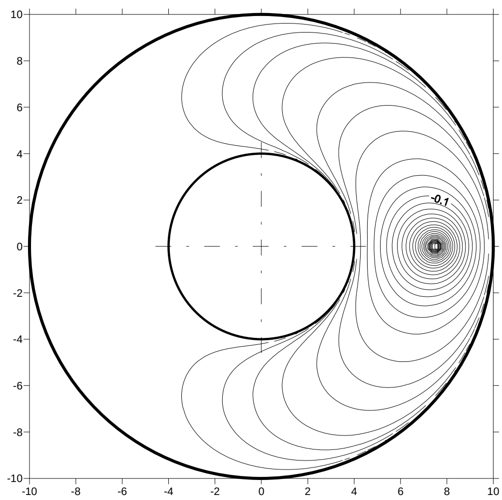

Figure 2-3(b) Potential contour by using the BIE approach

Figure 2-3(c) Potential contour by using the present method (M=50)

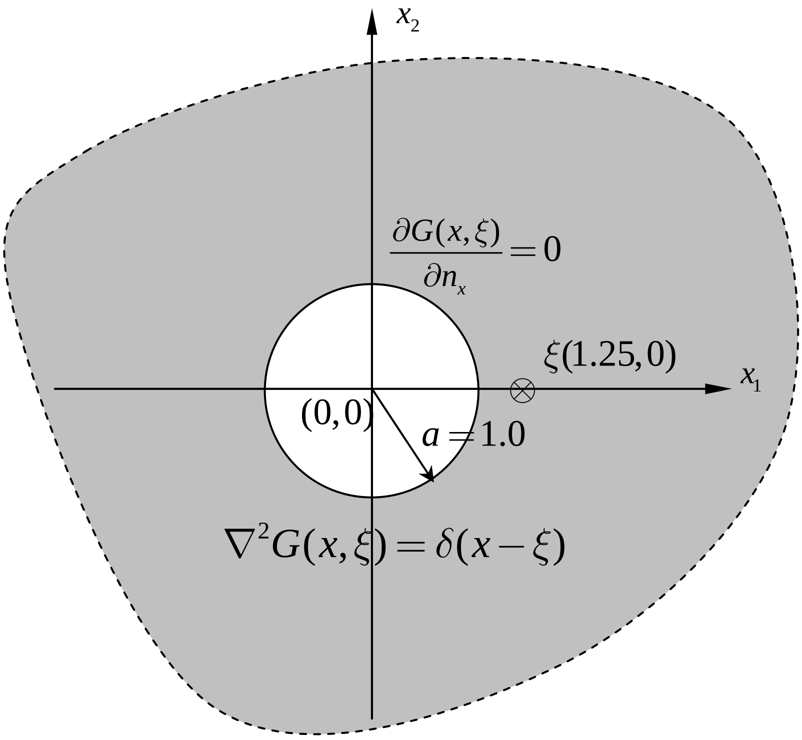

Figure 2-4(a) Green’s function for an infinite plane with an aperture

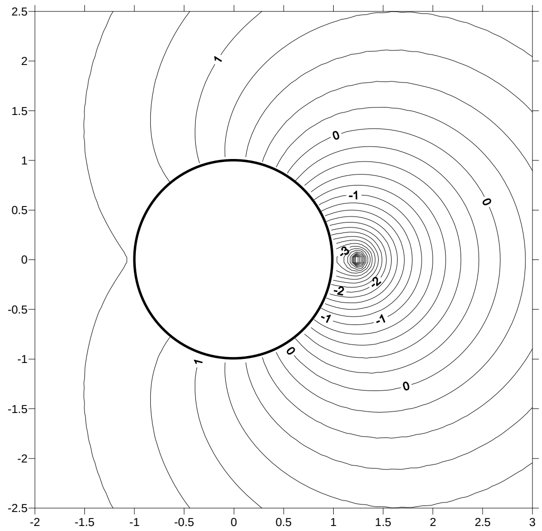

Figure 2-4(b) Potential contour by using the image method

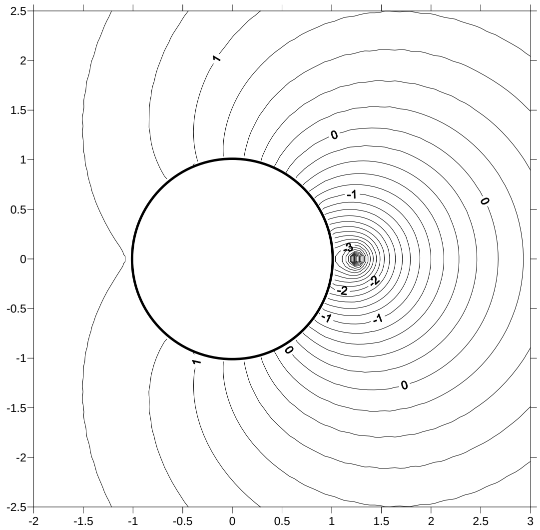

Figure 2-4(c) Potential contour by using the present method (M=50)

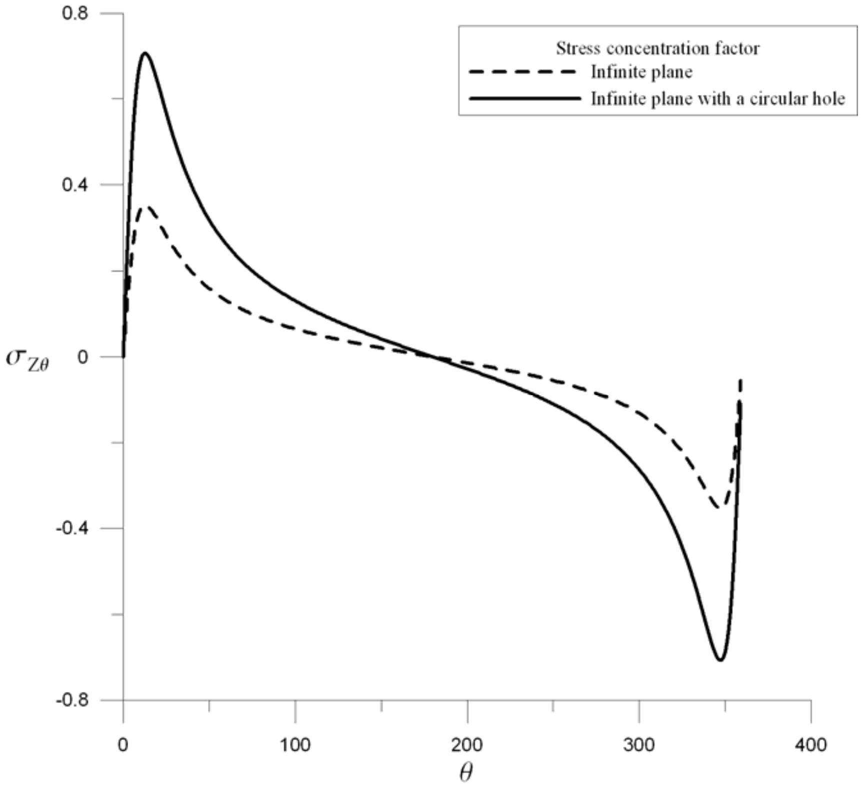

Figure 2-4(d) Stress distribution along the circular hole ($a = 1.0$ and $\xi = (1.25, 0)$)

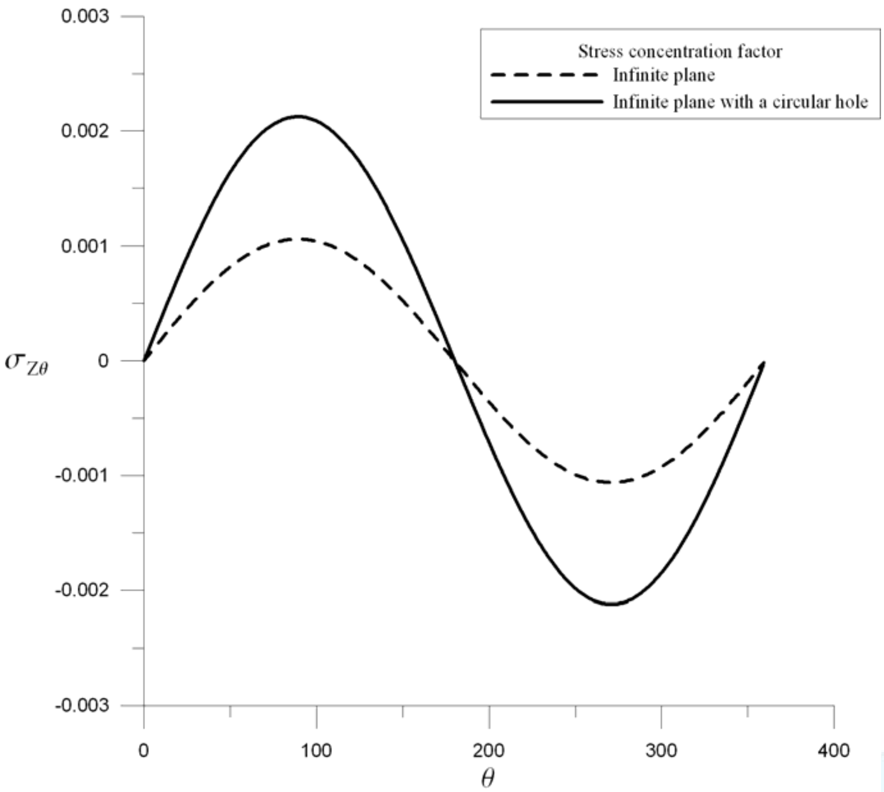

Figure 2-4(e) Stress distribution along the interface ($a = 1.0$ and $\xi = (150, 0)$)

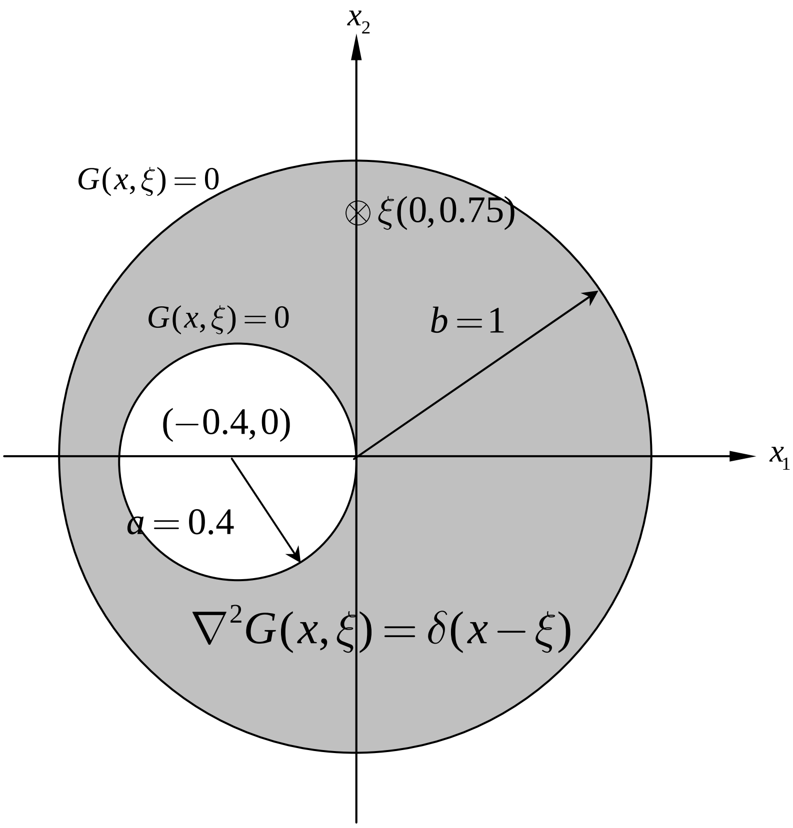

Figure 2-5(a) Green's function for the eccentric ring

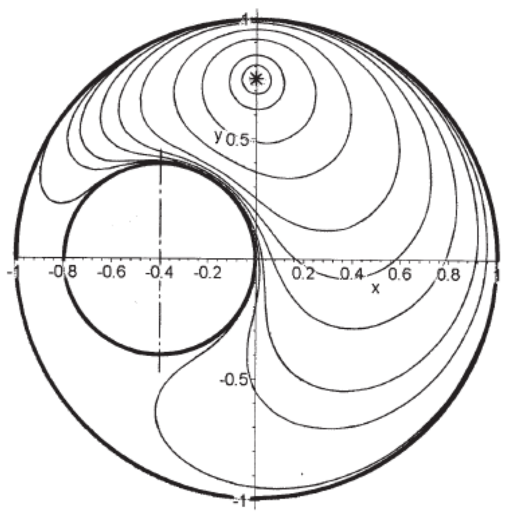

Figure 2-5(b) Potential contour by using the Melnikov's method [Melnikov and Melnikvo (2001)]

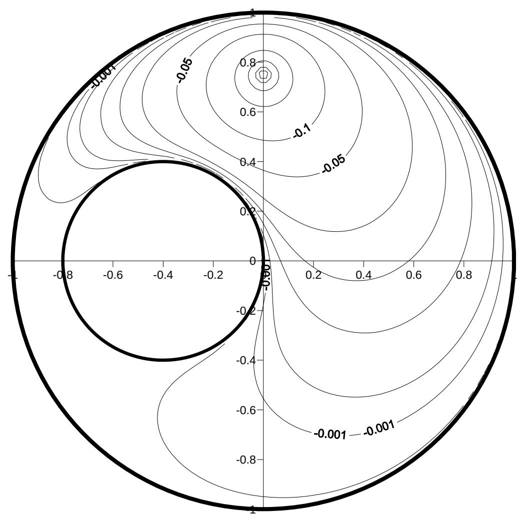

Figure 2-5(c) Potential contour by using the present method (M=50)

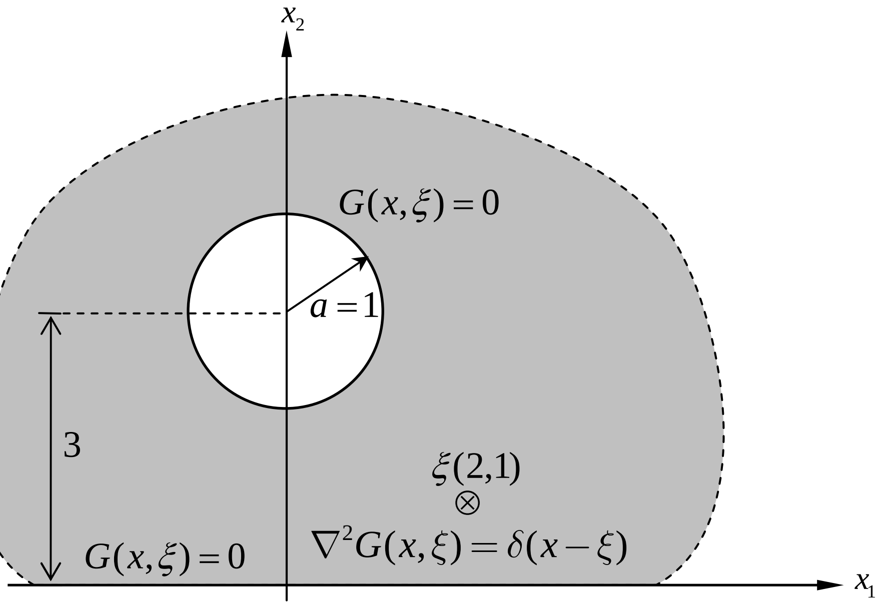

Figure 2-6(a) Green’s function for the half-plane problem with the Dirichlet boundary condition

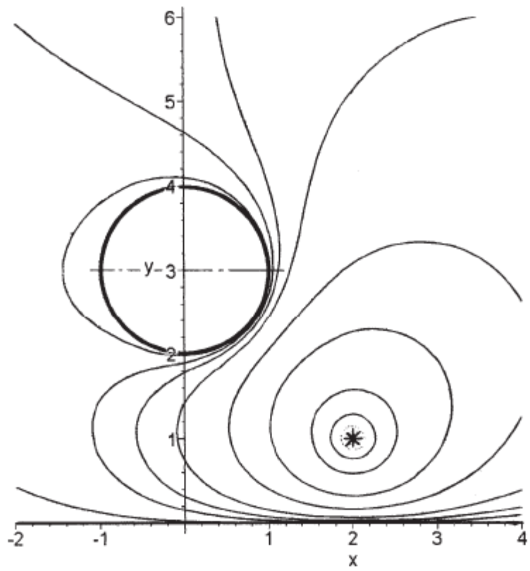

Figure 2-6(b) Potential contour by using the Melnikov’s method [Melnikov and Melnikvo (2001)]

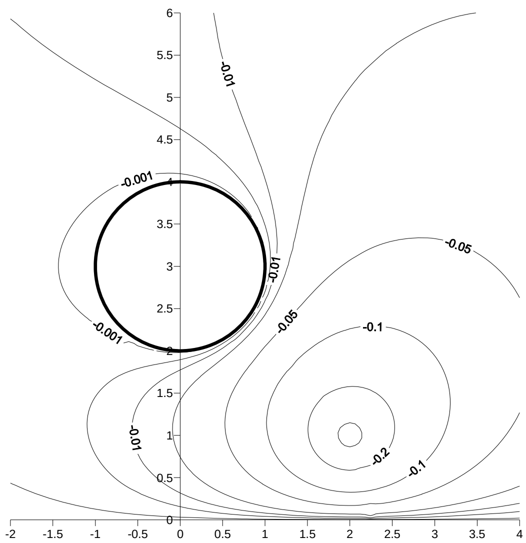

Figure 2-6(c) Potential contour by using the present method (M=50)

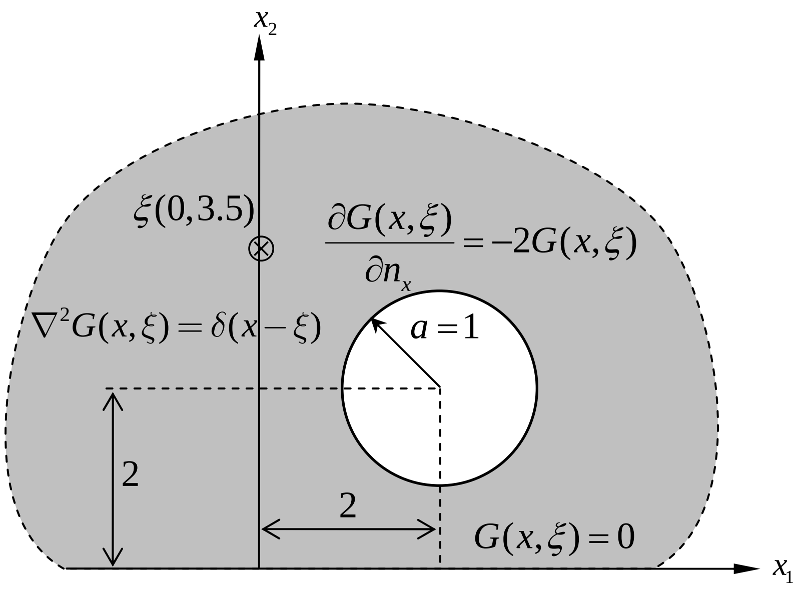

Figure 2-7(a) Green's function for the half-plane problem with the Robin boundary condition

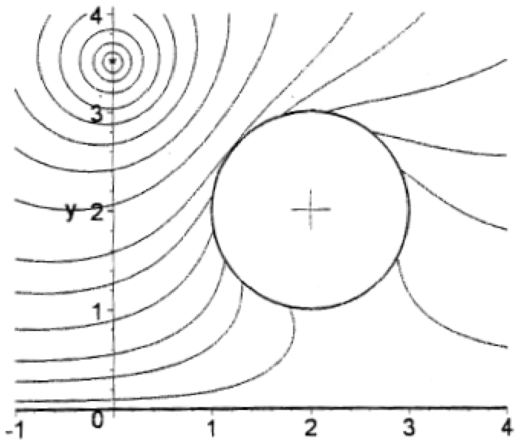

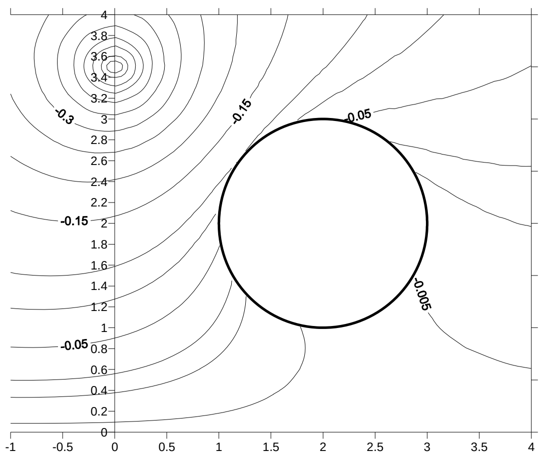

Figure 2-7(b) Potential contour by using the Melnikov's approach [Melnikov and Melnikvo (2006)]

Figure 2-7(c) Potential contour by using the present method (M=50)

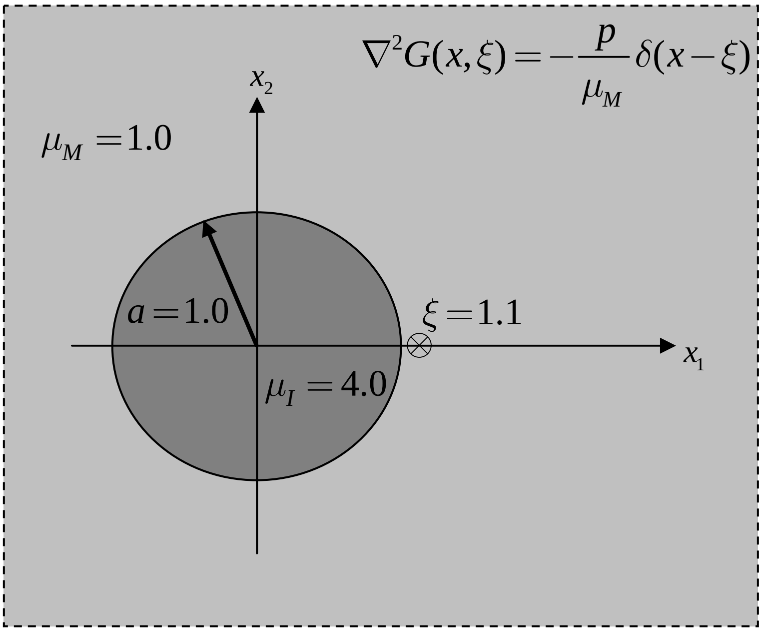

Figure 2-8(a) Green's function for the infinite plane with a circular inclusion

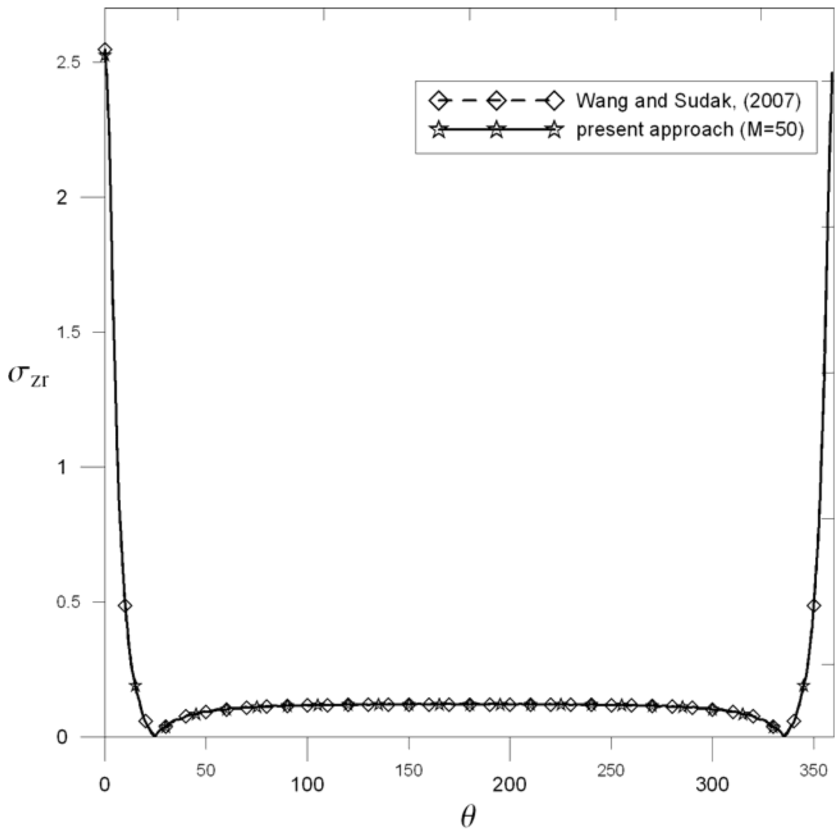

Figure 2-8(b) Stress distribution along the interface

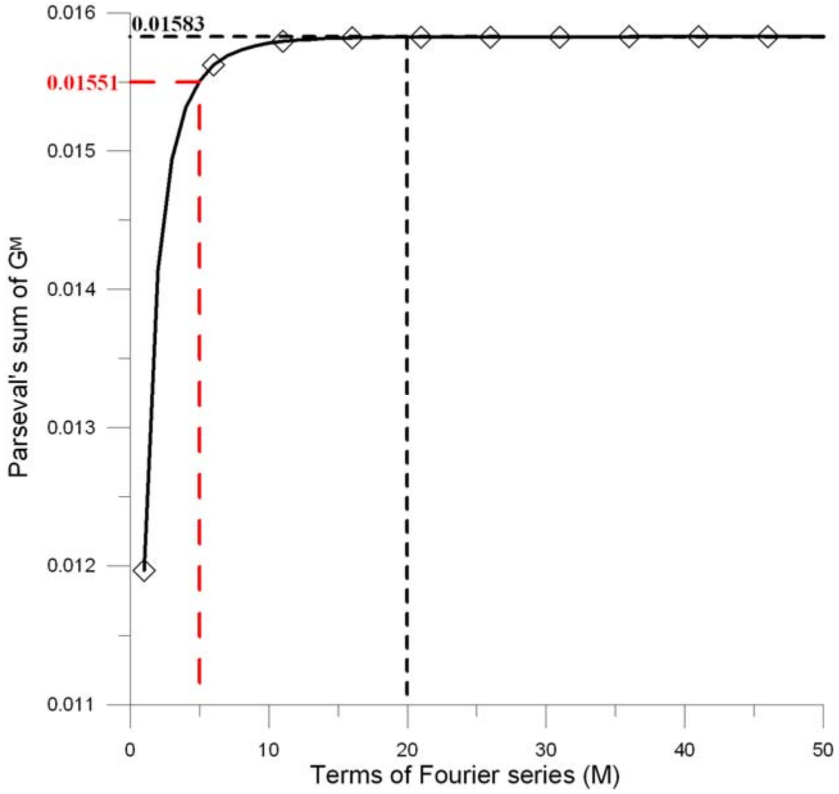

Figure 2-8(c) Parseval's sum for G^M with $a = 1.0$ and $\xi = (1.1, 0)$

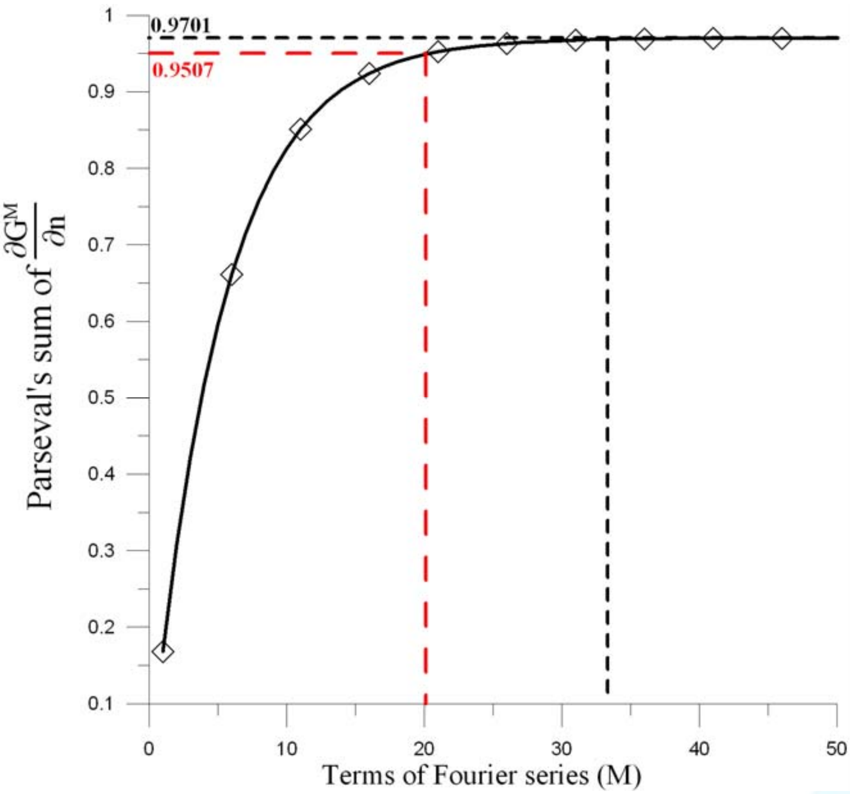

Figure 2-8(d) Parseval's sum for $\dfrac{\partial G^M}{\partial n}$ with $a = 1.0$ and $\xi = (1.1, 0)$

Chapter 3 Derivation of screw dislocation solution for Laplace problem with circular boundaries using addition theorem and superposition technique

Summary

In this chapter, the addition theorem and superposition technique are extended to solve the screw dislocation problems with several circular holes or inclusions. After taking the free body between the interface of the matrix and inclusions, the problem is decomposed into two parts. One is the screw dislocation problem with several circular holes and the other is interior Laplace problem for several circular inclusions. The problem with circular holes can be formulated by using superposition technique of the chapter 2. The interior problem is formulated by using the null-field formulation. According to the continuity of displacement and equilibrium of traction along the interface, the influence matrix can be constructed. The kernel functions and unknown boundary densities are expanded by using the degenerate kernel and Fourier series, respectively. To the author's best knowledge, the angle-type fundamental solution is first derived in this thesis. Finally, infinite-plane problems with circular holes or inclusions are demonstrated to verify the validity of present approach.

3.1 Introduction

The subject of dislocation is essential for an understanding of many of physical and mechanical properties of crystalline solids. Many researchers investigated the dislocation problems in the past years. Smith [Smith, 1968] successfully solved the problem of the interaction between a screw dislocation and a circular or elliptic inclusion contained within an infinite body. by using the complex-varialbe function and circle theorem. Besides, uniform anti-plane remote shear can bee considered at the same time. Dundurs [Dundurs, 1969] solved the screw dislocation with circular inclusion problem by using the image technique. Later, Sendeckyj [Sendeckyj, 1970] employed the complex-varialbe function in conjunction with the inverse point method to solve the problem of the screw dislocation near an arbitrary number of circular inclusions. Honein et al. [Honein et al., 1992] extended the circle theorem to solve the problem of an elastic body containing an elastic circular inclusion and subject to arbitrary loading. Sudak [Sudak, 2002] and Jin and Fang [Jin and Fang, 2007] solved the problem of the screw dislocation interacting with an imperfect interface by using the complex-variable technique. Such a problem was solved by using the image technique and Fourier transform by Fan and Wang [Fan and Wang, 2002]. In 2006, Fang and Liu [Fang and Liu, 2006] extended the complex-variable function and Riemann-Schwarz's symmetry principle to solve the problem of the interaction of a screw dislocation with a circular nano-inhomogeneity incorporating interface stress. Almost all the above problems were solved by using the complex-variable technique. Its extension to three-dimensional cases may be limited. A more general approach is nontrivial for further investigation.

In this chapter, we introduce the degenerate (or so-called separable) kernel for the angle-based fundamental solution (θ) instead of radial-basis one ($\ln r$). To our best knowledge, the degenerate kernel for angle-type fundamental solution was not found in the literature. A screw dislocation solution is decomposed into two parts. One is screw dislocation problem with several holes, and the other is the interior Laplace problems for several circular inclusions. After superposing the two solutions, the governing equation and boundary conditions can be satisfied automatically. The present approach offers a few attractive features. First, the integrals are made simple by avoiding the senses of Cauchy and Hadamard principal values. Secondly, the extension to three-dimensional problem is possible. Besides, this method can be seen as one kind of meshless method since no boundary element discretization is required. Finally, several illustrative examples are demonstrated to see the validity of the present method.

3.2 Problem statements and mathematical formulation

The physical problem to be considered is shown in Figure 3-1, where circular inclusions are imbedded in an infinite plane. For the anti-plane problem, we only consider the anti-plane displacement w such that

$$u = v = 0, \quad w = w(x, y) \tag{3-1}$$

where u and v are the vanishing components of displacement. The governing equation for anti-plane elasticity w in the absence of body forces is simplified to

$$\nabla^2 w(x,y) = 0 \tag{3-2}$$

where ∇^2 is the two-dimensional Laplacian operator. Therefore, the screw dislocation can be described as

$$\lim_{y\to 0}[w(x,-y) - w(x,y)] = b, \quad x \geq \xi \tag{3-3}$$

where b denotes the Burgers' vector and ξ denotes the location of the screw dislocation. By taking the free body along the interface between the matrix and inclusions, the problem is decomposed into two systems. One is an infinite plane with N circular holes subject to a screw dislocation as shown in Figure 3-2 (a). The other is N circular inclusions bounded by B_i contour which satisfies the Laplace equation as shown in Figure 3-2 (b). For the problem in Figure 3-2 (a), it can be superimposed by two parts again. One is an infinite plane subjected to screw dislocation and the other is an infinite plane with N circular holes which satisfies the specified boundary conditions as shown in Figures 3-2 (c) and 3-2 (d), respectively.

3.3 Expansions of fundamental solutions and boundary densities

To fully employ the property of circular geometry, the mathematical tools, separable kernel (so-called degenerate kernel or addition theorem) and Fourier series, are utilized for an analytical study.

3.3.1 Degenerate (Separable) kernel for the angle-based fundamental solution

In order to derive the degenerate kernel, the polar coordinate is utilized to replace the Cartesian coordinate. Therefore, the location of the screw dislocation and collocation points are expressed as (R,θ) and (ρ,ϕ), respectively, in the polar coordinate. The position vector of screw dislocation point is $z_s = Re^{i\theta}$. Similarly, the collocation point can be expressed by $z_x = \rho e^{i\phi}$, as shown in Figure 3-3. In order to derive the screw dislocation fundamental solution of Laplace equation ($\varphi(s,x)$) into the separable form, we have

$$\ln(z_x - z_s) = \ln(re^{i\varphi}) = \ln r + i\varphi \tag{3-4}$$

For the exterior case $(R < \rho)$, Eq.(3-4) can be expanded as follows

$$\begin{aligned}
\ln(z_x - z_s) &= \ln(z_x) + \ln(1 - \frac{z_s}{z_x}) \\
&= \ln(\rho e^{i\phi}) - \sum_{m=1}^{\infty} \frac{1}{m} (\frac{z_s}{z_x})^m \\
&= \ln\rho + i\phi - \sum_{m=1}^{\infty} \frac{1}{m} (\frac{\mathrm{R} e^{i\theta}}{\rho e^{i\phi}})^m \\
&= \ln\rho + i\phi - \sum_{m=1}^{\infty} \frac{1}{m} (\frac{\mathrm{R}}{\rho})^m [\cos m(\theta - \phi) + i \sin m(\theta - \phi)].
\end{aligned} \tag{3-5}$$

Thus, the degenerate (or so-called separable) form for the fundamental solution of the screw dislocation for the Laplace equation ($\varphi(s,x)$) is obtained

$$\varphi(s,x) = \phi - \sum_{m=1}^{\infty} \frac{1}{m} (\frac{\mathrm{R}}{\rho})^m \sin m(\theta - \phi), \quad R < \rho, \tag{3-6}$$

Similarly, we also obtain

$$\varphi(s,x) = \theta + \pi + \sum_{m=1}^{\infty} \frac{1}{m} (\frac{\rho}{R})^m \sin m(\theta - \phi), \quad R \geq \rho, \tag{3-7}$$

for the interior case $(R > \rho)$. In Figure 3-3, the range of $\varphi(s,x)$ is defined between 0 and 2π. To match the physical meaning and mathematical requirement, we modify the range of the interest between $-\pi$ and π. Thus, the fundamental solution of the screw dislocation ($\varphi(s,x)$) is expressed by

$$\varphi(s,x) = \begin{cases} \varphi^I(\rho,\phi;R,\theta) = \theta + \sum_{m=1}^{\infty} \frac{1}{m} (\frac{\rho}{R})^m \sin m(\theta - \phi), & \rho \leq R \\ \varphi^E(\rho,\phi;R,\theta) = \phi - \pi - \sum_{m=1}^{\infty} \frac{1}{m} (\frac{\mathrm{R}}{\rho})^m \sin m(\theta - \phi), & \rho > R \end{cases} \tag{3-8}$$

where the superscripts I and E denote the interior and exterior cases, respectively. It is noted that the numerator in Eq. (3-8) involve the larger argument to ensure the series convergence. By using Eq. (3-8) to plot the contour plots for the screw dislocation in the four quadrants are shown in Figure 3-4 (a) to Figure 3-4 (d). When the screw dislocation locates at the four quadrants, there are certain areas falling outside the range between $-\pi$ and π. We subtract 2π where the value is greater than π to ensure the value in the range. Similarly, we add 2π where the value is smaller than $-\pi$. When the response is in the defined range, Figure 3-5 shows the screw-dislocation response. To the author's best knowledge, the degenerate kernel for the angle-type fundamental solution was not found in the literature.

3.3.2 Fourier series expansion for boundary density

The unknown boundary densities are represented by using the Fourier series as shown below:

$$u(s_k) = a_0^k + \sum_{n=1}^{M} (a_n^k \cos n\theta_k + b_n^k \sin n\theta_k), \quad s_k \in B_k, \quad k = 1, 2, \cdots, N, \tag{3-9}$$

$$t(s_k) = \frac{\partial u(s_k)}{\partial n_s} = p_0^k + \sum_{n=1}^{M} (p_n^k \cos n\theta_k + q_n^k \sin n\theta_k), \quad s_k \in B_k, \quad k = 1, 2, \cdots, N, \tag{3-10}$$

where a_n^k, b_n^k, p_n^k and q_n^k ($n = 0, 1, 2, \cdots$) are the Fourier coefficients, θ_k is the polar angle measured related to the x-direction and N is the number of circular boundary. In the real computation, the finite number of terms M for boundary density is adopted.

3.4 Matching of interface conditions and solution procedures

After decomposing the inclusion problems into two parts, we employ the null-field equation approach to handle one exterior Laplace problems for the matrix and several interior Laplace problems for the inclusions as shown in Figures 3-2 (b) and 3-2 (d), respectively. By collocating the null-field point exactly on the real boundary, the linear algebraic system is obtained. For the exterior problem of matrix in Figure 3-2 (d), we have

$$\left[\mathbf{U}^M\right]\left\{\frac{\partial \mathbf{w}^M}{\partial \mathbf{n}} - \frac{\partial \mathbf{w}^{sd}}{\partial \mathbf{n}}\right\} = \left[\mathbf{T}^M\right]\left\{\mathbf{w}^M - \mathbf{w}^{sd}\right\}. \tag{3-11}$$

where the superscript M denotes the matrix and superscript sd denotes the screw dislocation. For the interior problem of each inclusion in Figure 3-2 (b), we have

$$\left[\mathbf{U}^I\right]\left\{\frac{\partial \mathbf{w}^I}{\partial \mathbf{n}}\right\} = \left[\mathbf{T}^I\right]\left\{\mathbf{w}^I\right\}, \tag{3-12}$$

where the superscript I denotes the inclusion. The $\left[\mathbf{U}^M\right]$, $\left[\mathbf{T}^M\right]$, $\left[\mathbf{U}^I\right]$ and $\left[\mathbf{T}^I\right]$ are the influence matrices due to degenerate kernels of single and double-layer potentials. The boundary data of $\left\{\frac{\partial \mathbf{w}^M}{\partial \mathbf{n}}\right\}$, $\left\{\frac{\partial \mathbf{w}^{sd}}{\partial \mathbf{n}}\right\}$, $\left\{\mathbf{w}^M\right\}$ and $\left\{\mathbf{w}^{sd}\right\}$ are the vectors of

Fourier coefficients. It is denoted that $\{\mathbf{w}^{sd}\}$ and $\left\{\frac{\partial \mathbf{w}^{sd}}{\partial \mathbf{n}}\right\}$ in Figure 3-2 (c) are the displacement and traction fields due to the screw dislocation. According to the continuity of displacement and equilibrium of traction along the ideal interface, we have the constraints

$$\{w_j^M\} = \{w_j^I\}, \qquad \text{on } B_j, \tag{3-13}$$

$$[\mu_M]\left\{\frac{\partial t_j^M}{\partial n}\right\} = -[\mu_I]\left\{\frac{\partial w_j^I}{\partial n}\right\}, \text{ on } B_j, \tag{3-14}$$

where $[\mu_I]$ and $[\mu_M]$ are shown as follows:

$$[\mu_I] = \begin{bmatrix} \mu_I & 0 & \cdots & 0 \\ 0 & \mu_I & \cdots & 0 \\ \vdots & \vdots & \ddots & \vdots \\ 0 & 0 & \cdots & \mu_I \end{bmatrix}, \ [\mu_M] = \begin{bmatrix} \mu_M & 0 & \cdots & 0 \\ 0 & \mu_M & \cdots & 0 \\ \vdots & \vdots & \ddots & \vdots \\ 0 & 0 & \cdots & \mu_M \end{bmatrix}, \tag{3-15}$$

in which μ_I and μ_M denote the shear modulus of the matrix and the inclusion, respectively. By assembling matrices in Eqs. (3-11)~(3-14), a global algebraic system can be obtained.

$$\begin{bmatrix} T_j^M & -U_j^M & 0 & 0 \\ 0 & 0 & T_j^I & -U_j^I \\ I & 0 & -I & 0 \\ 0 & \mu_M & 0 & \mu_I \end{bmatrix} \begin{Bmatrix} w_j^M \\ \frac{\partial w_j^M}{\partial n} \\ w_j^I \\ \frac{\partial w_j^I}{\partial n} \end{Bmatrix} = \begin{Bmatrix} c \\ 0 \\ 0 \\ 0 \end{Bmatrix}, \tag{3-16}$$

where $\{c\}$ is the forcing terms due to the screw dislocation. The matrix $[I]$ is an identity matrix. By comparing Eq. (3-11) with the first row of Eq. (3-16), we have

$$\{c\} = [T^M]\{w^{sd}\} - [U^M]\left\{\frac{\partial w^{sd}}{\partial n}\right\}. \tag{3-17}$$

By translating the screw dislocation to the origin of the circular hole, the boundary distribution of w^{sd} and t^{sd} due to the screw dislocation are expressed as

$$w^{sd} = \begin{cases} \theta + \sum_{m=1}^{\infty} \frac{1}{m}\left(\frac{a_i}{R}\right)^m \sin m(\theta - \phi), & a_i \le R \\ \phi - \pi - \sum_{m=1}^{\infty} \frac{1}{m}\left(\frac{\mathrm{R}}{a_i}\right)^m \sin m(\theta - \phi), & a_i > R \end{cases}, \tag{3-18}$$

$$\frac{\partial w^{sd}}{\partial n}=\begin{cases}\sum_{m=1}^{\infty}\frac{a_i^{m-1}}{R^m}\sin m(\theta-\phi), & a_i\le R\\ \sum_{m=1}^{\infty}\frac{R^m}{a_i^{m+1}}\sin m(\theta-\phi), & a_i>R\end{cases}, \tag{3-19}$$

where R and θ denote the distance and polar angle, respectively, between the screw dislocation and the origin as shown in Figure 3-3 and a_i denotes the radius of the ith circle. The flowchart of the present approach is shown in the Figure 3-6.

3.5 Illustrative examples and discussions

Case 1: An infinite plane with a rigid inclusion subject to the Dirichlet boundary condition (an analytical solution)

Figure 3-7 (a) shows the geometry of a single rigid inclusion in the infinite plane under the screw dislocation. The screw dislocation is located at $\xi=(1.75,0)$. The center of the rigid inclusion is set at $(0,0)$ and the radius a is 1.0. An analytical solution was derived by Smith (Smith, 1968) as shown below:

$$\begin{aligned}F(z)&=\frac{\mu_E b}{2\pi i}\log(z-z_0)+\frac{\mu_E b}{2\pi i}\log(\frac{a^2}{z}-\overline{z}_0)\\ w(x,y)&=\frac{1}{\mu_E}\mathrm{Re}[F(z)]\end{aligned} \tag{3-20}$$

where $F(z)$ and μ_E denote the complex variable function and shear modulus, respectively, $\overline{z}_0$ denotes the conjugate of the position vector of the screw dislocation, b denotes the Burgers' vector, and $\mathrm{Re}[\bullet]$ denotes the real part. By using the present formulation, the analytical solution is shown below:

$$w(\rho,\phi)=\begin{cases}(1-\frac{\ln\rho}{\ln a})\frac{b\theta}{2\pi}+\sum_{m=1}^{\infty}\frac{b}{2\pi m}[(\frac{\rho}{R})^m-(\frac{a^2}{\rho R})^m]\sin m(\theta-\phi), & R\ge\rho\\ \frac{b\phi}{2\pi}-\frac{b}{2}-\frac{\ln\rho}{\ln a}\frac{b\theta}{2\pi}-\sum_{m=1}^{\infty}\frac{b}{2\pi m}[(\frac{R}{\rho})^m+(\frac{a^2}{\rho R})^m]\sin m(\theta-\phi), & R<\rho\end{cases} \tag{3-21}$$

Figures 3-7 (b) and 3-7 (c) show the potential distribution by using the Smith method (Smith, 1969) and the present method, respectively. It is found that the result of the present approach is in good agreement. Based on the addition theorem, it is easier to find the image location of (a^2/R) with negative strength. A similar work can be found for the image location of source case [Chen and Wu, 2006].

Case 2: An infinite plane with a hole subject to the Neumann boundary condition (an analytical solution)

Figure 3-8 (a) shows the geometry of a single hole in the infinite plane under the screw dislocation. The screw dislocation is located at $\xi = (1.75, 0)$. The center of the hole is set at $(0,0)$ and the radius a is 1.5. The analytical solution proposed by Smith is found in [Smith, 1969] as

$$\begin{aligned} F(z) &= \frac{\mu_E b}{2\pi i}\log(z - z_0) - \frac{\mu_E b}{2\pi i}\log(\frac{a^2}{z} - \overline{z}_0) \\ w(x,y) &= \frac{1}{\mu_E}\mathrm{Re}[F(z)] \end{aligned} \tag{3-22}$$

By using the present formulation, the analytical solution is shown below:

$$w(\rho,\phi) = \begin{cases} \dfrac{b\theta}{2\pi} + \displaystyle\sum_{m=1}^{\infty}\frac{1}{2\pi m}[(\frac{\rho}{R})^m + (\frac{a^2}{\rho R})^m]\sin m(\theta-\phi), & R \ge \rho \\ \dfrac{b\phi}{2\pi} - \dfrac{b}{\pi} - \displaystyle\sum_{m=1}^{\infty}\frac{1}{2\pi m}[(\frac{R}{\rho})^m - (\frac{a^2}{\rho R})^m]\sin m(\theta-\phi), & R < \rho \end{cases} \tag{3-23}$$

Figures 3-8 (b) and 3-8 (c) show the potential distribution by using the Smith method [Smith, 1969] and the present method, respectively. Good agreement is made. Comparisons of the two analytical solutions by using the addition theorem are given in the Appendix 2. The stress distribution along the circular hole is shown in the Figure 3-8 (d). The stress concentration factor is 2.

Case 3: An infinite plane with a circular inclusion (an analytical solution)

Figure 3-9 (a) shows the geometry of a single inclusion in the infinite plane under the screw dislocation. The screw dislocation is located at $\xi = (1.75, 0)$. The center of the hole is set at $(0,0)$ and the radius a is 1.5. The analytical solution proposed by Smith is found in [Smith, 1969] as

$$
\begin{aligned}
F_I(z) &= \frac{(1+k)\mu_E b}{2\pi i}\log(z-z_0) \\
F_E(z) &= \frac{\mu_E b}{2\pi i}\log(z-z_0) + \frac{k\mu_E b}{2\pi i}\log(\frac{a^2}{z}-\overline{z}_0) \\
w_I(x,y) &= \frac{1}{\mu_I}\mathrm{Re}[F_I(z)] \\
w_E(x,y) &= \frac{1}{\mu_E}\mathrm{Re}[F_E(z)]
\end{aligned}
\tag{3-22}
$$

where the indexes I and E denote the inside and outside the inclusion, respectively, μ_I and μ_E denote the shear modulus for the inclusion and matrix, respectively and $k=(\mu_I-\mu_E)/(\mu_I+\mu_E)$. By using the present formulation, the analytical solution is shown below:

$$
w(\rho,\phi)= \begin{cases} \dfrac{b\theta}{2\pi}+\sum_{m=1}^{\infty}\dfrac{b}{2\pi m}[(\dfrac{\rho}{R})^m+\dfrac{\mu_M-\mu_I}{\mu_M+\mu_I}(\dfrac{a^2}{\rho R})^m]\sin m(\theta-\phi), & \rho\geq a \text{ and } \rho<R \\ \dfrac{b(\phi-\pi)}{2\pi}-\sum_{m=1}^{\infty}\dfrac{b}{2\pi m}[(\dfrac{R}{\rho})^m-\dfrac{\mu_M-\mu_I}{\mu_M+\mu_I}(\dfrac{a^2}{\rho R})^m]\sin m(\theta-\phi), & \rho\geq a \text{ and } \rho\geq R \\ \dfrac{b\theta}{2\pi}+\sum_{m=1}^{\infty}\dfrac{b}{\pi m}(\dfrac{\rho}{R})^m\dfrac{\mu_M}{\mu_M+\mu_I}\sin m(\theta-\phi), & \rho<a \end{cases}, \tag{3-24}
$$

where μ_M and μ_I denote the shear modulus of the matrix and inclusion, respectively. Figures 3-9 (b) and 3-9 (c) show the potential distribution by using the Smith method [Smith, 1969] and the present method, respectively. The result of case 2 can be obtained by using the limiting process ($\mu_I\to 0$). Furthermore, the Parseval's theorem is adopted to test the convergence for different number of terms (M) for Fourier series since the boundary densities are continuous on $[0,2\pi]$. The Parseval's theorem is defined as shown below:

$$
\int_0^{2\pi} f^2(\theta)d\theta \doteqdot 2\pi a_0^{\,2}+\pi\sum_{n=1}^{M}(a_n^{\,2}+b_n^{\,2}), \tag{3-25}
$$

where

$$
f(\theta)=a_0+\sum_{n=1}^{M}(a_n\cos n\theta+b_n\sin n\theta). \tag{3-26}
$$

According to Eq. (3-26), the Parseval's sum versus various number of terms (M) for Fourier series of boundary densities on each circular boundary in the screw dislocation is plotted in Figure 3-10 (a) to 3-10 (b).

Case 4: An infinite plane with two circular holes (semi-analytical solution)

Following the success of the single-hole case to compare well with the Smith's result, we extend to two circular holes as shown in Figure 3-11 (a). The screw dislocation is located at $\xi = (0,0)$. The center of the two holes are set at $(-a_1, 0.01a_1)$ and $(d + a_2, 0.01a_1)$. The radii a_1 and a_2 are 1.0 and $2.0a_1$, respectively. Three cases of $d = 2.0a_1$, $0.1a_1$ and $0.01a_1$ are demonstrated to show the validity of the present method. The contour of displacement for the two circular holes problem is shown in Figure 3-11 (b) to 3-11 (d).

3.6 Conclusions

For the screw dislocation problem with circular boundaries, we have proposed an indirect approach to construct the screw dislocation solution by using the addition theorem and superposition technique. The angle-type fundamental solution for screw dislocation was derived in terms of degenerate kernel in this chapter. Several examples, including an infinite plane with a circular hole subject to the Dirichlet or Neumann boundary condition and a circular inclusion imbedded in an infinite plane, were demonstrated to check the validity of the present formulation. A case of two holes is also addressed. Neither complex-variable technique nor senses of principal values were required. Good agreements were made after comparing with the previous results. Based on this concept, the extension to three-dimensional problem may be possible and is now under investigation.

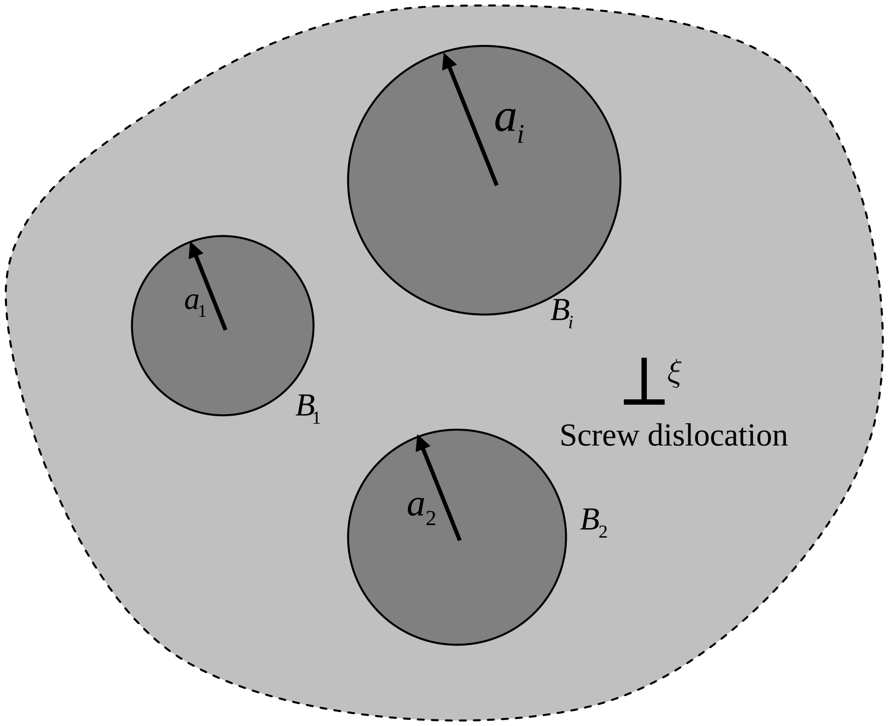

Figure 3-1 Infinite plane problem with arbitrary number of circular inclusions under the screw dislocation

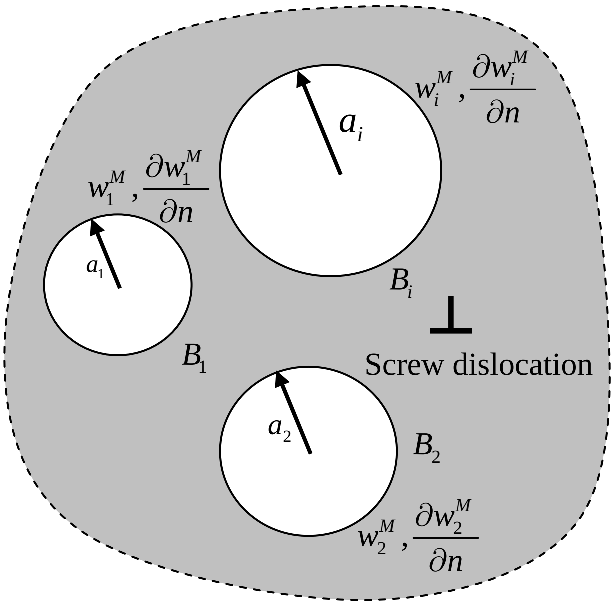

Figure 3-2 (a) Infinite matrix with circular holes subject to a screw dislocation

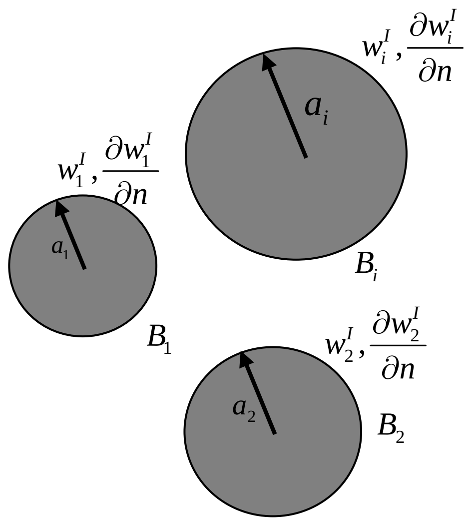

Figure 3-2 (b) Interior Laplace problems for each circular inclusion

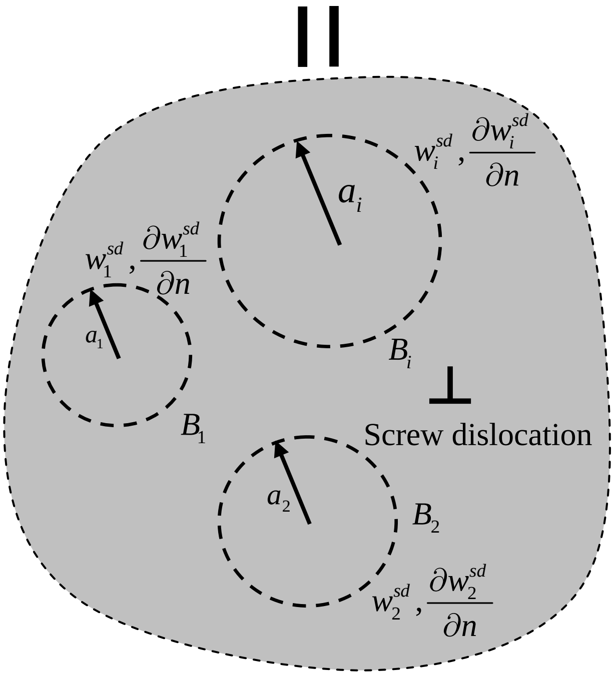

Figure 3-2 (c) Infinite matrix under the screw dislocation

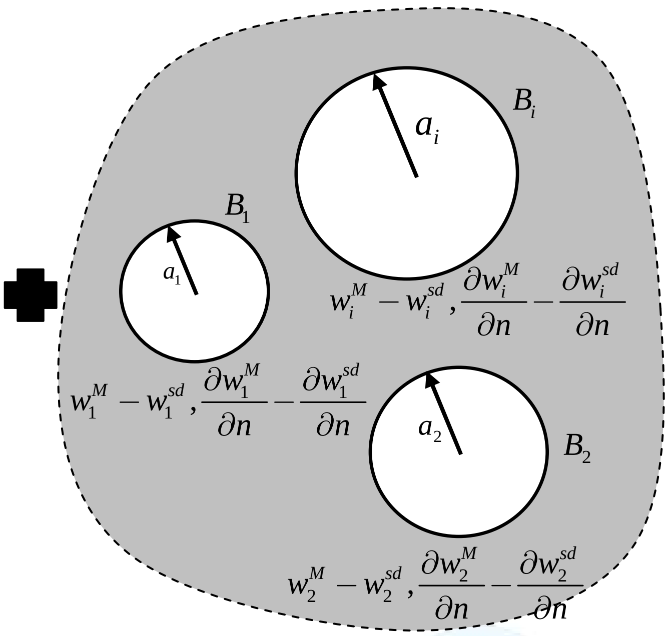

Figure 3-2 (d) Exterior Laplace problems for the matrix

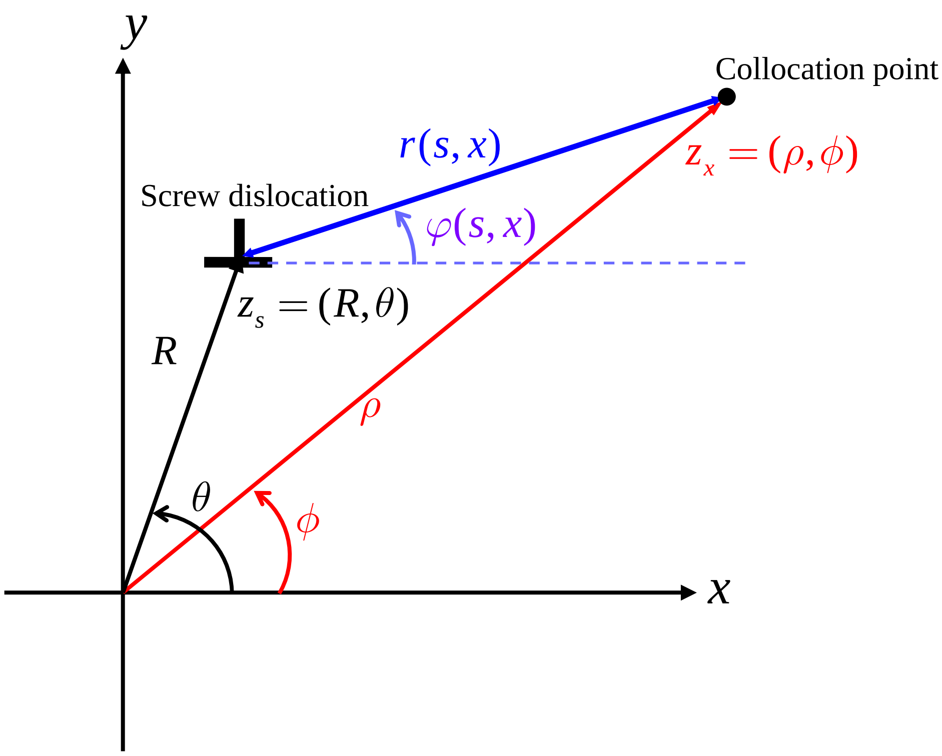

Figure 3-3 Figure sketch for the screw dislocation

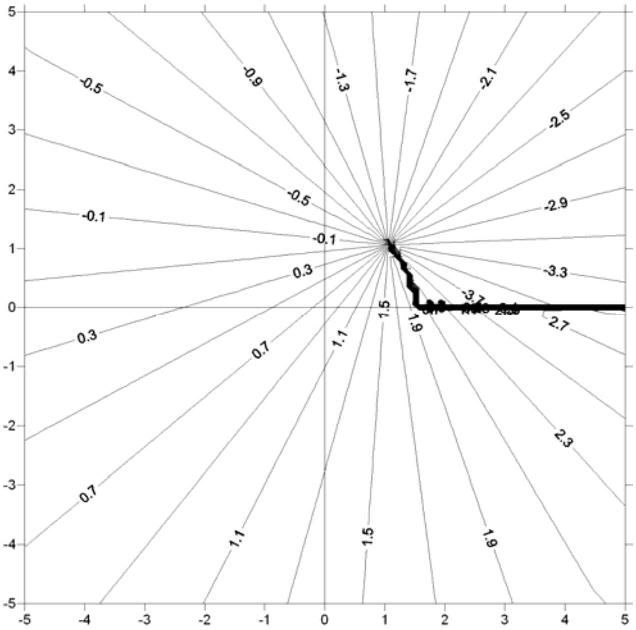

Figure 3-4 (a) Screw dislocation in the first quadrant without the constrain ($R=1.5$, $\theta=\pi/4$)

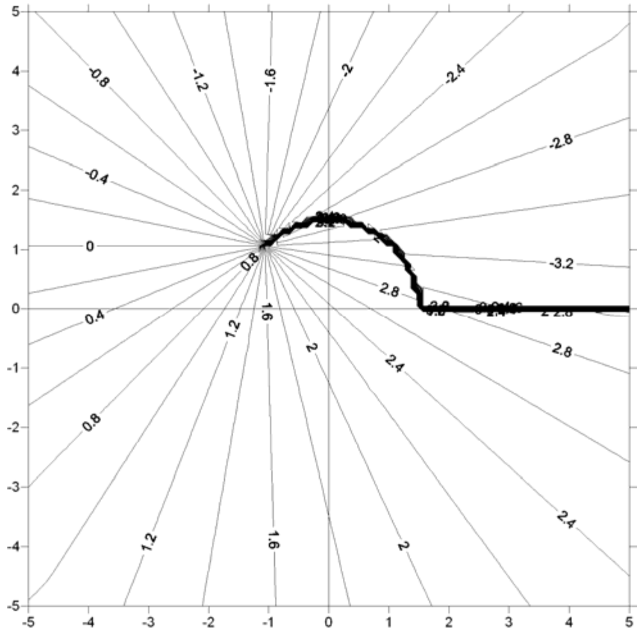

Figure 3-4 (b) Screw dislocation in the second quadrant without the constrain ($R=1.5$, $\theta=3\pi/4$)

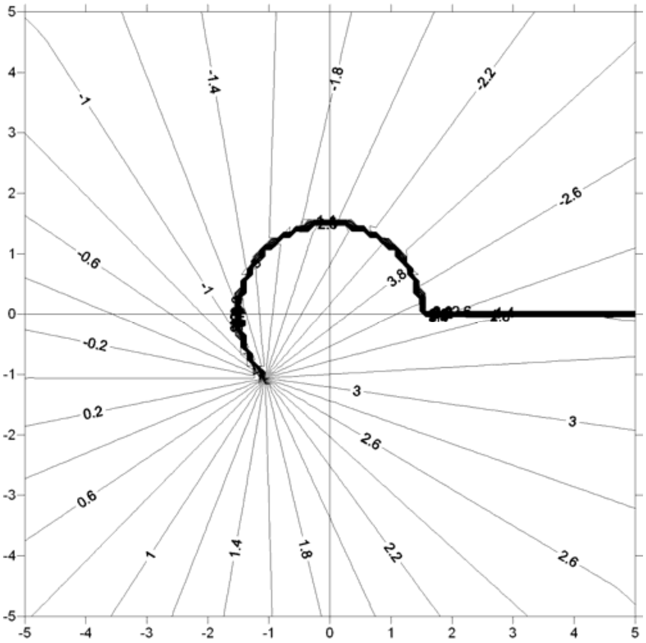

Figure 3-4 (c) Screw dislocation in the third quadrant without the constrain ($R=1.5$, $\theta=5\pi/4$)

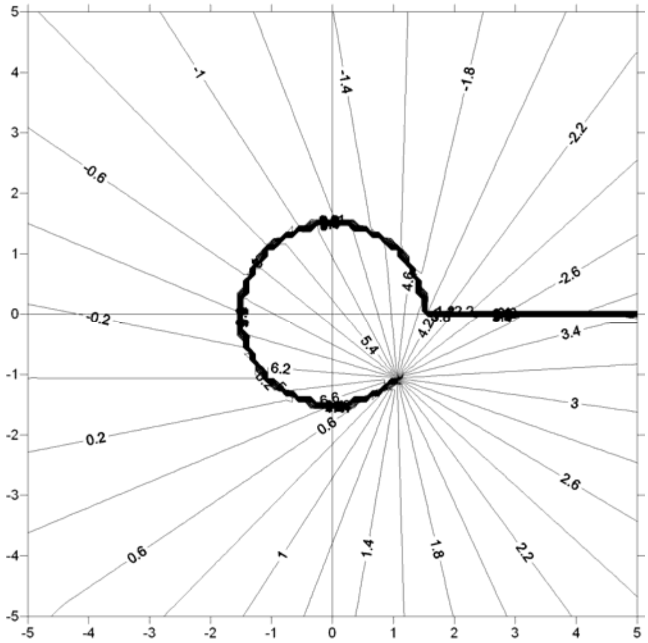

Figure 3-4 (d) Screw dislocation in the forth quadrant without the constrain ($R=1.5$, $\theta=7\pi/4$)

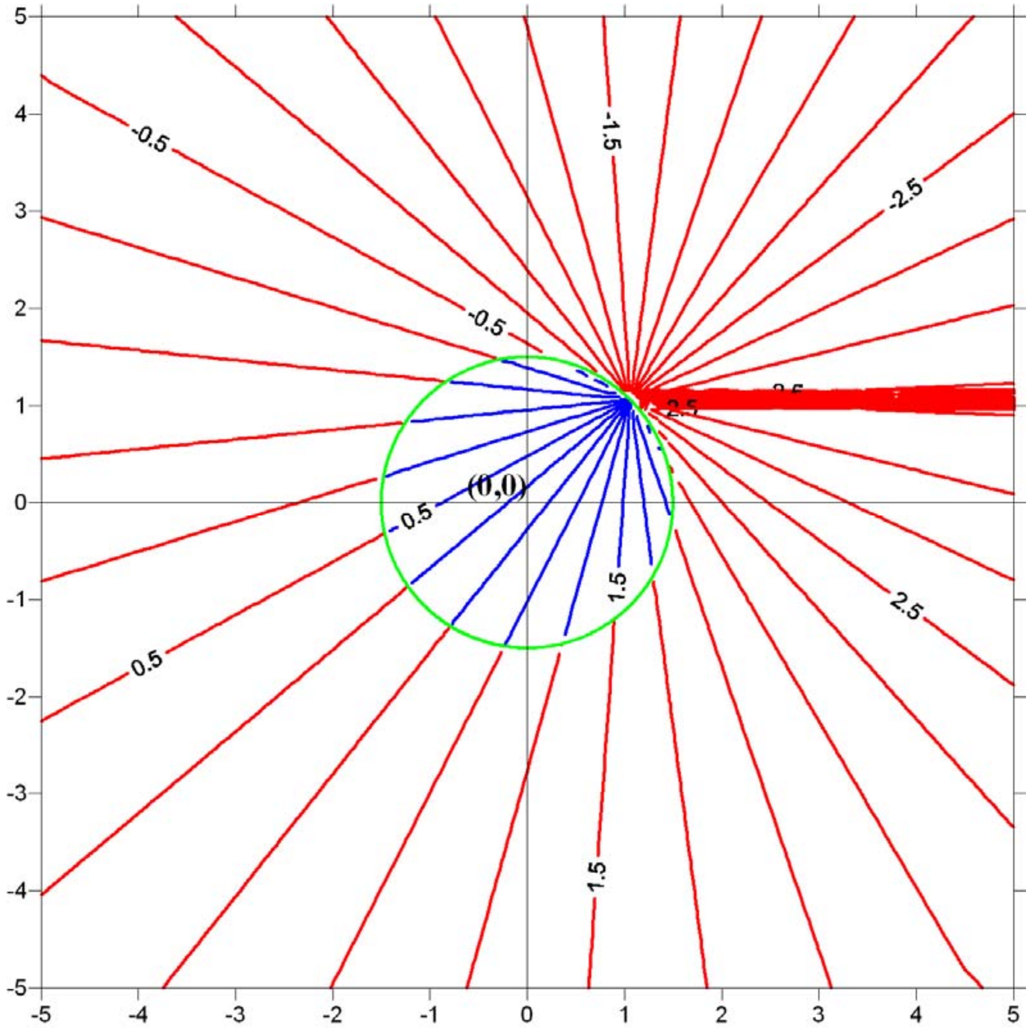

Figure 3-5 Screw dislocation in the first quadrant under the constrain

$(R = 1.5, \theta = \pi/4)$

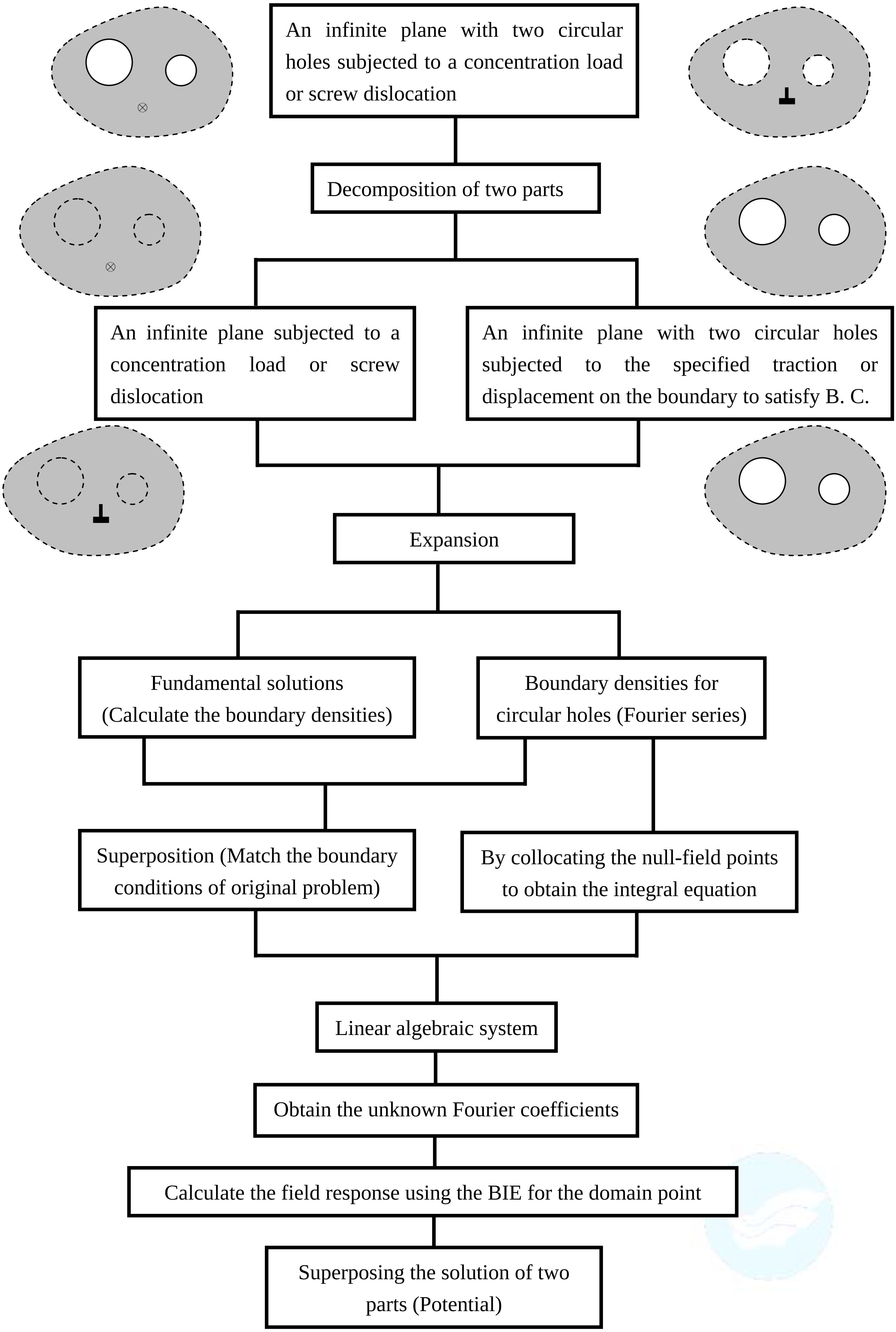

Figure 3-6 Flowchart of the present method

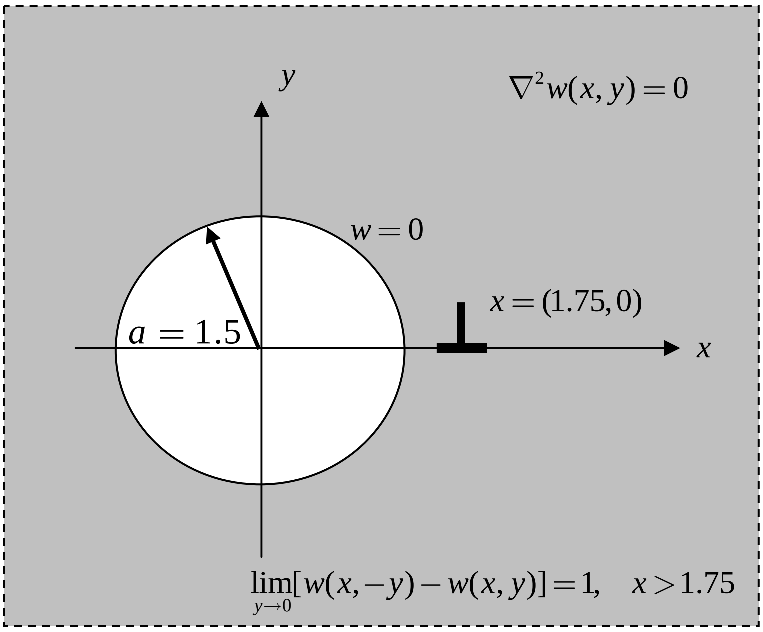

Figure 3-7 (a) Infinite plane with a circular rigid inclusion subject to the Dirichlet boundary condition under the screw dislocation

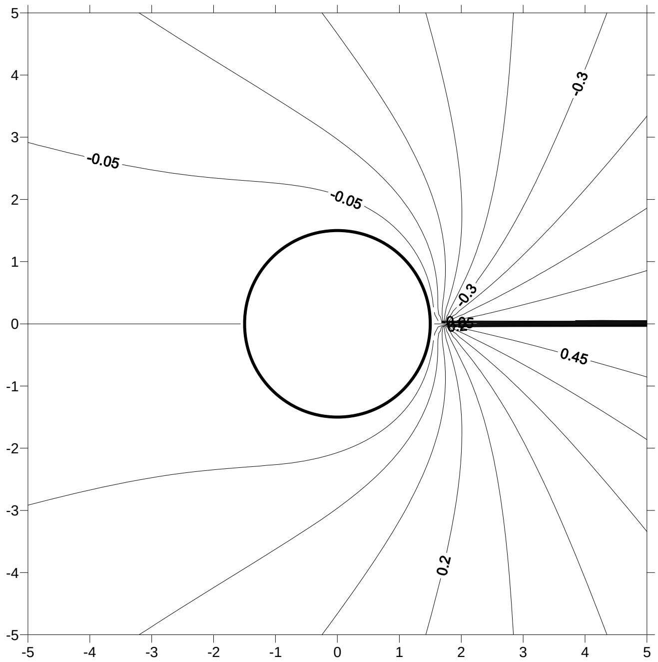

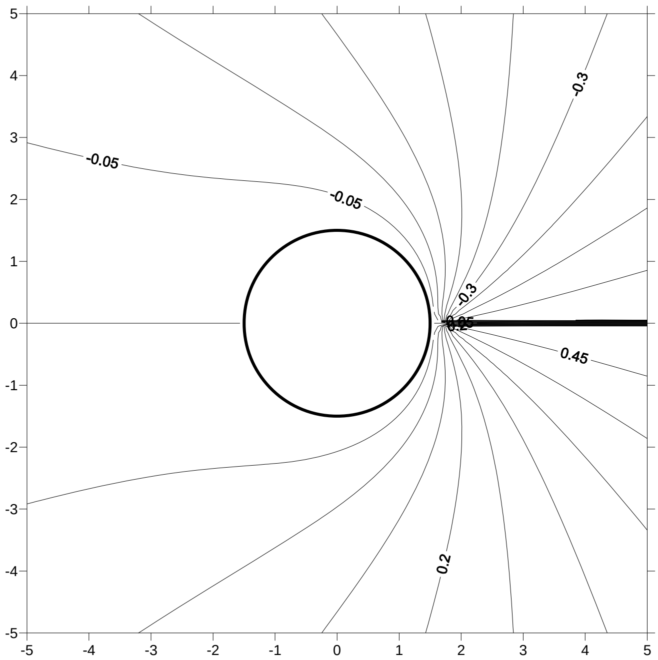

Figure 3-7 (b) Potential contour by using the Smith method [Smith, 1968]

Figure 3-7 (c) Potential contour by using the present method (M=50)

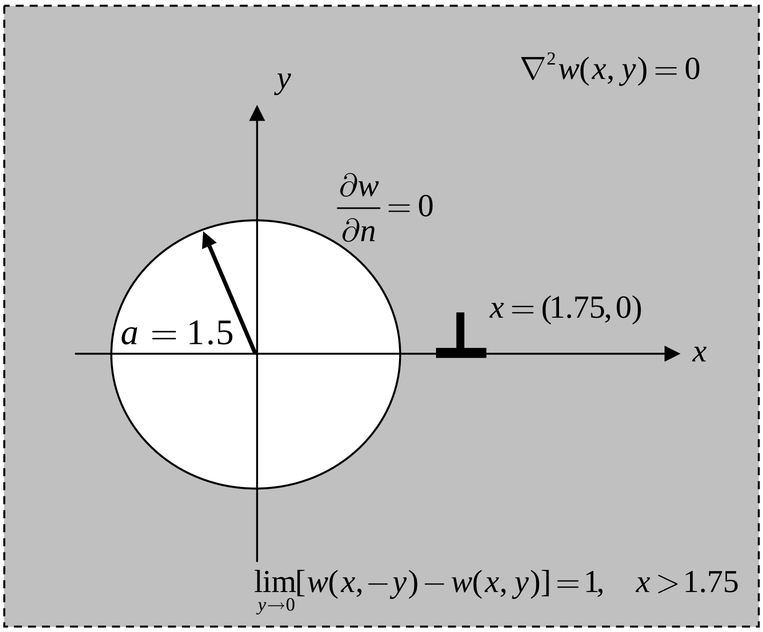

Figure 3-8 (a) Infinite plane with a circular hole subject to the Neumann boundary condition under the screw dislocation

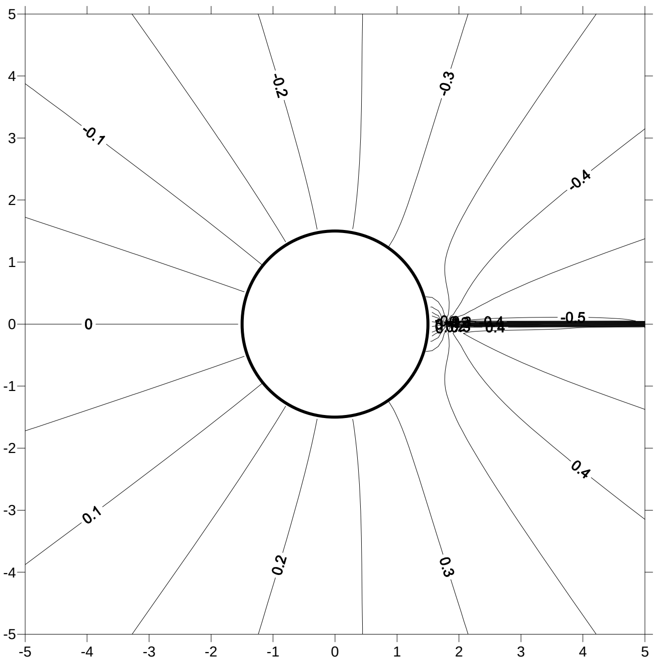

Figure 3-8 (b) Potential contour by using the Smith method [Smith, 1968]

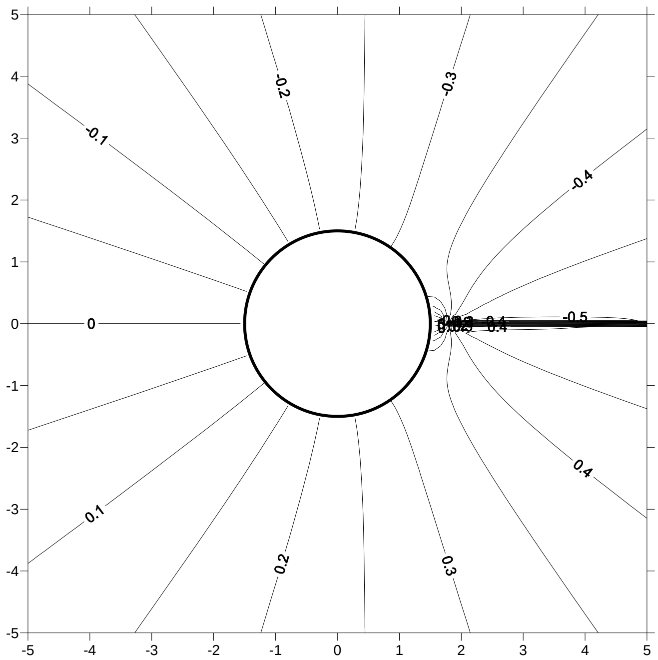

Figure 3-8 (c) Potential contour by using the present method (M=50)

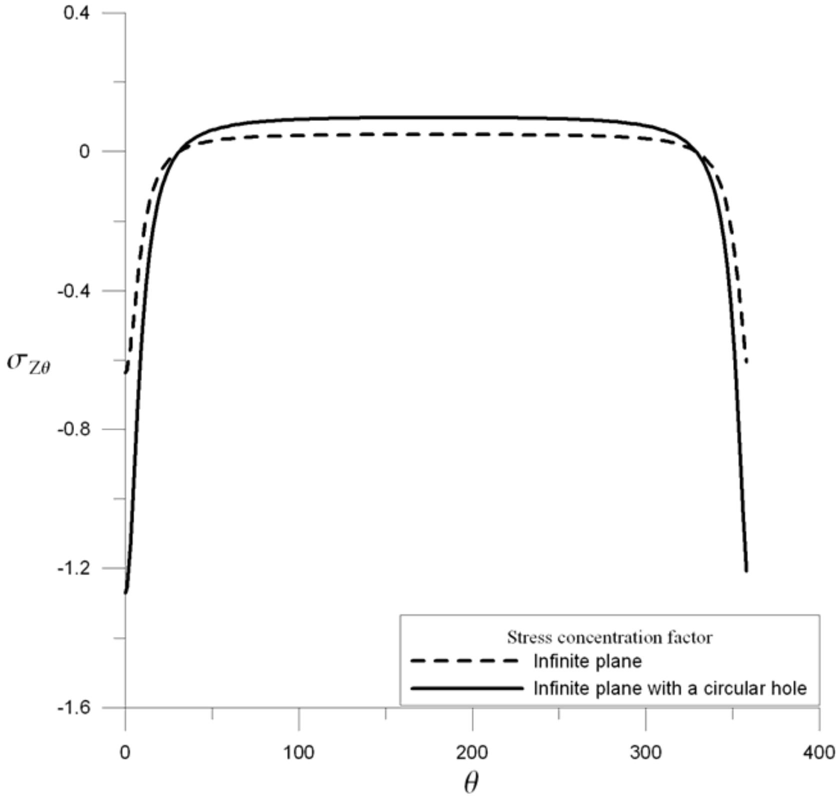

Figure 3-8(d) Stress distribution along the circular hole

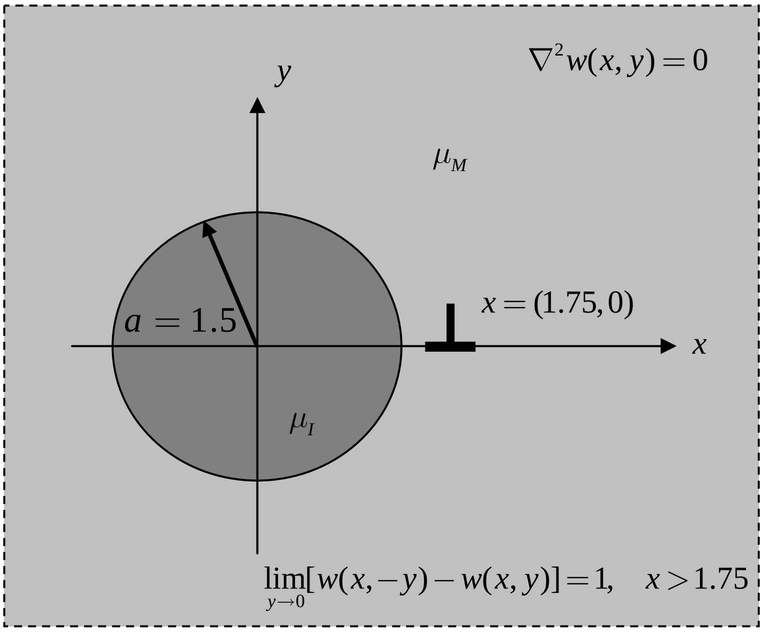

Figure 3-9 (a) A circular inclusion embedded in the matrix under the screw dislocation

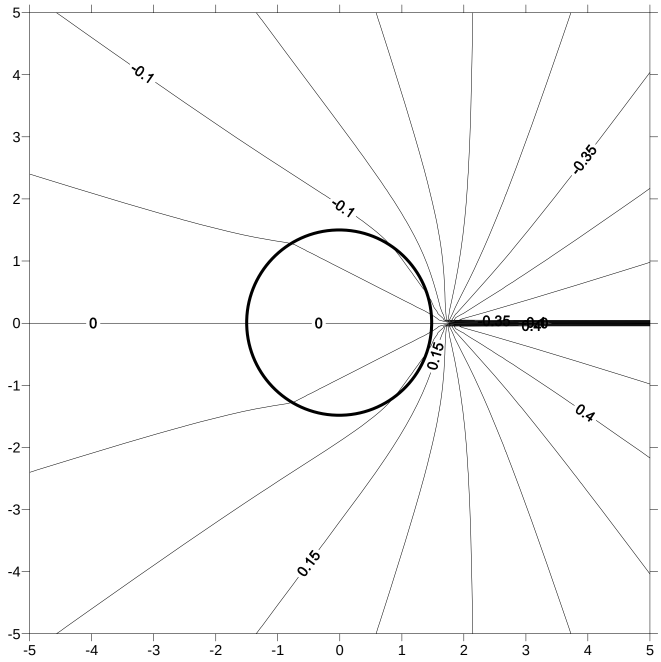

Figure 3-9 (b) Potential contour by using the Smith method [Smith, 1968]

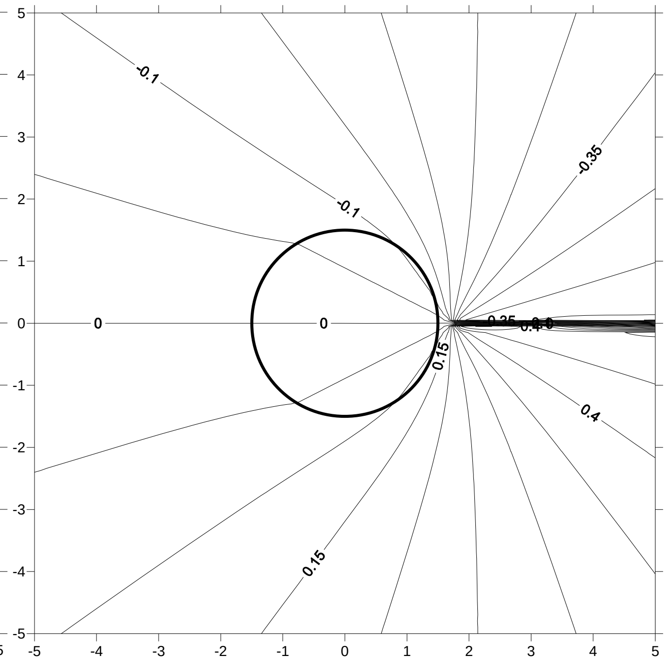

Figure 3-9 (c) Potential contour by using the present method (M=50)

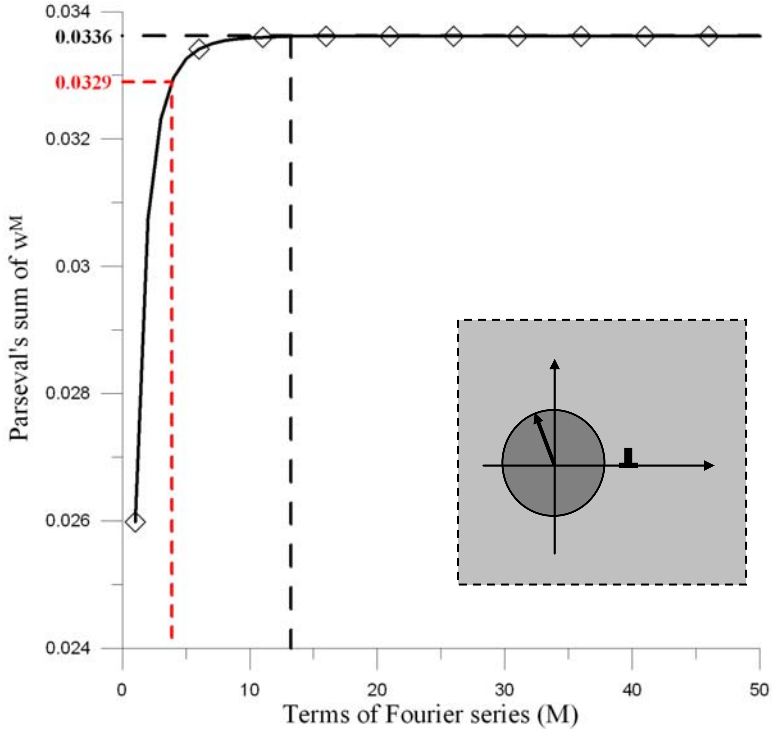

Figure 3-10 (a) Parseval's sum for w^M with $a = 1.5$ and $\xi = (1.75, 0)$

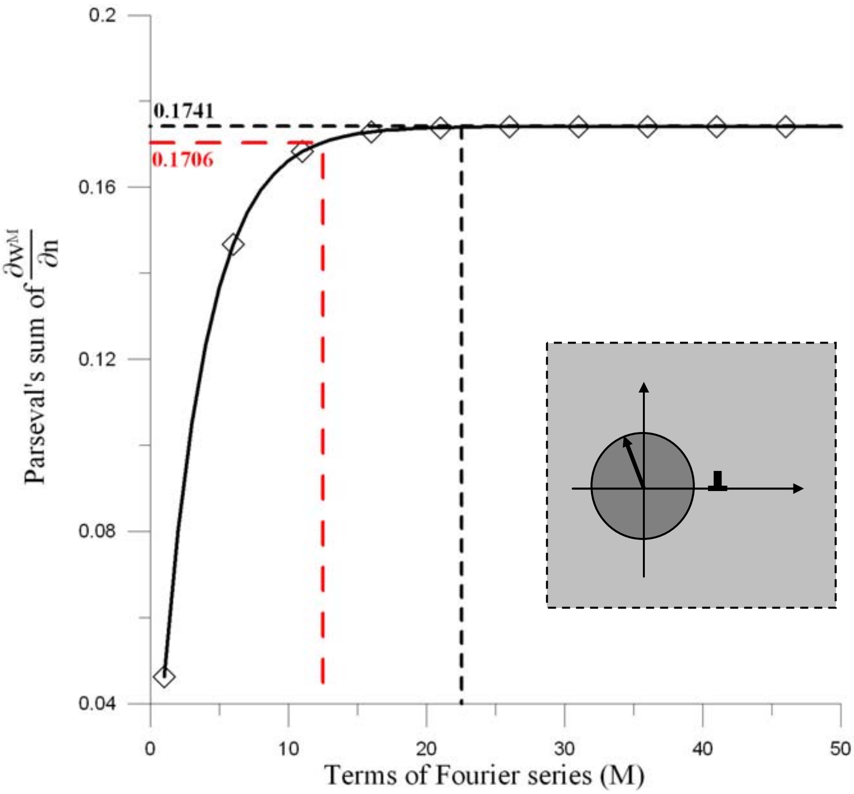

Figure 3-10 (b) Parseval's sum for $\dfrac{\partial w^M}{\partial n}$ with $a = 1.5$ and $\xi = (1.75, 0)$

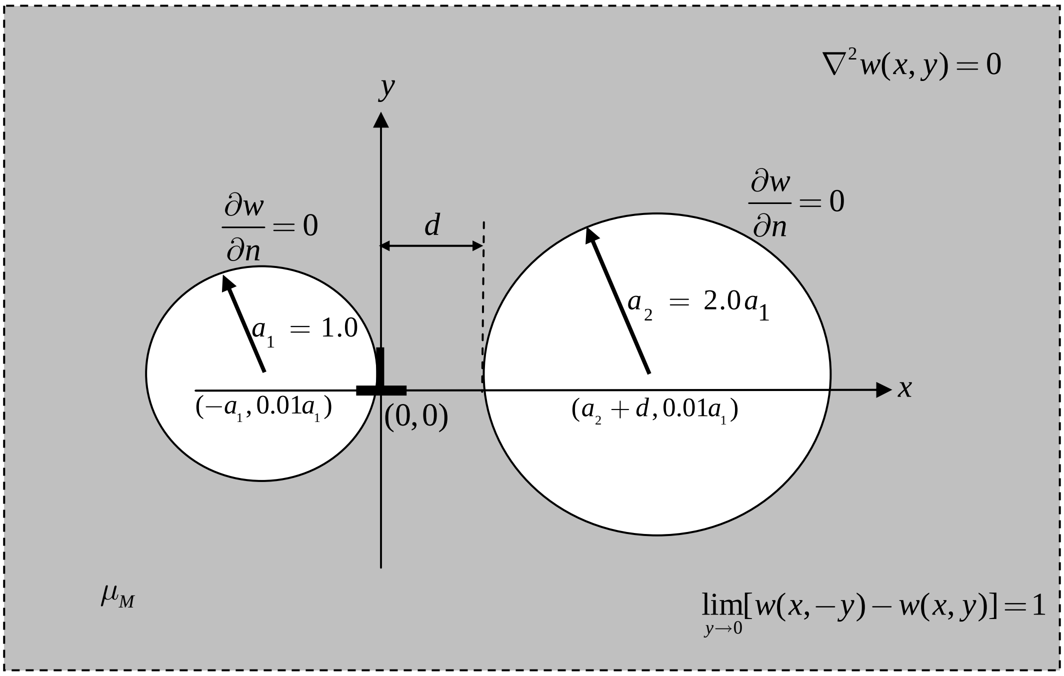

Figure 3-11 (a) Infinite plane with two circular holes subject to the Neumann boundary condition under the screw dislocation

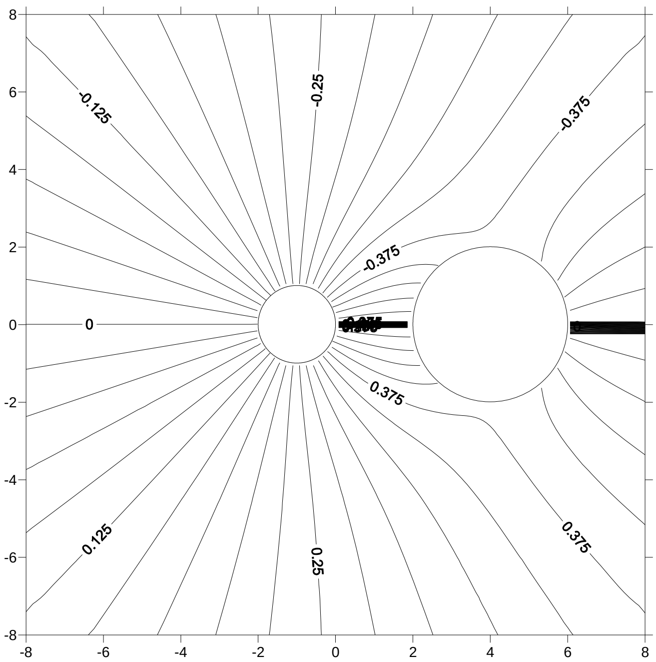

Figure 3-11 (b) The displacement contour for the two circular holes problem ($d = 2.0a_1$, $M = 50$)

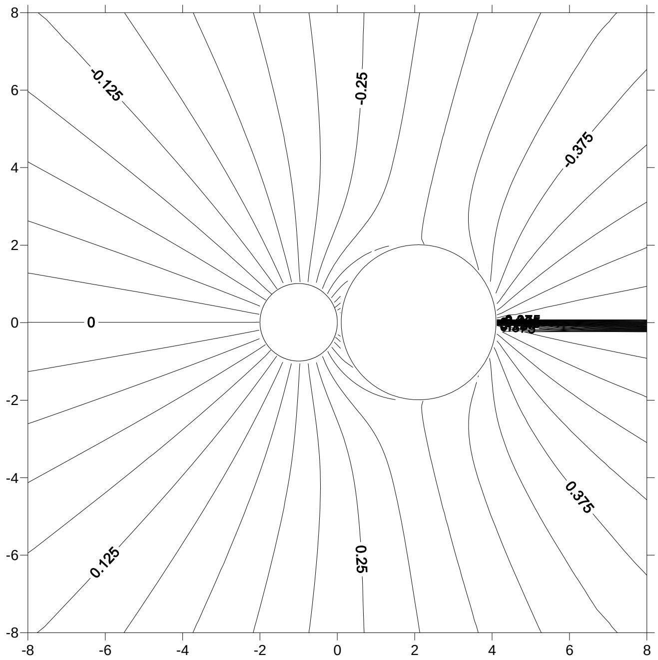

Figure 3-11 (c) The displacement contour for the two circular holes problem ($d = 0.1a_1$, $M = 50$)

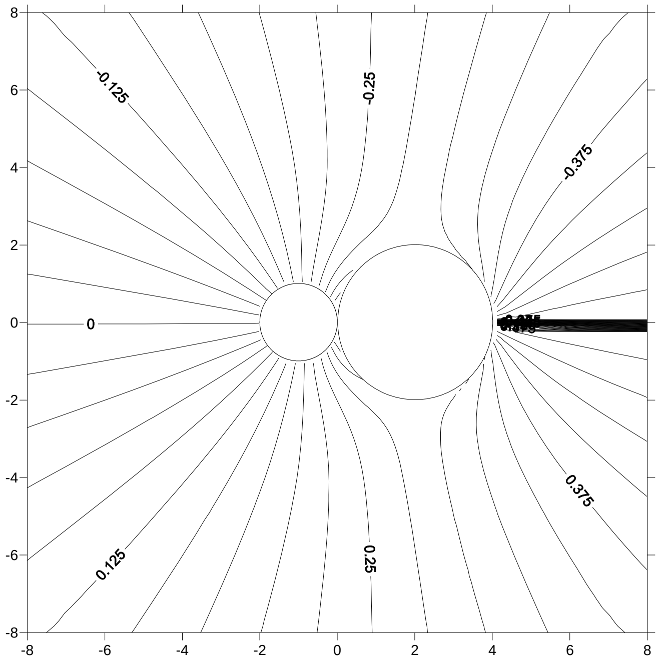

Figure 3-11 (d) The displacement contour for the two circular holes problem ($d = 0.01a_1$, $M = 50$)

Chapter 4 Conclusions and further research

4.1 Conclusions

The thesis is concerned about the derivation of Green's function for concentrated force and screw dislocation problems with circular holes and/or inclusions by using the superposition technique and addition theorem. In the context of this thesis, we have demonstrated that our approach is useful and effective. Based on the proposed formulation for solving the problems involving circular apertures and/or inclusions with perfect interface, some concluding remarks are itemized as follows:

1. Instead of directly using Green's third identity as proposed by Ke [Chen and Ke, 2008], a systematic approach to derive the Green's function for Laplace problems with circular apertures and/or inclusions was proposed successfully in this thesis by using the superposition technique and addition theorem. Problems involving infinite, semi-infinite and bounded domains with perfect circular boundaries were examined to check the accuracy of the present formulation.

2. The singularity and hypersingularity were avoided by using the addition theorem or the degenerate kernel for interior and exterior regions separated by the circular boundary. Instead of directly calculating principal values, all the boundary integrals can be performed analytically by using the degenerate kernel and Fourier expansion.

3. The Green's function can be obtained by using the null-field integral equation in conjunction with the degenerate kernel and Fourier series through the Green's third identity. It is also solved by using the present approach. The two methods are proved to be mathematically equivalent as given in the Appendix 1.

4. The convergence study shows that only a few terms of Fourier series can yield acceptable results and the convergence rate is fast since the kernel functions and boundary densities are expanded into the degenerate form and Fourier series, respectively.

5. We derived the analytical Green's function for one aperture or inclusion problem by using the superposition technique and addition theorem. Also, the present approach can be utilized to construct semi-analytical Green's functions for the concentrated force and screw dislocation problem with several circular aperture or inclusions. The present method is seen as a "semi-analytical" approach since error only stems from the truncation Fourier series.

6. After introducing the degenerate kernel, the BIEs is nothing more than the linear algebra for the unknown Fourier coefficients.

7. The angle-type fundamental solution is first successfully expanded into the degenerate form. Thus, we employ the kernel function to solve the screw dislocation problems with circular holes or inclusions.

8. A program for deriving the Green's function due to the concentrated force and screw dislocation with the circular apertures or inclusions of arbitrary radii and various positions involving Dirichlet, Neumann and mixed boundary condition was developed.

4.2 Further research

In this thesis, our formulation has been applied to derive the Green’s function for the concentrated forces and screw dislocation problems with circular boundaries by using the addition theorem and superposition technique. However, several issues are worth to be further investigated as follows:

1. In this thesis, we only consider the perfect interface. The general case of the imperfect interface which is circumferentially inhomogeneous can also be solved by using the present method.

2. Although the Green’s function for the screw dislocation problems is solved by using the superposition technique, we may also employ the Green’s third identity to solve the screw dislocation problems in the future study.

3. The degenerate kernels are expanded in the polar coordinate and only problems with circular boundaries are solved. For boundary value problems with ellipse or crack, further investigation should be considered.

4. According to our successful experiences for half-plane problems, it is straightforward to quarter-plane problems which can be studied by employing the symmetric or anti-symmetric property of image method.

5. Following the success of applications in two-dimensional problems, it is straightforward to extend this formulation to 3-D problems with spherical inclusions and/or apertures with perfect or imperfect circular boundaries using the corresponding 3-D degenerate kernel functions for fundamental solutions and spherical harmonic expansions for boundary densities.

References

[1] Achenbach, J. D.; Kechter, G. E.; Xu, Y. L**.,** 1988, Off-boundary approach to the boundary element method. *Computer Methods in Applied Mechanics and Engineering*, vol. 70, pp. 191-201.

[2] Adewale, A. O., 2006, Isotropic clamped-free thin annular plate subjected to a concentrated load. *ASME Journal of Applied Mechanics*, vol. 73, no. 4, pp. 658-663.

[3] Ang, W. T.; Telles, J. C. F., 2004, A numerical Green's function for multiple cracks in anisotropic bodies. *J. Eng. Math*, vol. 49, pp. 197-207.

[4] Barone, M. R.; Caulk, D. A., 1981, Special boundary integral equations for approximate solution of Laplace’s equation in two-dimensional regions with circular holes. *Quarterly Journal of Mechanics and Applied Mathematics*, vol. 34, pp. 265-286.

[5] Barone, M. R.; Caulk, D. A., 1982, Optimal arrangement of holes in a two-dimensional heat conductor by a special boundary integral method. *International Journal for Numerical Methods in Engineering*, vol. 18, pp. 675-685.

[6] Barone, M. R.; Caulk, D. A., 1985, Special boundary integral equations for approximate solution of potential problems in three-dimensional regions with slender cavities of circular cross-section. *IMA Journal of Applied Mathematics*, vol. 35, pp. 311-325.

[7] Barone, M. R.; Caulk, D. A., 2000, Analysis of liquid metal flow in die casting. *International Journal of Engineering Science*, vol. 38, pp. 1279-1302.

[8] Bird, M. D., 1992, A Fourier series method for determining the interaction of circular in homogeneities in harmonic and biharminic problems, Ph. D. Dissertation, *Department of Mechanical Engineering*, Stanford University, USA.

[9] Bergman, S.; Schiffer, M., 1953, Kernel functions and elliptic differential equations in mathematical physics, New York: *Academic Press*.

[10] Bird, M. D.; Steele, C. R., 1991, Separated solution procedure for bending of circular plates with circular holes. *ASME Applied Mechanics Reviews*, vol. 44, pp. 27-35.

[11] Bird, M. D.; Steele, C. R., 1992, A solution procedure for Laplace equation on multiply-connected circular domains. *ASME Journal of Applied Mechanics*, vol. 59, pp. 398-404.

[12] Boley, B. A., 1956, A method for the construction of Green's functions. *Quarterly of Applied Mathematics*, vol. 14, pp. 249-257.

[13] Caulk, D. A., 1983, Analysis of elastic torsion in a bar with circular holes by a special boundary integral method. *ASME Journal of Applied Mechanics*. vol. 50, pp. 101-108.

[14] Caulk, D. A., 1983, Analysis of steady heat conduction in regions with circular holes by a special boundary integral method. *IMA Journal of Applied Mathematics*, vol. 30, pp. 231-246.

[15] Caulk, D. A., 1983, Steady heat conduction from an infinite row of holes in a half-space or a uniform slab. *International Journal of Heat and Mass Transfer*, vol. 26, pp. 1509-1513.

[16] Caulk, D. A., 1984, Special boundary integral equations for potential problems in regions with circular holes. *ASME Journal of Applied Mechanics*, vol. 51, pp. 713-716.

[17] Chen, H. B.; Lu, P.; Schnack, E., 2001, Regularized algorithms for the calculation of values on and near boundaries in 2D elastic BEM. *Engineering Analysis with Boundary Elements*, vol. 25, pp. 851-876.

[18] Chen, J. T.; Hong, H. K., 1994, Dual boundary integral equations at a corner using contour approach around singularity. *Advances in Engineering Software*, vol. 21, pp. 169-178.

[19] Chen J. T. and Hong H-K, 1999, Review of dual boundary element methods with emphasis on hypersingular integrals and divergent series, *ASME Applied Mechanics Reviews*, Vol. **52**, pp. 17-33.

[20] Chen C. T., 2005, *Null-field integral equation approach for Helmholtz (interior and exterior acoustic) problems with circular boundaries*. Master Thesis, Department of Harbor and River Engineering, National Taiwan Ocean

University, Taiwan.

[21] Chen, J. T.; Ke J. N., 2008, Construction of Green's function using null field integral approach for Laplace problems with circular boundaries. CMC, accepted.

[22] Chen J. T., Hsiao C. C. and Leu S. Y., 2006, Null-field integral equation approach for plate problems with circular boundaries, *Journal of Applied Mechanics, ASME*, Vol. 73, pp. 679-693.

[23] Chen, J. T.; Wu, C. S., 2006, Alternative derivations for the Poisson integral formula. *International Journal of Mathematical Education in Science and Technology*, vol. 37, pp. 165-185.

[24] Chen, J. T.; Shen, W. C., 2007, Degenerate scale for multiply connected Laplace problems. *Mechanics Research Communications*, vol. 34, pp. 69-77.

[25] Chen, J. T.; Wu, C. S.; Lee, Y. T.; Chen, K. H., 2007, On the equivalence of the Trefftz method and method of fundamental solutions for Laplace and biharmonic equations. *Computers and Mathematics with Applications*, vol. 53, pp. 851-879.

[26] Chen J. T., Shen W. C. and Wu A. C., 2005, Null-field integral equations for stress field around circular holes under anti-plane shear. *Engineering Analysis with Boundary Elements*, Vol. 30, pp. 205-217.

[27] Chen P. Y., Chen C. T. and Chen J. T., 2005, A semi-analytical approach for dynamic stress concentration factor of Helmholtz problems with circular holes, *The 29th National Conference on Theoretical and Applied Mechanics*, NTHU, Hsinchu.

[28] Chen C. T., Chen I. L. and Chen J. T., 2005, Null-field integral equation approach for Helmholtz (interior and exterior acoustic) problems with circular boundaries, *九十四年電子計算機於土木水利工程應用研討會*, 台南成大.

[29] Chen J. T., Shen W. C. and Chen P. Y., 2006, Analysis of circular torsion bar with circular holes using null-field approach, *Computer Modeling in Engineering Science*, Vol. 12, pp. 109-119.

[30] Chen J. T., Wu C. S., Lee Y. T., K. H. Chen, 2007, On the equivalence of the Trefftz method and method of fundamental solution for Laplace and biharmonic equations. *Computers and Mathematics with Applications*, Vol. 53, pp. 851-879.

[31] Chen J. T. and Wu A. C., 2007, Null-field approach for the multi-inclusion problem under anti-plane shears. *Journal of Applied Mechanics, ASME*, Vol. 74, pp. 469-487.

[32] Chen J. T. and Wu A. C., 2006, Null-field approach for piezoelectricity problems with arbitrary circular inclusion. *Engineering Analysis with Boundary Elements*, Vol. 30, pp. 971-993.

[33] Cheng A. H. D. and Cheng D. T., Heritage and early history of the boundary element method, *Engineering Analysis with Boundary Elements*, Vol. 29, No. 3, pp. 268-302.

[34] Courant, R.; Hilbert, D., 1962, Methods of mathematical physics, vol. 2, New York: *Interscience*.

[35] Crouch, S. L.; Mogilevskaya, S. G., 2003, On the use of Somigliana's formula and Fourier series for elasticity problems with circular boundaries. *International Journal for Numerical Methods in Engineering*, vol. 58, pp. 537-578.

[36] Denda, M.; Wang, C. Y.; Yong, Y. K., 2003, 2-D time-harmonic BEM for solids of general anisotrophy with application to eigenvalue problems. *Journal of Sound and Vibration*, vol. 261, pp. 247-276.

[37] Denda, M.; Araki, Y.; Yong, Y. K., 2004, Time-harmonic BEM for 2-D piezoelectricity applied to eigenvalue problem. *International Journal of Solids and Structures*, vol. 41, pp. 7241-7265.

[38] Dundurs J., 1969, Elastic interaction of dislocations with inhomogeneities, Mathematical Theory of Dislocations, pp. 70-115.

[39] Fang Q. H. and Lin Y. W., 2006, Size-dependent elastic interaction between a screw dislocation and a circular nano-hole with surface stress, Physica Status Solidi, Vol. 243, No. 4, pp. R28-R30.

[40] Fan H. and Wang G. F., 2003, Screw dislocation interacting with imperfect interface, Mechanics of Materials, Vol.35, pp. 943-953.

[41] Fang Qihong, Liu Youwen and Jiang Chiping, 2005, Interaction between a screw dislocation and an elastic elliptical inhomogeneity with interfacial cracks, *Acta Mechanica Sinica*, Vol. 21, pp. 151-159.

[42] Fang Q. H. and Liu Y. W., 2006, Size-dependent elastic interaction of a screw dislocation with a circular nano-inhomogeneity incorporating interface stress, Scripta Materialia, Vol. 55, pp. 99-102.

[43] Golberg M. A., 1978, Solution methods for integral equations, Plenum press, New York and London.

[44] Guiggiani M, 1995, Hypersingular boundary integral equations have an additional free term, *Computational Mechanics*, Vol. **16**, pp. 245-248.

[45] Guimaraes, S and Telles, J. C. F., 2000, General application of numerical Green's functions for SIF Computations with boundary elements. CMES, vol. 1, no. 3, pp. 131-139.

[46] Honein E., Honein T. and Herrmann G., 1992, On two circular inclusions in Harmonic problems, *Quarterly of Applied Mathematics*, Vol. L, No. 3 pp. 479-499.

[47] Huang, Q.; Cruse, T. A., 1993, Some notes on singular integral techniques in boundary element analysis. *International Journal for Numerical Methods in Engineering*, vol. 36, pp. 2643-2659.

[48] Sloan I. H., Burn B. J. and Datyner N., 1975, A new approach to the numerical solution of integral equations, *Journal of Computational Physics*, Vol. 18, pp. 92-105.

[49] Jaswon, M. A.; Symm, G. T., 1977, Integral equation methods in potential theory and electrostatics, Academic Press, New York.

[50] Jin B. and Fang Q. H., 2008, Piezoelectric screw dislocations interacting with a circular inclusion with imperfect interface, *Archive of Applied Mechanics*, Vol.78, pp. 105-116.

[51] Jiang Chi-Ping, Liu You-wen and Xu Yao-long, 2003, Interaction of a screw dislocation in the interphase layer with the inclusion and matrix, *Mechanics Research Communications*, Vol.24, No. 8, pp.979-988.

[52] Kisu, H.; Kawahara, T., 1988, Boundary element analysis system based on a formulation with relative quantity. Boundary Elements X, Brebbia CA, eds., *Springer-Verlag*, vol. 1, pp. 111-121.

[53] Kitahara, M., 1985, Boundary integral equation methods in eigenvalue problems of elastodynamics and thin plates, *Elsevier*, Amsterdam.

[54] Kress, R., 1989, Linear integral equations, *Springer-Verlag*, Berlin.

[55] Kellogg, O. D., 1953, Foundations of potential theory, New York: *Dover*.

[56] Lee W. M. Lee, Chen J. T. and Lee Y. T., 2007, Free vibration analysis of circular plates with multiple circular holes using indirect BIEMs. *Journal of Sound and Vibration*, Vol. 304, pp. 811–830.

[57] Li, Z. and Shi, J., 2002, The interaction of a screw dislocation with inclusion analyzed by Eshelby equivalent inclusion method, Scripta Materialia, Vol.47, pp.371-375.

[58] Lin Y. W. and Fang Q. H., 2003, Electro-elastic interaction between a piezoelectric screw dislocation and circular interfacial rigid lines, International

Journal of Solids and Structures, Vol. 40, pp.5353-5370.

[59] Liu Y. W., Fang Q. H. and Jiang C. P., 2004, A piezoelectric screw dislocation interacting with an interphase layer between a circular inclusion and the matrix, *International Journal of Solids and Structures*, Vol.41, pp.3255-3274.

[60] Lin Y. W., Jiang C. P. and Cheung Y. K., 2003, A screw dislocation interacting with an interphase layer between a circular inhomogeneity and the matrix, *International Journal of Engineering Science*, Vol. 41, pp. 1883-1898.

[61] Lin Y. W., Fang Q. W. and Jiang C. P., 2004, A piezoelectric screw dislocation interacting with an interphase layer between a circular inclusion and the matrix, *International Journal of Solids and Structures*, Vol. 41, pp.3255-3274.

[62] Liu Y., Li B. and Fang Q., 2006, Interaction between a screw dislocation and a piezoelectric circular inhomogeneity with interfacial cracks in viscoelastic martrix, *Applied Rheology*, Vol. 16, pp. 102-109.

[63] Li Bo, Lin You-Wen and Fang Qi-Hong, 2007, Interaction between a screw dislocation and an interfacial crack in viscoelastic media, *Journal of Central South University of Technology*, Vol.14, pp. 1005-9784 (Print) 1993-0666 (Online)

[64] Lazar, M., 2004, On the correspondence between a screw dislocation in gradient elasticity and a regularized vortex, *Annalen der Physik (Leipzig)*, Vol. 13, pp. 617-622.

[65] Melnikov, Y. A.; Melnikov, M. Y., 2001, Modified potential as a tool for computing Green's functions in continuum mechanics. *CMES*, vol. 2, pp. 291-305.

[66] Melnikov, Y. A., 1995. Green's functions in applied mechanics, Computational Mechanics Publications, Boston-Southampton.

[67] Melnikov, Y. A.; Melnikov, M. Y., 2006, Green's functions for mixed boundary value problems in regions of irregular shape. *Electron. J. Boundary Elem.*, vol. 4, pp. 82-104.

[68] Melnikov, Y. A., 1982. A basis for computation of thermo-mechanical fields in elements of constructions of complex con figuration. Thesis Dr. Technical Sciences, Moscow Institute of Civil Engineering (in Russian).

[69] Melnikov, Y. A., 1977, Some application of the Green's function method in mechanics. *International Journal of Solids and Structures*, vol. 13, pp. 1045-1058.

[70] Morse, P. M.; Fechbach, H., 1953, Methods of theoretical physics, vols. 1 and 2, New York, Toronto, London: *McGraw-Hill*.

[71] Roach, G. F., 1982, Green's functions, New York: *Cambridge University Press*.

[72] Smith E., 1968, The interaction between dislocations and inhomogeneities-I, *International Journal of Engineering Science,* Vol. 6, pp. 129-143.

[73] Sladek, V.; Sladek, J., 1991, Elimination of the boundary layer effect in BEM computation of stresses. *Communications in Applied Numerical Methods*, vol. 7, pp. 539-550.

[74] Sudak L. J., 2002, On the interaction between a dislocation and a circular inhomogeneity with imperfect interface in antiplane shear, *Mechanics Research Communications,* Vol.30, pp.53-59.

[75] Schaback R., 2007, Adaptive Numerical Solution of MFS Systems, *ICCES Special Symposium on Meshless Methods*., Cyprus.

[76] Sendeckyj G.. P., 1970, Screw dislocations near circular inclusions, *Physica Status Solidi*, Vol.3, pp.529-535.

[77] Sudak L. J., 2003, On the interaction between a dislocation and a circular inhomogeneity with imperfect interface in antiplane shear, *Mechanics Research Communications*, Vol.30, pp.53-59.

[78] Shen Ming-Ho, 2008, A magnetoelectric screw dislocation interacting with a circular layered inclusion, *European Journal of Mechanics A/Soli*ds, Vol. 27, pp.429-442.

[79] Talbot, D. R. S.; Willis, J. R., 1983, Variational estimates for dispersion and attenuation of waves in random composite—III. Fiber-reinforced materials. *International Journal of Solids and Structures*, vol. 19, pp. 793-811.

[80] Telles, J. C. F., 1987, A self-adaptative coordinate transformation for efficient numerical evaluation of general boundary element integrals. *International Journal for Numerical Methods in Engineering*, vol. 24, pp. 959-973.

[81] Telles, J. C. F.; Castor, G. S.; Guimaraes, S. 1995, Numerical Green's function approach for boundary elements applied to fracture mechanics. *International Journal for Numerical Methods In Engineering*, vol. 38, no. 19, pp. 3259-3274.

[82] Thomson, W., 1848. Maxwell in his treatise, vol. I., Chap. XI, quotes a paper in the Cambridge and Dublin Math. Journ. of 1848.

[83] Waterman PC, 1965, Matrix formulation of electromagnetic scattering, *Proceedings of the IEEE*, Vol. **53**, pp. 805-812.

[84] Wang, X., Zhong, Z., 2003, Two-dimensional time-harmonic dynamic Green's functions in transversely isotropic piezoelectric solids. *Mechanics Research Communications*, vol. 30, pp. 589-593.

[85] Willis, J. R., 1980a, A polarization approach to the scattering of elastic waves—Ⅰ. scattering by a single inclusion. *Journal of the Mechanics and Physics of Solids*, vol. 28, pp. 287-305.

[86] Wu M. S. and Kirchner H. O. K. K. , 2004, An exact analytical formula for the line tension of screw dislocations in bcc metals, Philosophical Magazine, Vol. 84, No. 24, pp.2485-5499.

[87] Wu, 2006, Null-field approach for multiple circular inclusion problems in anti-plane piezoelectricity, Master thesis, *National Taiwan Ocean University.*

[88] Wang Xu and Sudak L. J., 2006, Interaction of a screw dislocation with an arbitrary shaped elastic inhomogeneity, *Journal of Applied Mechanics,* Transaction ASME, Vol.73, pp.206-211.

[89] Wang, X., Sudak, L. J., 2007, Antiplane time-harmonic Green’s functions for a circular inhomogeneity with an imperfect interface. *Mechanics Research Communications*, Vol. 34 pp. 352-358.

[90] Wang X. and Pan E., 2008, On the screw dislocation in a functionally graded piezoelectric plane and half-plane, *Mechanics Research Communications*, Vol. 35, No. 4, pp 229-236.

[91] Xiao Z. M. and Chen B. J., 2000, A crew dislocation interacting with a coated fiber, Mechanics of Materials, Vol.32, pp.485-494.

[92] Yen, Wen J. , Hwu, Chysnbin and Liang, Yin Ko, 1995, Dislocation inside of an anisotropic elliptical inclusion, *Journal of Applied Mechanics*, Transaction ASME, Vol. 62, pp.306-311.

Appendix 1 Equivalence between the solution using Green's third identity and that using superposition technique

According to the Chen and Ke (Chen and Ke, 2007) work, the Green's function can be represented by using the Green's third identity as shown below:

$$2\pi G(x,\xi)=\int_B T(s,x)G(s,\xi)dB(s)-\int_B U(s,x)\frac{\partial G(s,\xi)}{\partial n_s}dB(s)+U(\xi,x)\,, \quad \mathrm{x}\in D\,, \tag{A1-1}$$

After introducing the superposition technique, the Green's function is decomposed into two parts. The part of the fundamental solution can be written by using the boundary integral equation as given below:

$$2\pi G^1(x,\xi)=\int_B T(s,x)G^1(s)dB(s)-\int_B U(s,x)\frac{\partial G^1(s)}{\partial n_s}dB(s)+U(\xi,x)\,, \quad \mathrm{x}\in D\,. \tag{A1-2}$$

The figure is shown in Fig. 2 (b). The boundary integral equation for the typical boundary value problem can be also written as

$$2\pi G^2(x,\xi)=\int_B T(s,x)G^2(s)dB(s)-\int_B U(s,x)\frac{\partial G^2(s)}{\partial n_s}dB(s)\,, \quad \mathrm{x}\in D\,. \tag{A1-3}$$

as shown in Fig. 2 (c). By superposing Eqs. (A2-2) with (A2-3), we can obtain the equation as shown below:

$$\begin{aligned}2\pi(G^1(x,\xi)+G^2(x,\xi))=&\int_B T(s,x)(G^1(s)+G^2(s))dB(s)-\\&\int_B U(s,x)\left(\frac{\partial G^1(s)}{\partial n_s}+\frac{\partial G^2(s)}{\partial n_s}\right)dB(s)+U(\xi,x), \quad \mathrm{x}\in D\,,\end{aligned} \tag{A1-4}$$

where $u_1(s)+u_2(s)$ and $\frac{\partial u_2(s)}{\partial n_s}+\frac{\partial u_1(s)}{\partial n_s}$ must satisfy the original boundary conditions. Thus, Eq. (A1-4) is rewritten as

$$\begin{aligned}2\pi(G^1(x,\xi)+G^2(x,\xi))=&\int_B T(s,x)G(s,\xi)dB(s)-\int_B U(s,x)\frac{\partial G(s,\xi)}{\partial n_s}dB(s)\,,\\&+U(\xi,x), \quad \mathrm{x}\in D\end{aligned} \tag{A1-5}$$

where $G^1(x,\xi)+G^2(x,\xi)=G(x,\xi)$. Therefore, we have proved the equivalence between the solution of Green's third identity and that of superposition technique.

Appendix 2 Relation between the Smith solution and the present solution for screw dislocation by using the addition theorem

According to the Smith (Smith, 1969) work, an analytical solution for the screw dislocation problem with a circular hole subject to the Neumann boundary condition is shown below:

$$F(z)=\frac{\mu_E b}{2\pi i}\log(z-z_0)-\frac{\mu_E b}{2\pi i}\log(\frac{a^2}{z}-\bar{z}_0)$$
$$w(x,y)=\frac{1}{\mu_E}\mathrm{Re}[F(z)] \quad . \qquad \text{(A2-1)}$$

By using the addition theorem, the term $\log(z-z_0)$ can be separated as shown in Eq. (3-8). Similarly, the term $\log(\frac{a^2}{z}-\bar{z}_0)$ is also separated into the separable form as

$$\log(\frac{a_0^2}{z}-\bar{z}_0)=\log R-i\theta-\sum_{m=1}^{\infty}(\frac{a^2}{R\rho})^m[\cos m(\theta-\phi)+i\sin m(\theta-\phi)]\,. \qquad \text{(A2-2)}$$

Thus, we separated the analytical solution into the separable form as shown below:

$$w_S(\rho,\phi)=\begin{cases}\dfrac{b\theta}{\pi}+\displaystyle\sum_{m=1}^{\infty}\frac{b}{2\pi m}((\frac{\rho}{R})^m+(\frac{a^2}{R\rho})^m)\sin m(\theta-\phi), & \rho\le R\\ \dfrac{b\phi}{2\pi}+\dfrac{b\theta}{2\pi}-\dfrac{b}{2}-\displaystyle\sum_{m=1}^{\infty}\frac{b}{2\pi m}((\frac{R}{\rho})^m-(\frac{a^2}{R\rho})^m)\sin m(\theta-\phi), & \rho>R\end{cases}, \qquad \text{(A2-3)}$$

where the subscript S denotes the Smith's solution. The solution is also obtained by using the present approach as shown below:

$$w_P(\rho,\phi)=\begin{cases}\dfrac{b\theta}{2\pi}+\displaystyle\sum_{m=1}^{\infty}\frac{b}{2\pi m}[(\frac{\rho}{R})^m+(\frac{a^2}{\rho R})^m]\sin m(\theta-\phi), & R\ge\rho\\ \dfrac{b\phi}{2\pi}-\dfrac{b}{2}-\displaystyle\sum_{m=1}^{\infty}\frac{b}{2\pi m}[(\frac{R}{\rho})^m-(\frac{a^2}{\rho R})^m]\sin m(\theta-\phi), & R<\rho\end{cases}. \qquad \text{(A2-4)}$$

where the subscript P denotes the present solution. After comparing with the two solutions, there is a little difference between the present approach and Smith's work. When the θ is not equal to zero, the present solution and the Smith's solution are different. The θ term can be viewed as a rigid body solution due to the Neumann problem.

作者簡歷

中文姓名：周克勳

英文姓名：Ke-Hsun Chou

出生日期：民國 72 年 01 月 12 日

籍　　貫：台灣省台北縣

聯絡地址：台北縣泰山鄉明志路二段 372 巷 9 弄 6 號 2 樓

聯絡電話：(02) 2908-9235

行動電話：0921147716

電子信箱：*M95520083@mail.ntou.edu.tw*

學　　歷：

國立台灣海洋大學河海工程研究所碩士 (2006.09 ~ 2008.07)

國立台灣海洋大學河海工程研究所學士(2001.09 ~ 2006.06)

台北縣國立三重高級中學 (1998.09 ~ 2001.06)

台北縣立義學國民中學 (1995.09 ~ 1998.06)

台北縣立明志國民小學 (1989.09 ~ 1995.06)

著作目錄：

(A) 期刊論文

1 Chen, J. T.; Chou, K. S.; Hsieh, C. C., (2007): Derivation of stiffness and flexibility for rods and beams by using dual integral equations, Engineering Analysis with Boundary Elements, Vol. 32, pp. 108-121.

2 Chen, J. T.; Chou, K. S.; Kao, S. K., (2008) One-dimensional wave animation using Mathematica, Computer Applications in Engineering Education, Accepted.

3 Chen, J. T.; Chou, K. H.; Kao, S. K., (2007): Derivation of Green’s function using addition theorem, Submitted.

4 陳正宗，周克勳，(2008): 圓周積分的三種看法，數學傳播，32 卷 1 期，pp. 66-76。

(B) 會議論文

1 Lee, Y. T.; Chen, J. T.; Chou, K. H. (2007): Revisit of two classical elasticity problems by using the null-field BIE, *APCOM’07*, Kyoto, Japan.

(C) 榮譽

1 榮獲中華顧問工程司 96 年度『工程科技獎學金』。

2 榮獲中華民國斐陶斐榮譽學會之榮譽會員。